Imperial College London

Computational Study of Failure of Curtain Wall Facade Systems Exposed to Fire

Author
Francesca Lugaresi

Academic Supervisor
Prof. Guillermo Rein

Department of Mechanical Engineering

A thesis submitted in partial fulfilment of the requirements for the degree of Doctor of Philosophy in Mechanical Engineering of Imperial College London

London, UK
November 2023

Abstract

Fires involving building facades pose challenges for fire safety engineers and the fire service. This thesis examines the critical, yet often overlooked aspect of mechanical failure in facade systems during fires. The impact of fire on the structural integrity of the facade is critical for safe evacuation and fire-fighter access, particularly for tall buildings where facade elements falling off the building pose a life threat and swift evacuation is essential. High-profile fires in buildings with curtain walls, such as the Mercantile Credit building and the Relay building, highlight these dangers.

The absence of reliable tools for predicting the failure of facade systems during fires prompted this research. Focusing on the failure mechanisms, various facade support systems were examined. A comparative analysis of the mechanical and thermal properties influencing the failure of non-combustible components is presented.

Through computational models, the thermal response of curtain wall framing systems to fire exposure is studied. Validation against experimental data, alongside a sensitivity study, enhances the reliability of the model's predictions. The exploration of the role of screw connectors, thermal breaks and gaskets, gives insights on the complex interactions defining the system's thermal response.

The mechanical behaviour of a generic curtain wall frame was analysed, focusing on thermal degradation, load-bearing and buckling failure. Simulation results reveal that failure mode is influenced largely by both material and level of restraint. Aluminium mullions fail at temperatures from 170°C to 400°C, while transoms, due to shorter and stockier profiles, fail at lower temperatures. Stainless steel transoms fail due to extensive deflection, while carbon steel performs best but is not commonly used due to corrosion concerns.

These findings advance our understanding of curtain wall frame behaviour during fires. By identifying optimal fire protection measures and systems with increased fire resistance, this research aims to enable safer facade designs.

Declaration of Originality

I hereby declare that the work contained in this thesis is my own unless stated otherwise. In such cases the work will be appropriately referenced.

Francesca Lugaresi

Copyright Declaration

The copyright of this thesis rests with the author. Unless otherwise indicated, its contents are licensed under a Creative Commons Attribution-Non Commercial 4.0 International Licence (CC BY-NC). Under this licence, you may copy and redistribute the material in any medium or format. You may also create and distribute modified versions of the work. This is on the condition that: you credit the author and do not use it, or any derivative works, for a commercial purpose. When reusing or sharing this work, ensure you make the licence terms clear to others by naming the licence and linking to the licence text. Where a work has been adapted, you should indicate that the work has been changed and describe those changes. Please seek permission from the copyright holder for uses of this work that are not included in this licence or permitted under UK Copyright Law.

Acknowledgements

In the years it took to complete this thesis I have received incalculable help and support from friends, colleagues, and family. While I cannot possibly thank everyone here, I will do my best.

Foremost, I am indebted to Professor Guillermo Rein, my esteemed supervisor. He is really one in a million. Not only a smart and creative scientist, but also a person of great humanity and extremely funny. He has helped me in the highs and lows of this long journey, always with a smile on his face.

Thank you to all of my colleagues in Hazelab, both past and present, who are an inestimable source of expertise, and also great company. Thank you particularly to Matt and Ben for being the facade research dream-team. The time we spent in Poland burning facade mock-up was fun but also so useful - a crash course in fire dynamics! Harry helped me so much in so many different activities, I can't even begin to list them here. Rik was always a great chat and a great buddy at conferences – specially in Detroit. Wuquan and Dwi, since they left, the office has not been the same. They are the most hard-working and unique minds, their work was always an inspiration. Finally, thanks to the last arrivals: Nick, Alexander and Carlos (craziest guy in the office and a great babysitter).

I would like to thank Arup and Partners for sponsoring this research, and Imperial College London for providing the best environment and the best support net possibly imaginable. During my placement with the Arup facade and fire team, I learnt so much and their work ethic was inspiring. I want to acknowledge in particular Dr Panagiotis Kotsovinos and Dr Peter Lenk for their guidance and supervision.

I express sincere appreciation to ITB and, specifically, to Dr Wojciech Wegrzynski and Dr Bartek Sedlak for their collaborative efforts and the access granted to essential data. The practical experiences gained in their fire lab have been instrumental in shaping my research.

Lisa and Chiara, we started our PhD together in different research groups and from day one we have always had each other back. Thank you for supporting me while writing this thesis and always having great advice for me. Nieves and Soraia, thank you for being the kind of academic and women I would like to become one day. During my transition to motherhood you help me navigate the difficulties, I will always be in debt for this. You showed me balance between academic pursuits and personal responsibilities.

Thank you to all of my family for their love and kindness over the years. To my mum for her selflessness and encouragement, for guiding me and mostly for being my number one inspiration. Daniel, thank you for being there everyday, everynight, in sickness and in health. Lastly, to my son, Tommy, whose presence added unforeseen challenges in the final stages of my PhD, helping me put everything in prospective.

Contents

Abstract i

List of Figures xvii

List of Tables xix

1 Introduction 1
- 1.1 Motivation and Backgroud . . . 1
  - 1.1.1 The Relay Building Fire . . . 3
- 1.2 Aims and Objectives . . . 6
- 1.3 Thesis Structure . . . 7

2 Mechanical Failure of Non-Combustible Facade Systems in Fire 9
- 2.1 Introduction . . . 9
- 2.2 Mechanical Behaviour of Facade Systems . . . 11
  - 2.2.1 Heat Transfer . . . 12
  - 2.2.2 Material degradation . . . 13
  - 2.2.3 Thermal Expansion . . . 13
  - 2.2.4 Failure Temperature due to Thermal Expansion . . . 14
- 2.3 Support Systems . . . 15
  - 2.3.1 Cladding . . . 15
    - 2.3.1.1 Rails . . . 17
    - 2.3.1.2 Light Steel Frame . . . 18
  - 2.3.2 Curtain Walls . . . 19
- 2.4 Non-combustible Facades Materials . . . 21
  - 2.4.1 Stone and Ceramics . . . 21
  - 2.4.2 Concrete . . . 24
  - 2.4.3 Metals . . . 25
  - 2.4.4 Glass . . . 26
- 2.5 Combustible Facades Materials . . . 28
  - 2.5.1 Concrete Sandwich Panels . . . 29

2.5.2 Metal Sandwich Panels . . . 30
2.6 Comparison of Material Properties . . . 31
2.6.1 Material Failure . . . 32
2.6.2 Thermal Expansion and Element Failure . . . 33
2.7 Conclusions . . . 35

3 Development of Thermal Model for Curtain Wall Systems with Increasing Complexity 37
3.1 Introduction . . . 37
3.2 Curtain Wall Heat Transfer Methodology . . . 38
3.2.1 Curtain Wall Components . . . 38
3.2.2 Heat Transfer Mechanisms for Glass Panels . . . 40
3.2.3 Heat Transfer in Frame chamber . . . 41
3.3 Boundary Conditions . . . 42
3.3.1 Convective Heating . . . 42
3.3.2 Radiative Heating . . . 43
3.3.3 Ambient Cooling . . . 44
3.4 Models with Increasing Complexity . . . 45
3.4.1 Lumped Capacitance - 0D Model . . . 45
3.4.2 Lumped Capacitance Network - 1D Model . . . 46
3.4.3 Finite Element - 2D Model . . . 47
3.4.4 Finite Element - 3D Model . . . 48
3.5 Material Thermal Properties . . . 49
3.6 Model comparison . . . 50
3.7 Conclusions . . . 51

4 Validation and Parameter Sensitivity Study of 2D and 3D Models 53
4.1 Introduction . . . 53
4.2 Experimental Data in Literature . . . 54
4.3 Korean Experiments . . . 57
4.3.1 Comparison with Korean Experiments . . . 58
4.4 Polish Experiments . . . 61
4.4.1 Partition wall . . . 62
4.4.2 Curtain wall . . . 63
4.4.2.1 The Screw Effect . . . 65
4.5 Parametric Study . . . 67
4.6 Conclusions . . . 69

5 Thermal Failure Criteria of Curtain Wall Framing System Exposed to Fire 71
5.1 Introduction . . . 71
5.2 Behaviour of Curtain Wall Support Structure . . . 72
5.3 Results . . . 73

5.3.1 Influence of insulation insert and thermal break . . . 73
5.3.2 Thermally protected Frame . . . 76
5.3.3 Steel Frame . . . 76
5.3.4 Fire scenarios . . . 78
5.4 Discussion . . . 79
5.5 Conclusions . . . 81

6 Mechanical Failure Criteria of Curtain Wall Framing System Exposed to Fire 83
6.1 Introduction . . . 83
6.2 Modelling the Mechanical Response . . . 84
6.2.1 Boundary Conditions . . . 84
6.2.2 Ambient Loading . . . 85
6.2.3 Mechanical Failure . . . 86
6.3 Results and Discussion . . . 88
6.3.1 Mechanical Failure of Mullion . . . 88
6.3.1.1 Aluminium Mullions . . . 88
6.3.1.2 Steel Mullion . . . 89
6.3.1.3 Failure . . . 90
6.3.2 Mechanical Failure of Transom . . . 91
6.3.3 Behaviour of Glass in Fire . . . 92
6.4 Conclusions . . . 93

7 Conclusions 95
7.1 Outcome of presented research . . . 95
7.2 Future Work . . . 97
7.3 Conclusions . . . 98

List of Figures

1.1 Major fires involving a curtain wall facade system. From left to right: One Meridiana Plaza fire in 1991, Philadelphia, USA; Mercantile Credit Building fire in 1991, Basingstoke, UK; Office Building fire in 2011, Bucharest, Romania; Lotus Building fire in 2014, Mumbai, India. 2

1.2 Satellite image of the Relay building and surrounding area. Highlighted in red the flat of fire origin on the 17th floor. Adapted from Google Maps 3

1.3 (a) Photo of Relay fire on 17th and 18th floor. In the red circle the flames from the burning wooden balcony, in the red rectangles flames coming from the glass panels. Adapted from Quadri (2022) (b) Flames under the wood decking of the balcony on the 18th floor. The flames inside the building seem to be extinguished while sections of the balcony are still flaming. Adapted from Lodge and Terry (2022) 4

1.4 Large curtain wall panel falling from the Relay building during the fire. Adapted from Carter (2022). 5

1.5 (a) The flat on 17th and 18th floor after the fire. All glass panels have been destroyed and parts of the metal frame supporting the glass have been consumed. (b) Curtain wall after the fire with visible extensive damage to the glass panels and the aluminium frame. Bowing of the horizontal component of the aluminium frame is indicated by the red arrow. Adapted from London Fire Brigades (2022). 5

2.1 Photo of large panel falling off the 22-storey commercial building Lotus Business Park during the 2014 fire, Mumbai, India. Photo from Hindustan Times with permission. 10

2.2 Heat transfer through a material with high thermal diffusivity (left) and low thermal diffusivity (right). Material with high diffusivity will experience small thermal gradients, while materials with low values will experience large gradients. Figure from Roenner et al. (2019) with permission 12

2.3 Effect of temperature change on a facade element heated from one side considering two idealized cross-sectional temperature conditions – uniform temperature (A-top) and linear thermal gradient (B - top). Diagram of element deformation due to thermal expansion when unrestrained – uniform temperature (A - middle) and linear thermal gradient (B - middle). Diagram of element forces developed when element is fully restrained - uniform temperature (A - bottom) and linear thermal gradient (B - bottom). Figure by Author after Bisby (2016). 14
2.4 Failure of the support structure leading to detachment and fall-out of the cement-board cladding panel during experiments at ITB, Poland by Bonner and Rein (2018). Support structure composed of aluminium rails. 16
2.5 Diagram of vertical railing support system for cladding panels. The rails are connected to the load bearing external wall (primary structure). The cladding connectors will differ depending on the panel material and retrain required. . . . 17
2.6 Facade mock-up after being exposed to a wood crib fire. The facade was cladded with cement boards supported on aluminium vertical rails with mineral-wool cavity insulation. The rails were connected to a load bearing brick wall. Portions of the aluminium rail (marked with a dashed line) were consumed by the flames in sections directly exposed to flames (A) while the external rail buckled (B). 18
2.7 Diagram of a typical curtain wall assembly connected to the main structure concrete slab via metal brackets (A) and independent curtain wall unit including frame elements, glass panel and spandrel panel (B). 19
2.8 Details of typical curtain wall brackets, fixed to the side of the structural slab (A) and fixed to the top of the slab (B). 20
2.9 Properties of stone and ceramic plotted on a logarithmic scale. (A) Thermal expansion coefficient and thermal diffusivity. Materials used for connections are included (steel & epoxy). (B) Failure temperature due to thermal expansion (see Equation 2.4.) Material data from ANSYS (2021). 22
2.10 Details of dowel and pin connection typically used for stone panels. The steel pin is inserted in the pre-drilled holes of the panel. 23
2.11 Properties of unreinforced concrete plotted on a logarithmic scale. (A) Thermal expansion coefficient and thermal diffusivity. Materials used for connectors are included (steel & fibre reinforce polymers.) (B) Failure temperature due to thermal expansion (see Section 2.2.4, Equation 2.4) Material data from ANSYS (2021). . 24
2.12 Concrete panels connected to the main structure: suspended with tension bar (A) and fixed at the bottom with corbel bracket (B). Metal bars and brackets (in yellow) and steel bolts (in red), if affected by heat will deform and lose their load-bearing capacities. 25
2.13 Properties of metals plotted on a logarithmic scale. (A) Thermal expansion coefficient and thermal diffusivity. (B) Failure temperature due to thermal expansion (see Section 2.2.4, Equation 2.4) Material data from ANSYS (2021). 26

2.14 Fracture pattern of common construction glass: float annealed, heat-strengthened and fully tempered. . . . 27
2.15 Properties of glass plotted on a logarithmic scale. (A) Thermal expansion coefficient and thermal diffusivity, material used to frame glass are also included (steel, aluminium & silicone). (B) Failure temperature due to thermal expansion (see Section 2.2.4, Equation 2.4) Material data from ANSYS (2021). . . . 27
2.16 Delamination of steel sandwich panels after a fire test, with rockwool insulation (left) and PIR insulation (right), the PIR insulation has been completely consumed. Image from Pyl et al. (2012). . . . 31
2.17 Maximum service temperature of non-combustible facade materials on logarithmic scale. Data from ANSYS (2021) . . . 33
2.18 Thermal expansion and thermal diffusivity of non-combustible facade materials plotted on logarithmic scale. Data from ANSYS (2021). . . . 34
2.19 Failure temperature due to thermal expansion for fully restrained element with uniform temperature across its cross-section. For description of how the failure temperature is calculated see Section 2.2.4, Equation 2.4. Material data from ANSYS (2021) . . . 35

3.1 Exploded view of a curtain wall facade with glazed panels and supporting frame. 39
3.2 Section through a curtain wall framing system. . . . 39
3.3 Boundary conditions for a facade heated internally (e.g. compartment fire) . . . 42
3.4 Peak heat flux measured against a wall from propane burner fires with varying heat released from Lattimer (2016) . . . 44
3.5 Maximum flame temperature for a given convective heat transfer coefficient for the lumped mass capacitance assumption to be valid for different curtain wall components. . . . 46
3.6 Zero dimensional model schematic. . . . 46
3.7 One dimensional model discretisation schematic. . . . 46
3.8 Two dimensional model discretisation schematic. . . . 47
3.9 Three dimensional model mesh schematic. . . . 49
3.10 Thermal conductivity (left) and specific heat (right) for materials components a curtain wall frame. Thermal property plotted on logarithmic scale. . . . 50

4.1 Emissive power as a function of the pool fire diameter. Experimental data from Ji et al. (2021). . . . 58
4.2 Heat release rate of heptane pool fire calculated from Korean experiment, flame height obtained from Heskestad correlation, and irradiation from pool fire at target location (bottom and top of curtain wall) calculated via Shorki & Beyler method for pool fires. . . . 58

4.3 Temperature of exposed surface of the aluminium frame. Comparison of finite element model predictions and experimental data from Korean experiment. The thermocouple (TC) data from experiments was collected at two height on the frame, shown in the top left corner of the plot. Experimental data error bars include results from three repeats. 59
4.4 Temperature of exposed surface of the glass panel. Comparison of finite element model predictions with experimental data from Korean experiment. The thermocouple (TC) data from experiments was collected at two locations, shown in the top left corner of the plot. Experimental data error bars include results from three repeats. 60
4.5 Cross section of mullion of partition wall (left) and curtain wall (right). Dimensions in mm. Glazing highlighted in blue and thermal break in yellow. Figure adapted from Sędłak et al. (2013) and Sędłak et al. (2021). 61
4.6 Boundary condition for the mullions of the partition wall (left) and curtain wall (centre and right) in the Polish experiments. The curtain wall was tested under a compartment fire and external fire regimen. 62
4.7 Predictions of frame temperature compared to data recorded during the Partition Wall experiment (left). Boundary conditions and position of thermocouples (right). 63
4.8 Frame temperature variation with time. The thermal degradation of the frame is visible on the exposed side (complete degradation assumed at 600°C). Only half of the partition wall frame is shown due to symmetry. 63
4.9 Predictions of temperature of frame in compartment fire (left) and external fire (right) in comparison to experiments. The boundary conditions and thermocouple locations for each scenario are sketched. 64
4.10 Frame temperature distribution after 10, 20 and 30 minutes of heating during the compartment fire exposure. The thermal degradation of the frame is visible on the exposed side (complete degradation assumed at 600°C). The steel screw is not shown. 65
4.11 Predictions of 2D model with steel screw, 2D model with thermal break, and 3D model with screw and thermal break verified against data from Curtain wall experiment for the compartment fire test. Boundary conditions and location of temperature shown on the right. 66
4.12 Resultant heat flux in frame and along the pressure plate (shown in section A-A) for 3D model after 10 and 30 minutes of heating. Heat flux values are simplified as high and low as reporting the actual vaules is superfluous. 66
4.13 Scatter plot of one-at-a-time sensitivity study of material (left) and heat transfer input parameters (right). Results for output function t_{500} (top) and T_{max} (bottom). Material parameters colour coded for components: pink - structural frame, black - thermal break, green - insulation. Heat tranfer parameter colour coded: red - fire side, blue - ambient side. 68

4.14 Sensitivity coefficient for material and heat transfer input parameters. Results for output function t_{500}(above) and T_{max} (below). Sensitivity coefficient plotted in increasing order. 69

5.1 Strenght and stifness reduation for aluminium (left) and carbon steel (right) due to high temperature. From Eurocodes CEN (2002) and CEN (2007) 72

5.2 Section of frame system investigated. Form left to right: aluminium frame, aluminium frame with half of the frame chamber filled up with insulation, aluminium frame with a thermal break as connector element between external and internal sections. Red dashed line indicates heated surface. 73

5.3 Temperature development in aluminium frame, aluminium frame with insulation insert and aluminium frame with polymeric thermal break exposed to a ISO standard fire (left). Section of the frame with temperature location and heated surface (right). 74

5.4 Temperature development and distribution in aluminium frame (left) , aluminium frame with insulation insert (middle) and aluminium frame with polymeric thermal break (right) exposed to a standard fire (ISO). 75

5.5 Temperature distribution after 5 and 10 minutes of heating (left) and linear thermal gradient across structural frame during heating (right). Values reported for a aluminium frame, an aluminium frame with an insulation insert and an aluminium frame with polymeric thermal break exposed to a ISO standard fire. 76

5.6 Temperature development and distribution of aluminium frame (left) and encapsulated aluminium frame (right) exposed to a standard fire (ISO). 77

5.7 Temperature development for stainless steel frame and carbon steel frame exposed to a ISO standard fire. Temperature presented refer to location 1, 2 and 3 shown in sketch. 77

5.8 Temperature development of stainless steel frame (left) and carbon steel frame (right) exposed to a standard fire (ISO). Thermal gradients across the frame after 10 minutes of heating are show in sketches. 78

5.9 Gas temperatures for the considered fire scenarios. Standard fire curve (ISO), external fire curve, short-cool (SC) and log-hot(LH). 79

5.10 Temperature development of aluminum frame exposed to different fires. Temprature presented at three locations, T_1 and T_2 on two opposite sides of the structural frame, and T_3 on the external pressure late. For eah scenario the heated surface is shown in sketch by the red dashed line. 79

5.11 Temperature of pressure plate (left) and structural frame (right) of curtain wall systems with thermal protection and different materials. Location of temperature prediction marked by black dot in sketch. 80

5.12 Temperature distribution after 5 and 10 minutes of heating (left) and linear thermal gradient across structural frame during heating (right). Values reported for a simple aluminium frame, an encapsulated aluminium frame, a stainless steel and a carbon steel frame exposed to a standard fire (ISO). 80

6.1 Elevation of frame system with glass panel dead load G (left) mullion member axial load P (middle) and restrain conditions (right). 86

6.2 Dimension of the rectangular structural frame. 86

6.3 Critical buckling temperature as a function of slenderness ration for aluminium and steel elements. 87

6.4 Thermal strain due to uniform temperature rise, ε_{th}, and curvature due to thermal gradients, ε_{ϕ}, for aluminium, stainless steel and carbon steel mullion exposed to ISO temperature-time curve. 88

6.5 The effect of the spring stiffness on the thermal stress developed in an aluminium mullion framing member. For each spring stiffness the critical buckling temperature is shown as a grey line and the compressive stress due to thermal expansion as a black curve. The strength of the member is degrading as it is heated and is shown as a red curve. 89

6.6 The effect of encapsulation on the strenght (f_y) and stress ()σ_{th}) of the loadbearing mullion exposed to uniform heating following the ISO fire curve. Compared to the exposed frame failure is delayed. 89

6.7 The effect of the spring stiffness on the thermal stress developed in an stainless steel mullion framing member. Critical buckling temperature for the 100 % and 50% spring stiffness is shown as a grey line, for other stiffness values the critical buckling temperature was greater than the temperature experienced by the frame (above 800 ℃). The ultimate tensile strength and the 0.2% proof strength reduce as the frame is heated (red lines). 90

6.8 The effect of the spring stiffness on the thermal stress developed in an carbon steel mullion framing member. Critical buckling temperature for the 100 % and 50% spring stiffness are shown as a grey line, for other stiffness values the critical buckling temperature was grater than the range considered (above 800 ℃). The strength reduces as the frame is heated and the degradation is plotted for S355 and S275 steel. 90

6.9 Failure time (left) and failure temperature (right) for the mullion element in aluminium (AL), stainless steel (SS) and carbon steel (CS). Two failure modes analysed for each case: compression and buckling. 91

6.10 Failure time (left) and failure temperature (right) for the transom element with varying level of restrain (5-100% member stifness). 91

6.11 Midspan deflection due to thermal gradient of transom member. Evolution with temperature (left) and time (right). 92

7.1 Diagram illustrating the complexity levels of the models employed in the chapters of this thesis. 97

List of Tables

2.1 Summary of failure times and modes for different curtain wall assemblies from experiment with free burning wood crib in a compartment [33]. Element highlighted in bold and red is the element that failed first. 21
2.2 Primary material failure in fire of non-combustible facade elements. 32

3.1 Absorptance, transmittance and reflectance values for glass panels from Debuyser et al. (2017) 40
3.2 Calculation of convective heat transfer coefficient for natural convection on vertical plate. 43
3.3 Maximum effective heat transfer coefficient for lumped capacitance assumption to be valid (Bi=0.1) for different curtain wall components. 45
3.4 Comparison of model complexity. 50

4.1 Summary of Experimental data on thermal response of curtain walls components heated by different fire sources. The curtain wall components considered are glazed panels, frame and brackets. 56
4.2 Values of input parameters investigated in the sensitivity study. 67

5.1 Time to thermal degradation of aluminium frame, defined as the time when the cooler section of the frame not directly exposed to the hot temperature (T_2) reaches the melting temperature of aluminium. 75
5.2 Comparison of failure time for all cases. Failure is considered as complete thermal degradation. 81

6.1 Allowable temperature difference ΔT for glass [prEN thstr:2004]. 92

Chapter 1

Introduction

1.1 Motivation and Backgroud

When a fire breaks out in a building, the fire safety strategy in place should guarantee the safe evacuation of everyone in and around the building whilst giving safe access for firefighters to tackle the fire. This not only means preventing the fire and smoke from spreading within the building but also limiting the fire spreading externally between floors and preventing parts of the facade from detaching from the building due to stress and degradation caused by the fire. If a section of the facade was to detach and fall from the building, this would pose a life threat and could obstruct the passage of people and equipment at ground level. In addition, the failure of a large section of the facade can facilitate fire spread and can lead to huge economic losses to the building owners due to time and cost of repair.

Glazed curtain wall facades are particularly at risk of large parts of the facade detaching due to the poor fire performance of the glass panels and the aluminium frame which are the main components of the system. Aluminium expands and softens rapidly when heated, while glass is likely to crack due to thermal gradients or thermal shock.

There have been several fires involving curtain wall facades. In 1991 a fire ignited on 22nd floor of the One Meridian Plaza in Philadelphia, USA, and spread along the facade affecting nine floors. Three fire-fighters lost their life while tackling the fire and economic losses amounted to $325m. The building, a 38-storey office block, had to be demolished after the fire. In the same year a similar building burned in the UK; the Mercantile credit building in Basingstoke, a 14-storey office block enclosed completely in an aluminium frame glazed curtain wall. The fire started on 8th floor and spread up two floors of the building behind the curtain wall. The failure of a number of windows produced a strong ventilated fire. Damage due to fire was estimated at £15.6m.

More recently in Bucharest, Romania, during a fire in an office building a large portion of the

curtain wall facade was damaged. The fire started from inside the top floor plant room and spread outside. Similarly in the 2014 fire at Lotus Business Park in Mumbai, India, the curtain wall facade was destroyed on multiple floors. The fire started on the 21st floor and bulky elements were seen falling from the building.



Figure 1.1: Major fires involving a curtain wall facade system. From left to right: One Meridiana Plaza fire in 1991, Philadelphia, USA; Mercantile Credit Building fire in 1991, Basingstoke, UK; Office Building fire in 2011, Bucharest, Romania; Lotus Building fire in 2014, Mumbai, India.

Reports on these fires, shown in Figure 1.1, only mention whether the glass panels broke and discuss the flame spread behind the curtain wall or through the openings created by broken glass panels. However, when looking at photos we can observe that the metal frame supporting the glass panels has either melted away or deformed substantially. This suggests that the panels may have failed not only due to the heat from the flames but due to pressure from the deformed frame. In addition, extensive displacement of the frame elements, due to loss of stiffness and thermal strain, could cause the facade to bulk outward creating gaps which allowed for the spread of smoke and flame.

Furthermore, although they were not present in these fires, there is a possibility that, had fire resistant glass panels been included in a building that experienced such a fire, these panels may not have shattered, but instead remained intact in the frame. In this scenario, the deformation of the frame may have been enough to push out the intact panel, increasing risk to life safety. This could also be the case for other kinds of curtain wall panelling, for instance stone or metal panels.

There are four scenarios where a fire could threaten the facade:

1. A compartment fire developing in a room adjacent to the facade and impinging on the internal surface of the facade.

2. Fire at ground level in proximity of the facade (ex. garbage, vehicle fire) or large fire involving neighbouring structures. Radiative heat from flames could heat up the facade to critical temperatures.

3. Fire spreading externally from the compartment of origin and impinging on the facade above. The flames in this case will heat up the external part of the facade.

4. Where the facade is assembled with combustible components, the facade itself could burn.

In all four scenarios the flames could penetrate the facade from opening and cavities and spread vertically and horizontally. These cavities could be intentional, to allow ventilation, mechanical and electrical ducts, alternatively they could develop due to incorrect detailing, improper installation and maintenance.

1.1.1 The Relay Building Fire

On March 7th, 2022, an incident unfolded at the Relay Building situated near Aldgate East Station in East London. This section presents an analysis of the event, focusing on the fire's impact on the building's facade structure and the consequential observations of falling elements during the course of the fire.

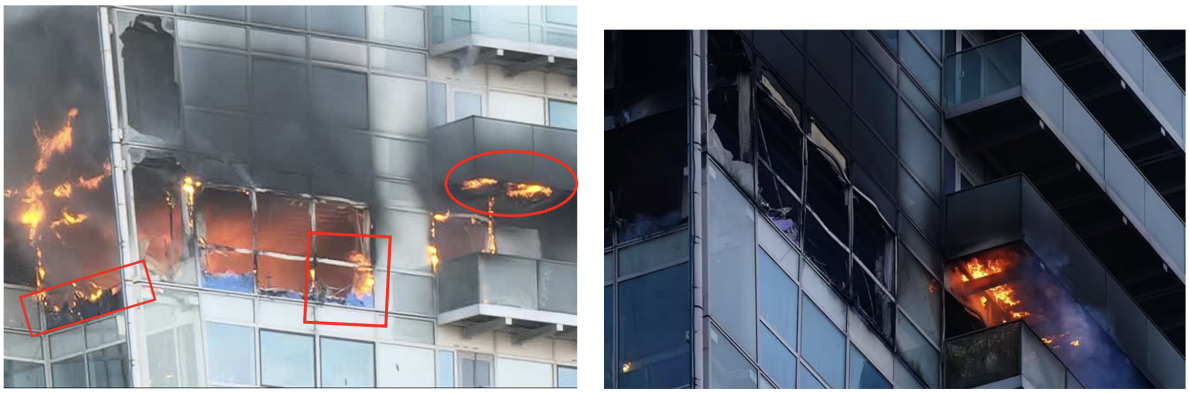
The Relay Building, a prominent 21-floor structure completed in 2014, stands at a height of 79 meters (Figure 1.2). Designed by Broadway Malyan, it serves as a mixed-use establishment, featuring office spaces on the lower levels and residential apartments from the 7th to the 21st floor (CTBUH (2023)). The fire primarily affected two residential flats on the 17th and 18th floors. The blaze originated in a flat on the building's South-East corner, causing substantial damage to the facade and balcony areas. Falling object were a large threat as the Aldgate East tube station exit is located at street level on the South-East corner of the building and in general Aldgate is a bustling business district and hub of high foot traffic.



Figure 1.2: Satellite image of the Relay building and surrounding area. Highlighted in red the flat of fire origin on the 17th floor. Adapted from Google Maps

A curtain wall facade envelops a significant portion of the building's exterior. The structural elements include an aluminium framing system and glass panels. The facade comprises double-glazed units featuring toughened laminate glass, with specific opaque sections utilizing external toughened ceramic panels.

The fire, which commenced at 3:53 pm and lasted approximately three hours until its extinguishment at 7:07 pm, triggered a substantial response involving 20 fire engines and 125 firefighters. The incident resulted in the evacuation of 70 individuals, with two hospitalizations and two on-site treatments due to smoke-related complications. The fire's spread, attributed to glass breakage and ignition within the facade, compromised the balconies, exacerbating the situation (Figures 1.3).



(a) (b)

Figure 1.3: (a) Photo of Relay fire on 17th and 18th floor. In the red circle the flames from the burning wooden balcony, in the red rectangles flames coming from the glass panels. Adapted from Quadri (2022) (b) Flames under the wood decking of the balcony on the 18th floor. The flames inside the building seem to be extinguished while sections of the balcony are still flaming. Adapted from Lodge and Terry (2022)

In Figure 1.3a we can see evidence of flaming elements within the facade (shown in red rectangles), the combustible components in flame could be the polymeric interlayer used in laminated glass panels. From Figure 1.3a we can also see evidence of the flaming of the wood decking on the balcony (shown in red circle). In Figure 1.3b we can observe the wooden balconies burning after the flames have extinguished elsewhere.

During the fire, large objects, including glass panels and metal elements from the building's upper floors, were observed detaching and falling approximately 60 meters to the ground (Figure 1.4). Glass panels shatter at impact with ground sending fragments across the street.

The fire resulted in the complete destruction of a three-room flat on the 17th floor and partial damage to the flat immediately above on the 18th floor. Extensive damage to the facade, including destroyed glass panels and deformed aluminium framing due to heat exposure, was observed (Figures 1.5).

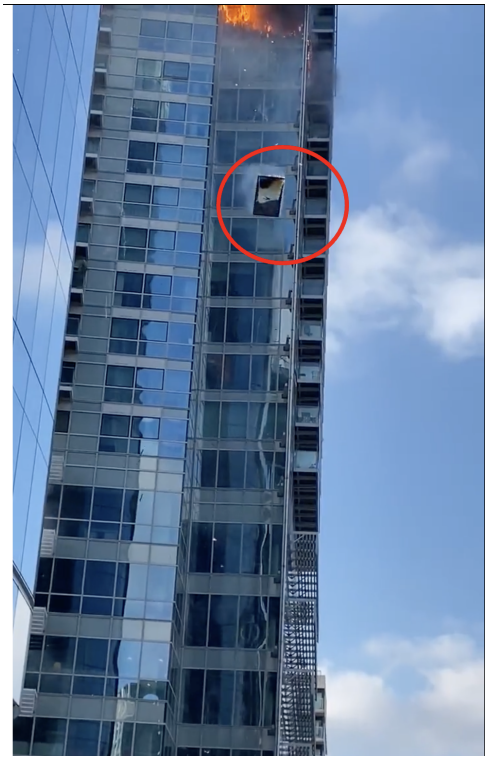
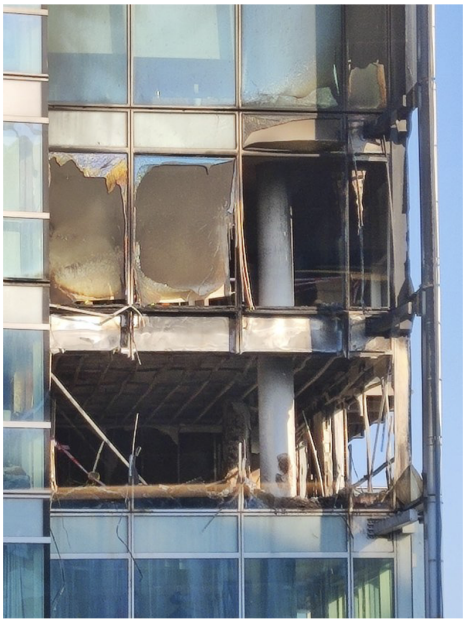


Figure 1.4: Large curtain wall panel falling from the Relay building during the fire. Adapted from Carter (2022).



(a)



(b)

Figure 1.5: (a) The flat on 17th and 18th floor after the fire. All glass panels have been destroyed and parts of the metal frame supporting the glass have been consumed. (b) Curtain wall after the fire with visible extensive damage to the glass panels and the aluminium frame. Bowing of the horizontal component of the aluminium frame is indicated by the red arrow. Adapted from London Fire Brigades (2022).

The fire alarm was only sounded on the ground floor of the building, as at the time of the fire a stay put strategy was in place for floors 12 to 21. However, the fire was not effectively contained in the compartment of fire origin, instead the external fire spread led to compartmentation breach and property damage on multiple floors.

Although there were no casualties this event was a near miss and demonstrated the challenges that failure of tall building facades can pose and was a major motivation in perusing this work.

1.2 Aims and Objectives

The aim of this thesis is to at assess the safety of a curtain wall systems under thermal effects and investigate how glazed curtain walls facades perform in fire. With fire performance/behaviour we refer to the performance of a facade system as a structure; we will investigate the deformation it will undergo, which elements will fail and the modes of failure.

Overall structure performance in a real fire depends on a number of factors: temperature rise and distribution, structural loading, restraint conditions, composite action effects and continuity within the structure. Therefore, we will consider the facade as a system of parts and not as parts in isolation. We will study the fire performance of a curtain wall assembly, to understand what the role of individual elements is and how these interact and work together at elevated temperatures. More specifically, the objectives of the present thesis are to:

- Build a heat transfer model that allows the prediction of thermal gradients within a curtain wall facade support structure (Chapter 3).
- Study the thermal behaviour of glazed curtain wall facade systems and validate the computational models with experimental data (Chapter 4).
- Investigate the thermal response of a curtain wall facade system exposed to standard design fires (Chapter 5).
- Investigate the structural response of a curtain wall assembly to temperatures induced by standard design fires (Chapter 6).
- Identify failure modes and elements that can cause early failure (Chapters 5- 5).
- Identify critical scenarios that could cause failure, with regards to facade assembly including materials, member dimensions and connections (Chapter 6).
- Gather information to guide facade engineers and architects in the design of more resilient facades that perform better when exposed to elevated temperatures.

1.3 Thesis Structure

Chapter 1 presents a brief discussion of the background to the research, and the definition of its aims and objectives.

Chapter 2 presents an extensive review on the fire behaviour of non-combustible facade components and systems. Material properties that influence the fire behaviour of facade components are analysed and compared.

Chapter 3 presents the methodology for modelling heat transfer across a curtain wall system. The model includes radiative and convective heat trasnfer from the fire source and conduction across the metal frame, and the screw connector and the thermal break where present, as well as heat transfer through the frame chamber.

Chapter 4 presents the validation against experimental data of the model prediction. A parameter sensitivity study is carried out to study the effect of various maaterial and heat trasnfer parameters on the models predictions.

Chapter 5 analyses and compared the thermal response of a curtain wall frame system subject to uniform fires utilizing a limiting temperature criterion. The effect of swapping material and adding passive protection on the thermal response is investigated.

Chapter 6 investigated the structural response of a curtain wall frame system subject to staic loading and uniform fire. The simple methodology investigartes failure due to thermal expansion and consideres buckling and compressive failure of the restrained frame elements.

Chapter 7 summarises the main conclusions from the work and outlines possible areas for further work.

Chapter 2

Mechanical Failure of Non-Combustible Facade Systems in Fire

Summary [1]

Fires involving the facade system are a modern and complex problem. Previous studies on fire safety of facades have typically addressed fire spread and flammability, but these are not the only hazards. In this chapter we undertake a review of the state-of-the-art research concerning the mechanical behaviour of facades in fire and their failure modes, and a comparison of mechanical and thermal properties of materials that influence such failures. Mechanical failure can cause portions of the facade to fall out threatening people evacuating and emergency personnel. We describe different support systems, including curtain walls, which are essential to maintaining the integrity of the facade during a fire. Stone, concrete, metal, and glass panels are discussed considering typical connections. The most vulnerable aspects of these systems and their possible failure modes are highlighted, thus allowing a better understanding of the safe design and construction of facades. The present discussion could aid researchers develop future research projects that have the greatest impact for the industry.

2.1 Introduction

Facade systems are not part of the primary structure of buildings and as such are not recognized in prescriptive legislation as critical for life safety during a fire event. However, if a facade element fails mechanically during a fire the consequences can be severe. A facade element that falls from a building can pose a threat to passers-by, people evacuating the building and firefighters attending the fire (Figure 2.1). Damage to the facade or to adjacent buildings could cause considerable economic losses. Additionally, the failure of one or more elements of a facade

[1] This chapter is based on " F. Lugaresi, P. Kotsovinos, P. Lenk, G. Rein (2020) *Review of the Mechanical Failure of Non-Combustible Facade Systems in Fire* , **Construction and Building Materials** 361."

could enhance the fire ventilation rate and facilitate fire growth. If flames and smoke exit the compartment they can impinge upon the facade of the building and damage external elements. In the most unfavourable of events the fire could then spread to the upper floor, breaching compartmentation, an essential layer of protection in tall buildings.



Figure 2.1: Photo of large panel falling off the 22-storey commercial building Lotus Business Park during the 2014 fire, Mumbai, India. Photo from Hindustan Times with permission.

Reviews on the topic of facades and fire have mainly addressed fire testing methods, building guidance, and the flammability of facades (Nguyen et al. (2016); Peng et al. (2013); White and Delichatsios (2015); Bonner and Rein (2018); Soja et al. (2022); Yuen et al. (2021)). Much attention has been directed to the study of combustible components due to the increasing number of fires involving flammable facades (Bonner and Rein (2018)). Although fire spread along the facade is a modern and dramatic issue, it is not the only fire risk for facade systems. Facade systems are at risk of mechanical failure when involved in fires, especially if their support structure is exposed to the flames. For non-combustible facades mechanical failure can potentially pose a greater threat compared to fire spread over the facade, and for facade systems with heavy components (e.g., glass, stone) the consequences of mechanical failure can be dramatic.

In this Chapter we undertake a state-of-the-art review of the literature regarding the mechanical behaviour of non-combustible components of facades systems and their failure modes in fire. A cohesive guidance is lacking in current literature. This work does not focus on the problem of flammability therefore aspects regarding fire spread and flammability of facades will only be considered in relation to their influence on the mechanical behaviour of facade systems. This review highlights non-combustible elements of facade systems that are vulnerable and illustrates possible failure behaviour when these are exposed to a fire, allowing a better understanding of the design and construction of fire-resistant facades. Knowledge gaps are also discussed to aid researchers identify and develop projects that can have the greatest impact for the industry.

This chapter is divided as follows. Section 2.2 discusses the principles of mechanical behaviour at high temperature that can lead to mechanical failure and the main parameters that define material response. In Section 2.3 different facade support systems are described and their vulnerability to fire is discussed. Non-combustible facade materials are considered in Section 2.4, focusing on natural stone and ceramics, concrete, metals, and glass. The fire characteristics of flammable materials is briefly discussed in Section 2.5. In Section **??**, the fire performance of different materials is discussed by comparing material properties in relation with functional performance.

2.2 Mechanical Behaviour of Facade Systems

The terms mechanical behaviour and structural behaviour both refer to induced deformations, stresses, and strains on a solid body. However, it is convenient to distinguish between the two terms. When we use the term mechanical behaviour, we are dealing with a system made up of small connected elements, whereas when dealing with load-bearing structures with bulky elements (e.g., buildings frame, skeleton) we are in the structural behaviour domain. In this chapter, we use the term mechanical behaviour as most facades are made of small individual components and are not part of the primary structural system that aims to ensure the stability of a building.

During a fire, the mechanical behaviour of a facade system depends on the interactions between the different elements, as well as the loads and restraint conditions of these elements. Therefore, the whole facade assembly, including support structure, fixings, connections, and openings, needs to be considered to accurately predict fire behaviour. Researchers and industry experts agree on this approach (Bonner and Rein (2018), Colwell and Baker (2013)) but despite this a very limited number of studies consider the whole assembly. In this thesis, we aim to discuss the behaviour of a facade element within the context of the assembly, and consequently point out vulnerable elements and failure mechanisms for different types of facades. There are instances where this is not possible, and we can only address the mechanical behaviour of an element in isolation from the assembly due to the current lack of knowledge. The behaviour of an isolated element can help in understanding the assembly behaviour but cannot necessarily be taken on its own as a proxy of the system behaviour.

Fire safety engineers often calculate the fire resistance of an assembly by testing only the load-supporting elements (Harmathy (1965) rules no. 9 and 10). This approximation is possible because some assemblies have simple load paths and well-defined deflection shapes in the event of a fire. Facade systems have multiple layers, complex load paths and restrain conditions, therefore predicting their deformation pattern is not straight for-ward and will depend on the direction of the heating (e.g., from the external side or from the internal side), interaction between different layers and materials.

When heated, the elements of a system will undergo material degradation and simultaneously will try to expand (or in some cases shrink) due to thermal dilation. Here we will define these mechanisms and describe how they can lead to mechanical failure in a fire scenario.

2.2.1 Heat Transfer

When discussing the transient transfer of heat across an element, we primary consider the material's thermal diffusivity, α, as discussed in Roenner et al. (2019). The thermal diffusivity (Eq. 2.1) relates to the rate of heat transfer by conduction, the higher the diffusivity, the faster the heat transfer across the material.

$$\alpha = \frac{k}{\rho c} \tag{2.1}$$

where, k is the thermal conductivity, ρ the density, and c the specific heat of a material.

Materials with low diffusivity experience high surface temperatures as the heat cannot travel easily to deeper sections of the thickness (Fig. 2.2). For flammable materials, a high surface temperature facilitates ignition. While non-combustible materials with low diffusivity tend to develop large thermal gradients that might be detrimental to the stability of the systems.

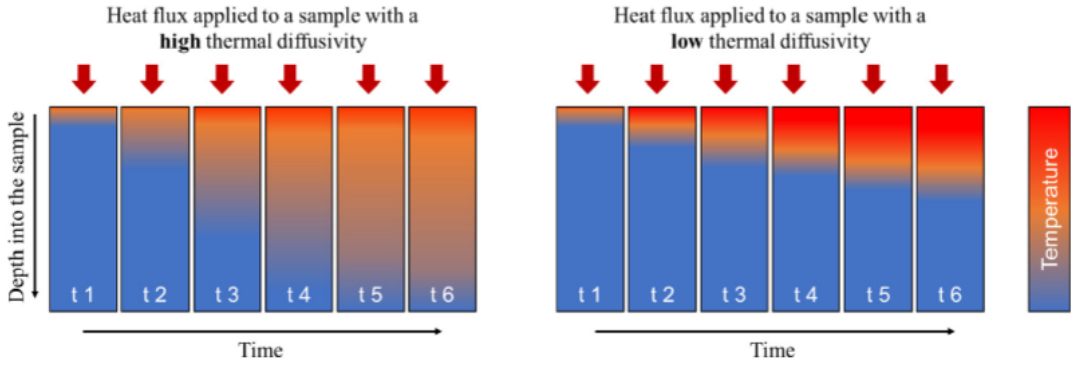


Figure 2.2: Heat transfer through a material with high thermal diffusivity (left) and low thermal diffusivity (right). Material with high diffusivity will experience small thermal gradients, while materials with low values will experience large gradients. Figure from Roenner et al. (2019) with permission

2.2.2 Material degradation

When heated, all materials will generally experience degradation of their mechanical properties due to changes in the microstructure and weakening of the chemical bonds between atoms (Callister and Rethwisch (2018)). Materials such as metal, glass, and thermoplastic polymers will eventually melt. Wood products and thermosetting polymers will char and turn into ash. Concrete and stones can experience spalling, while clay-based products will only degrade at very high temperatures.

Small increases in temperature can affect the mechanical properties and can sometimes lead to mechanical failure. The properties mostly affected by heat are strength (e.g., yield strength, σ_y, compressive strength, σ_c) and stiffness (Young's modulus, E). When an element loses its strength, its capacity to sustain a load will decrease and eventually reach a point where the material will fail due to overload (strength $<$ stress). A decrease in stiffness will allow greater inelastic deformations to develop which may lead to failure by buckling or accelerated creep. When thermal gradients develop the element will experience localized material degradation causing the neutral axis to shift.

The decrease in material properties is partly reversible when the material returns to ambient temperatures following the fire. Knowledge of the residual strength is essential for the evaluation of the stability of the system after the fire. Material degradation will not be discussed in detail, but its influence on mechanical failure will be considered in the following sections.

2.2.3 Thermal Expansion

To understand the mechanical behaviour of facade elements we need to consider how the material will heat up and how it will behave due to the thermal strains developed. While the rate of heat transfer across a material is defined by its thermal diffusivity α, the degree of expansion is captured by the linear thermal expansion coefficient β. The larger the value of β the greater the thermal strains, ε_T, caused by a change in temperature, ΔT (Eq. 2.2). Usmani et al. (2001) demonstrated that once thermal strains develop, they can either lead to deformations if the element is unrestrained (i.e., free to expand) or can lead to forces developing within the element if restrained.

$$\varepsilon = \beta \Delta T \tag{2.2}$$

For an element heated on one side, two idealized cross sectional temperature changes are sketched in Figure 2.3: uniform temperature (Figure 2.3A) and linear thermal gradient (Figure 2.3B). The former is representative of a material with an infinitely large thermal diffusivity value, the latter a material with a low thermal diffusivity. For the scenario where a uniform temperature develops across the cross-section (Figure 2.3A), if the element is unrestrained the whole cross-section will expand, and the element will elongate mainly in the longitudinal direction. If

restrained, compression forces will develop within the element and once the stresses exceed the strength capacity the element will fail (e.g., crush or buckle). When large thermal gradients develop within an element (Figure 2.3B) the element will experience differential thermal strains ($\beta\Delta T_1 < \beta\Delta T_2$). If unrestrained, the element will bend towards the heated side, a mechanism referred to as thermal bowing. Thermal bowing can lead to rupturing of brittle panels or buckling failure in compression elements. If restrained, bending moments will develop within the element and might induce a flexural failure.

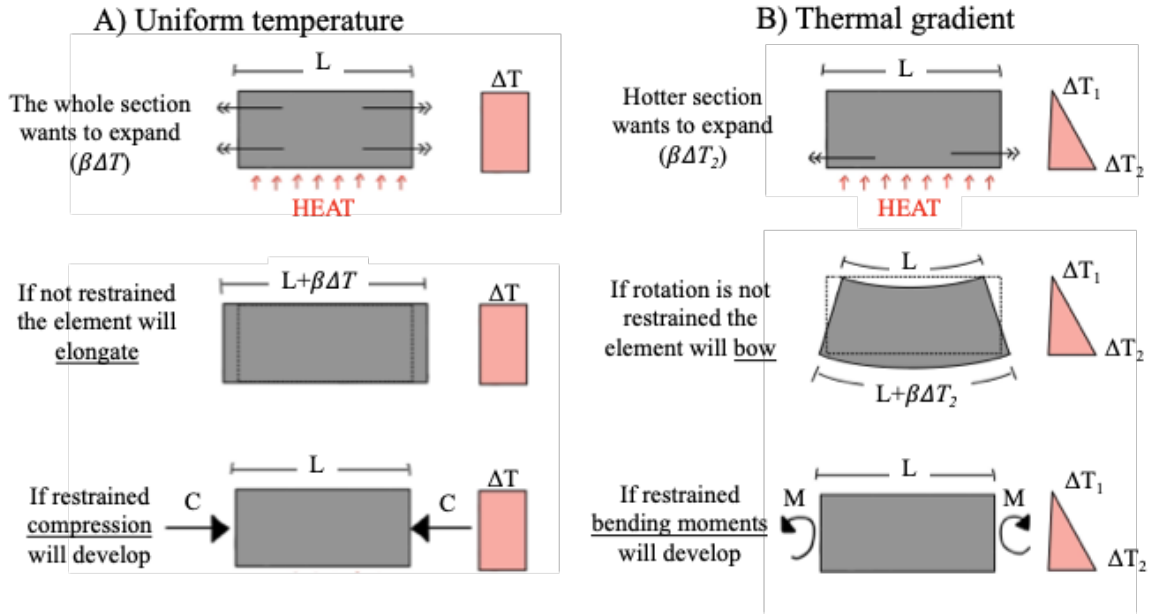


Figure 2.3: Effect of temperature change on a facade element heated from one side considering two idealized cross-sectional temperature conditions – uniform temperature (A- top) and linear thermal gradient (B - top). Diagram of element deformation due to thermal expansion when unrestrained – uniform temperature (A - middle) and linear thermal gradient (B - middle). Diagram of element forces developed when element is fully restrained - uniform temperature (A - bottom) and linear thermal gradient (B - bottom). Figure by Author after Bisby (2016).

2.2.4 Failure Temperature due to Thermal Expansion

For a fully restrained element with uniform temperature, which corresponds to the scenario in Figure 2.3A-bottom, we can calculate a failure temperature due to thermal expansion. In this scenario, thermal strains ε_T would lead to thermal stresses σ_T within the element that can be easily calculated with Equation 2.3, if the Young's Modulus, E, is known.

$$\sigma_T = E\varepsilon_T = E\beta\Delta T \tag{2.3}$$

By rearranging Equation 2.3, the failure temperature, ΔT_f, can be defined as the change in temperature from the ambient temperature which leads to stresses that are equal to the compressive strength σ_c of the material (Equation. 2.4).

$$\Delta T_f = \frac{\sigma_c}{E\beta} \tag{2.4}$$

In Sections 2.4 and 2.5 , we will utilize the failure temperature due to thermal expansion, ΔT_f, to compare the fire behaviour of different materials. Considering that most facade elements are thin and will therefore heat up uniformly, this has been chosen as a simple and realistic criteria of failure due to thermal loading.

The main limitations of the failure temperature ΔT_f are:

- *Considers the behaviour of an isolated element* - The thermal expansion of a panel, or of any other element within the facade assembly, can lead to deformations and stresses in adjacent and connected elements. For example, the elongation of a panel will generate stresses within the restrains holding that panel into place. Analogously, any deformations in the substructure will lead to deformation and stresses in the supported panels. The failure temperature defined here does not consider these interactions.

- *Elements within the facade are never fully restrained* - Tolerance gaps due to building movements are always included when designing facades, this means that a certain amount of movement can occur without stresses developing within the system. By assuming that the element is fully restrained we are calculating a conservative failure temperature.

- *Calculated utilizing ambient material properties* - The young's modulus and the compressive strength are temperature-dependant. However, for some materials this reduction is not well defined (material properties at high temperature can cover large ranges and vary from one test to another) therefore ambient values are used. This assumption is appropriate when both mechanical properties reduce at a similar rate, for example for steel, aluminium, and glass.

2.3 Support Systems

Facade systems differ from typical primary structural systems in materials, loading and construction methods. In this section we will discuss the most common facades – cladding and curtain wall – and the fire performance of their support systems.

2.3.1 Cladding

We define cladding as a non-loadbearing external skin that covers the underlying external wall. The underlying solid load-bearing walls are typically made of reinforced concrete or brickwork. Reinforced concrete walls are widely used in medium-rise and high-rise buildings and are subjected to both axial loads and out-of-plane. Brick walls are only used in low-rise buildings as they are weak in tension and cannot resist out-of-plane loads originating from wind. Concrete and brick walls are usually part of the main structure and will not be discussed in this thesis.

We will instead discuss the connectors and supports that are attached to such walls and are part of the facade system.

Often there will be an open cavity between the wall and the cladding to allow ventilation and improved moisture control. When a cavity is present the fire can be intensified due to the chimney effect which draws flames upwards and the re-radiation from the cavity walls, this mechnism was studied by Khoo Sheng Yeong (2023), Livkiss et al. (2018) and Sharma and Mishra (2021). If flames penetrate in the cavity, they can impinge directly on the support structure and the high heat fluxes typical of an small enclosed space can rapidly lead to a failure of the supports. In a series of experiments by Imperial College London and Instytut Techniki Budowlanej (ITB) and analysed in the thesis by Bonner (2020), cavity flames consumed the fixings of a large non-combustible panel which detached and reached the ground as one piece, disintegrating with the impact (Figure 2.4).

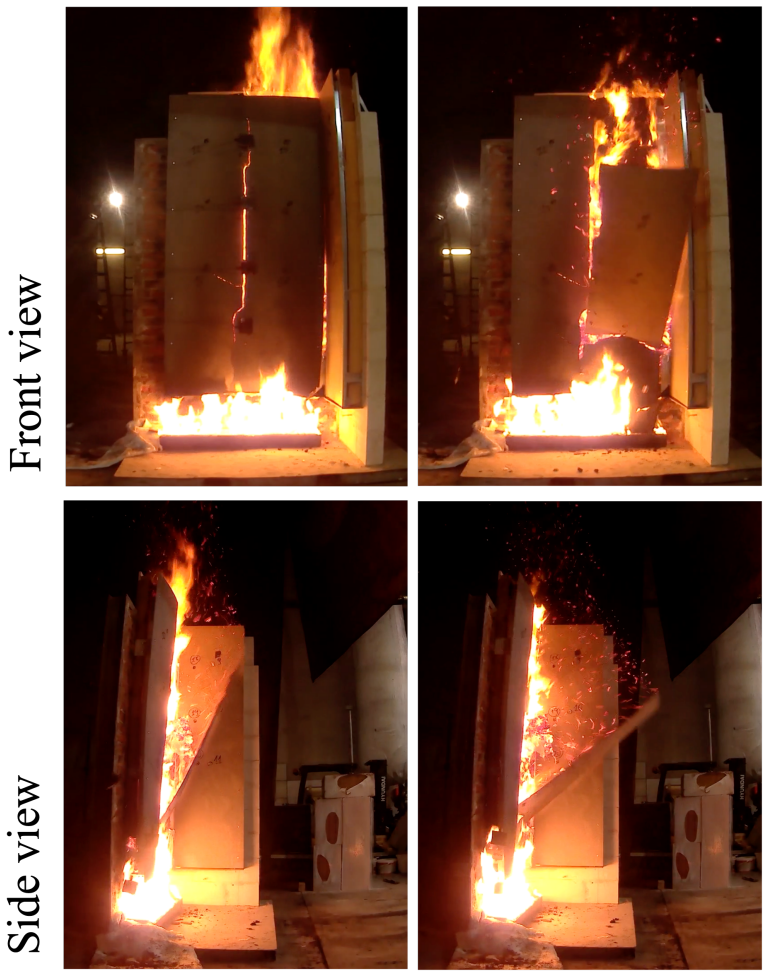


Figure 2.4: Failure of the support structure leading to detachment and fall-out of the cement-board cladding panel during experiments at ITB, Poland by Bonner and Rein (2018). Support structure composed of aluminium rails.

2.3.1.1 Rails

Cladding panels can be supported on metal railings (Figure 2.5) attached to the external walls of the main structure, these elements can be horizontal, vertical or both. They carry the load of the cladding to the load-bearing structure and form a cavity where insulation or other protective layers can be placed. Metal railings when heated will experience rapid degradation in material properties and will expand, this coupled with the eccentric loading of the cladding panels might induce buckling of the element. As these longitudinal elements expand, they will apply stresses on the fixing that might fail in shear or due to pull-out of the fasteners and could result in fall-out of the panels. Deformation of the railings might result in breakage of the cladding panels. To the knowledge of the authors there is no work in the literature intentionally investigating the fire behaviour of metal railings used in facade constructions.

Particularly of concern are aluminium railings as they have been seen to rapidly deteriorate and burn away in fire scenarios. During the fire at Knowsley Heights, Liverpool, in 1991 the aluminium support rails melted causing panels to fall to the ground, reported in BRE (1992). In a recent experimental programme by Bonner et al. (2020) sections of the rails engulfed by flames melted away (Fig. 2.6A) while buckling was observed in the aluminium rails that did not experience direct flame impingement (Fig. 2.6B).

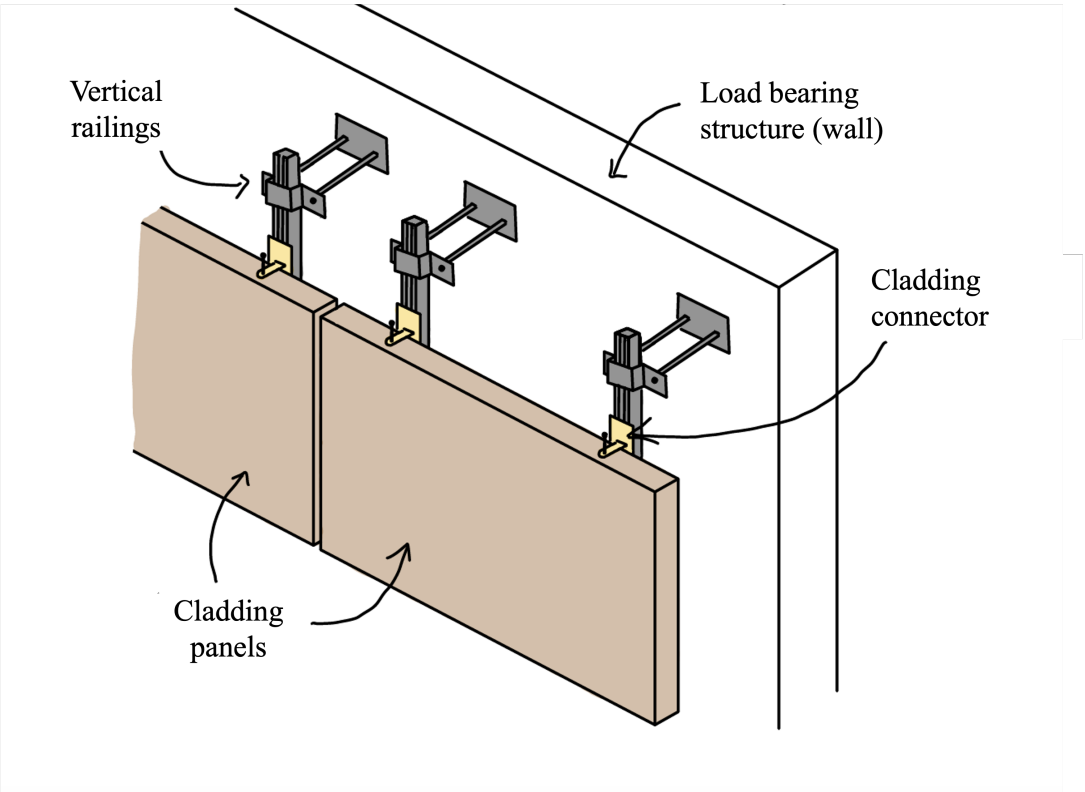


Figure 2.5: Diagram of vertical railing support system for cladding panels. The rails are connected to the load bearing external wall (primary structure). The cladding connectors will differ depending on the panel material and retrain required.

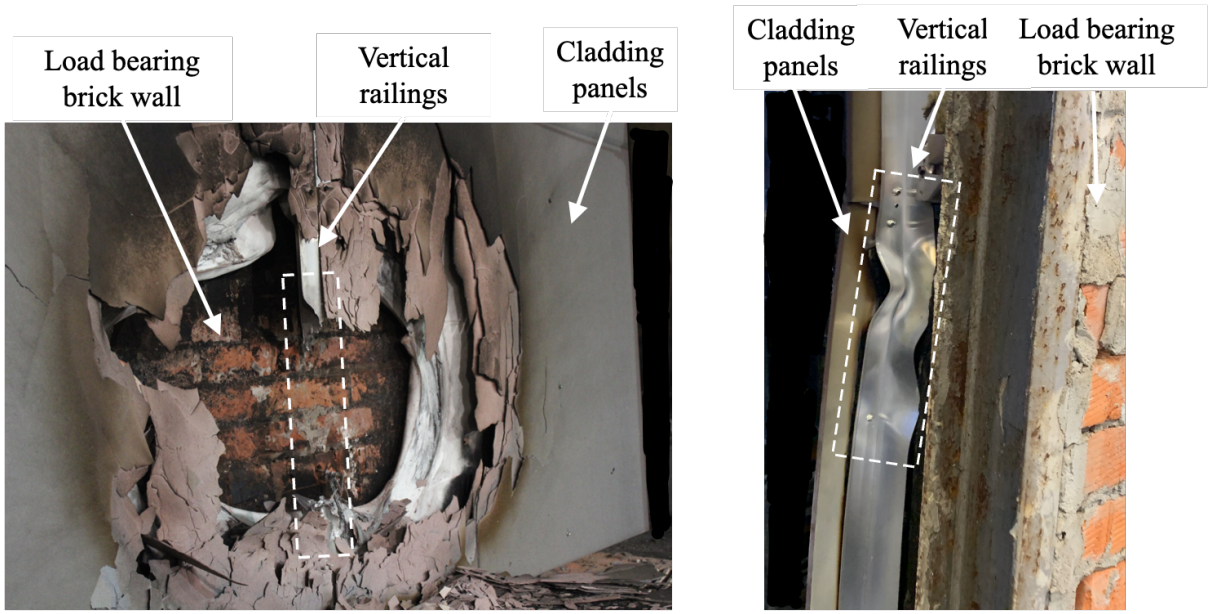


Figure 2.6: Facade mock-up after being exposed to a wood crib fire. The facade was cladded with cement boards supported on aluminium vertical rails with mineral-wool cavity insulation. The rails were connected to a load bearing brick wall. Portions of the aluminium rail (marked with a dashed line) were consumed by the flames in sections directly exposed to flames (A) while the external rail buckled (B).

Alternatively, metal connections are used to fix the facade panels directly to the main structural walls. Connections are usually fixed with steel bolts and screws, but adhesive bonded connections are also used. Kinowski et al. (2017) found that cladding panels fixed with adhesives are generally weaker than mechanically fixed panels and can fail early causing entire panels to fall off. Shear and tension resistance of bonded joints will decrease substantially when heated to temperature above 25 °C and have been discussed by Pasternak and Ciupack (2014). Therefore, in a fire scenario it is sensible to assume that an adhesive bond will fail very rapidly.

2.3.1.2 Light Steel Frame

In some cases, a facade system can be supported on a light steel frame sometimes referred to as Steel Framing System (SFS) which is separate from the main structure and structurally independent. These framing systems are assembled with cold-rolled C and U-shaped studs. Cold-formed steel is more susceptible to local buckling and loses strength more rapidly than hot-rolled steel when exposed to increasing temperatures (Kolarkar (2011)). These frame systems perform better in fire when the insulation is positioned externally to the frame, as cavity insulation leads to higher thermal gradients across the frame thickness and consequently to thermal bowing as discussed by Gunalan and Mahendran (2013b), Gunalan and Mahendran (2013a), Gunalan and Mahendran (2014), Keerthan and Mahendran (2012). Magnified thermal bowing due to eccentric loading can also be an issue and lead to failure of the system as shown in Gunalan and Mahendran (2013b). Analytical tools have been developed to aid designer in the performance-

based design of similar systems for fire resistance, where failure is defined as a critical hot flange temperature for a certain load ratio, presented in Gunalan et al. (2013) and Shahbazian and Wang (2014).

2.3.2 Curtain Walls

Curtain walls are lightweight, and non-loadbearing external walls. These systems are largely adopted in high-rise buildings as they can be easily and quickly installed. The main components, as sketched in Figure 2.7 , are glass panels, spandrel panels, metal frames and metal brackets. Independent units are usually hung from the main structure to avoid compression forces and buckling of the frame (Fig. 2.7 & 2.8) Two brackets are used, and each bracket is designed to carry the total weight of the unit for redundancy. Understanding and predicting the fire behaviour of curtain wall facade is difficult due to the complexity of these facade systems (Hu et al. (2016)).

Aluminium and steel, used typically for the framing element and the brackets respectively, expands and softens when heated, while glass is likely to crack and shatter due to thermal gradients or thermal shock (O'Connor (2016)). In addition, comparing the thermal diffusivities of the metals we observe that aluminium heats up 22 times faster than steel. By comparing under similar temperature conditions the thermal expansion coefficients, we observe that aluminium expands 1.6 times more than steel. Where the two metals are interacting, the difference in expansion and heating rates could lead to high stresses.

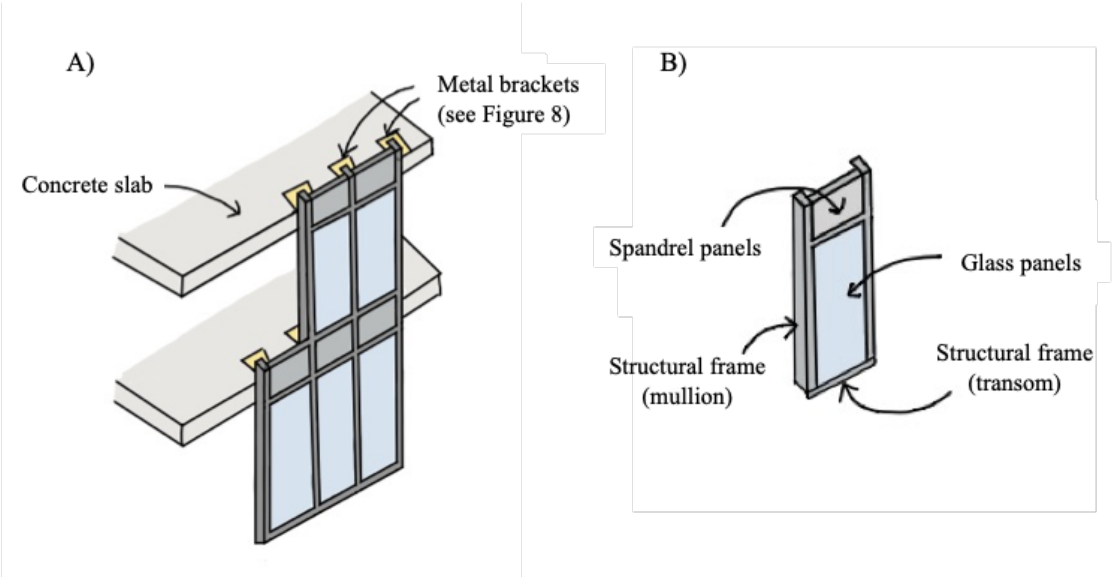


Figure 2.7: Diagram of a typical curtain wall assembly connected to the main structure concrete slab via metal brackets (A) and independent curtain wall unit including frame elements, glass panel and spandrel panel (B).

The fire behaviour of a curtain wall facade system could be analysed by means of laboratory experiments or computational stimulations (e.g. finite element methods). A combination of both would be the most comprehensive.

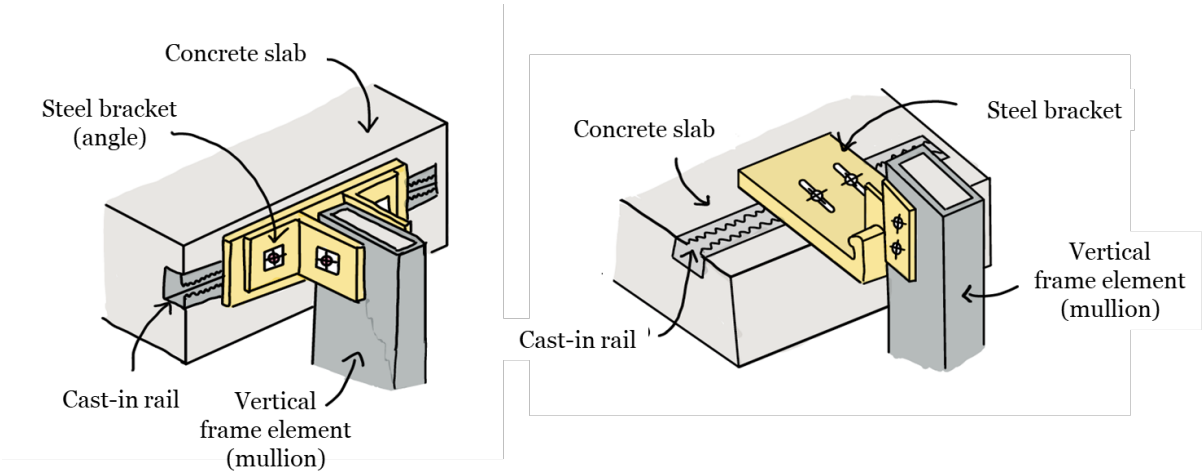


Figure 2.8: Details of typical curtain wall brackets, fixed to the side of the structural slab (A) and fixed to the top of the slab (B).

During a fire, the framing elements will experience large displacements due to non-uniform temperature loading. For example, in a compartment fire the facade would be heated on the internal face while being cooled on the external side by outdoor air, causing the frame to bulk inwards. The deformation of the frame could cause the glass panels to either shatter due to localized stresses or to fall out due to loss of restraint. The latter can be very dangerous as the panels can falls off as one piece. This phenomenon has been reported during a large-scale experiment by Srivastava et al. (2020) and in a recent fire in central London reported in Lugaresi and Rein (2022). Similarly, if the frame keeping the glass panel in position degrades the glass could fall-out. External or internal heating could lead to different failure mechanisms, therefore both fire scenarios should be explored.

Frequently the frame elements are composed of an outer and inner aluminium profile connected by a polymer section (usually made of polyamide) referred to as thermal break. Thermal breaks are insertions designed to create some resistance against the transfer of heat across the aluminium profiles. These small elements must be considered in a fire scenario as they will degrade at lower temperatures than the otherwise aluminium elements, accelerating failure. The influence of thermal breaks on the heating of a typical curtain wall frame was analysed and found to increase the thermal gradient within the aluminium frame (Lugaresi et al. (2021)) while its influence on failure was investigated in the context of window frames by Koohkan et al. (2021).

During a large-scale experimental programme, 19 experiments were conducted to identify the extent of damage in a scenario where fire spreads either internally or externally along a glazed facade (LPC (1999) & Morris and Jackman (2003)). The tests were conducted on a full-scale

curtain wall assembly attached to a two-storey building. The curtain wall was assembled with glass panels alternated to metal spandrel panels at floor level. To identify the performance of the different elements, three tests were run isolating one element at a time (brackets, frame, or panels) by using fire resistant substitutes for the other elements. Fire-stopping was appropriately installed in all three tests. From the tests, summarized in Table 2.1, the authors concluded that standard elements fail very rapidly, allowing flames to spread externally along the facade.

Table 2.1: Summary of failure times and modes for different curtain wall assemblies from experiment with free burning wood crib in a compartment [33]. Element highlighted in bold and red is the element that failed first.

Brackets	Frame	Panels	Failure Time (min)	Failure mode
aluminium (650 °C)	mild steel	calcium silicate	28	pull through of pin connection between bracket and mullion.
mild steel	aluminium (700 °C)	calcium silicate	24	consumption of framework and fall-out of panel.
aluminium	aluminium	glass (275 °C)	13	breakage of glass spandrel panel.

2.4 Non-combustible Facades Materials

2.4.1 Stone and Ceramics

Natural stone like granite and marble are commonly used for cladding historic, secular, and public buildings, whereas bricks and terracotta are used for their warm colours and optimal insulative properties. In general stone and ceramics have a low thermal diffusivity and low thermal expansion coefficients therefore are considered to perform well in fire, however they are brittle and can experience thermal induced fracture or spalling.

In Figure 2.9 the properties related to the fire behaviour of common stone and ceramic cladding materials are presented as a range of values - material properties can vary due to chemical compositions and manufacturing process. The properties plotted in Figure 2.9A are the ambient value of the thermal diffusivity and the thermal expansion coefficient. The failure temperature due to thermal expansion reported in Figure 2.9B is calculated assuming a fully restrained panel with uniform temperature and no material degradation (described in detail in Section 2.2.4.). The values reported in Fig. 2.9A and 2.9B can be used for comparison between materials, however if more detailed material properties are required the specific material composition should be looked up. For temperature dependant thermal and mechanical properties of natural stones refer to the state-of-the-art review by Sciarretta et al. (2021).

Looking at Figure 2.9A we observe that marbles and granites heat up quicker than other stone and ceramics due to their higher thermal diffusivity, and granites also expand at a faster rate.

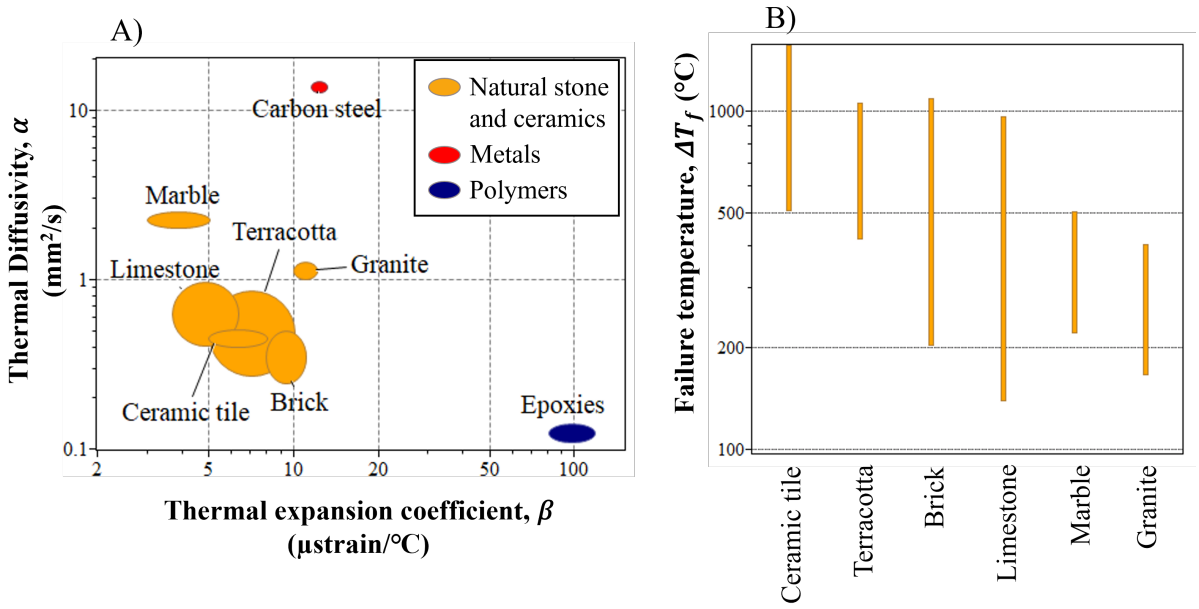


Figure 2.9: Properties of stone and ceramic plotted on a logarithmic scale. (A) Thermal expansion coefficient and thermal diffusivity. Materials used for connections are included (steel & epoxy). (B) Failure temperature due to thermal expansion (see Equation 2.4.) Material data from ANSYS (2021).

Comparing the failure temperature in Figure 2.9B, we can conclude that ceramic tiles and terracotta are the most inert materials, while natural stone are more at risk of failure in restrained conditions, especially granite and marble panels. Due to their low thermal diffusivity, these materials will experience a very non-uniform temperature across their thickness and therefore bowing and flexural failure will be critical. The differential thermal expansion between the panel and other materials in contact could cause the panels to break (Chin (2000)). An example is epoxy used to seal cracks, join pieces of stones or to attach connections to the panels - which expands 4 to 10 times more than stone materials as shown in Figure 2.9A. Likewise, embedded metals (e.g., steel pin or wire mesh) when heated could expand and apply pressure to the stone panel.

For natural stone, terracotta and brick cladding, the connectors and support structure (rails) are the vulnerable elements, however to the knowledge of the author no work has been carried out investigating the fire behaviour of these elements. Stone cladding panels are usually quite thin (approx. 30mm) due to the heavy weight of these materials and are fastened to the support structure using either dowels, screw anchors, profiled webs, clips, or adhesives. Dowel connections are the most common (Fig. 2.10), where the stone is fixed using steel pins that are inserted into pre-drilled holes – dowel holes. These connections are weak when loaded out of plane (e.g., wind loads) as discussed by Huang et al. (2020). Failure of the dowel connection is either due to shear failure of the steel pin and the stone, or due to spalling of a section of the stone around the dowel hole. Both mechanisms are expected to be accelerated at higher temperatures, due to

the material degradation of both the steel pin and the stone panel.

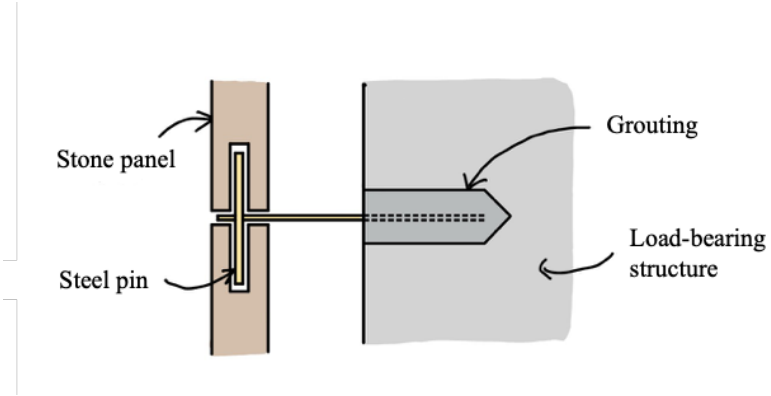


Figure 2.10: Details of dowel and pin connection typically used for stone panels. The steel pin is inserted in the pre-drilled holes of the panel.

The effect of fire on limestones, sandstones, granites and marbles has been tested and analysed by Sippel et al. (2007). For sandstones the generation of cracks at high temperatures is related to shrinkage of clay minerals due to the loss of structural waters. In limestones and sandstones, mineral transformation was also observed after testing. At room temperature, due to absorption of water vapour from the air, the stones experience important volume increase which leads to the disintegration of sandstone and severe scaling of limestone a few days after the heat shock. These mechanisms are discussed by Hajpál and Török (2004) and Sippel et al. (2007).

When a facade survives a fire, it is important to be able to understand and predict the residual degradation – irreversible mineral and chemical changes - as this could lead to failure after the fire event is over. The difficulty here is for the engineer to estimate the amount of damage sustained by the panel. Previous experimental work can help define the heat damaged experienced by granites (Pires et al. (2014)) and marbles (Zeisig et al. (2002) & Siegesmund et al. (2008)). Non-destructive testing techniques could also be utilized to measure post-fire properties in-situ.

Granites were observed by Zeisig et al. (2002)to change colour and experienced a reduction in both their Young's modulus and their flexural strength, up to 30% and 20% reduction from the pre-heating value respectively. In a series of experiments on marbles (Zeisig et al. (2002) & Siegesmund et al. (2008)) the authors observed that the residual strain after cooling-heating cycles was found to increase significantly where water was present. This should be considered when applying water for fire-fighting activities. Bowing due to thermal gradients was also observed and linked to a decrease of mechanical properties (Siegesmund et al. (2008). When the bowing was substantial, cracks were observed at the dowel. Available work investigates physical weathering (night-day cycles and rain) therefore the damage caused by fire, a quick event with rapidly changing environment, will be different and needs to be investigated. Yet, the lessons learnt can be useful in understating the type of damage that a temperature change can cause.

2.4.2 Concrete

Concrete is durable, easy to work and has good insulative properties, therefore its often used to produce facade elements, especially when original forms and shapes are required. Like stone and ceramics, concrete has a low thermal diffusivity and relatively low thermal expansion coefficient (see 2.11A) and therefore has a good resistance to heat. How-ever, the failure temperatures reported in Figure 2.11B for a perfectly restrained uniformly heated element are very low (100-200℃) due to the low compressive strength of unrein-forced concrete. High-Performance Concrete (HPC) has a higher compressive strength and therefore a higher failure temperature, however it can experience enhanced local cracking and explosive spalling. The failure temperature here is calculated ignoring material degradation and heat induced spalling.

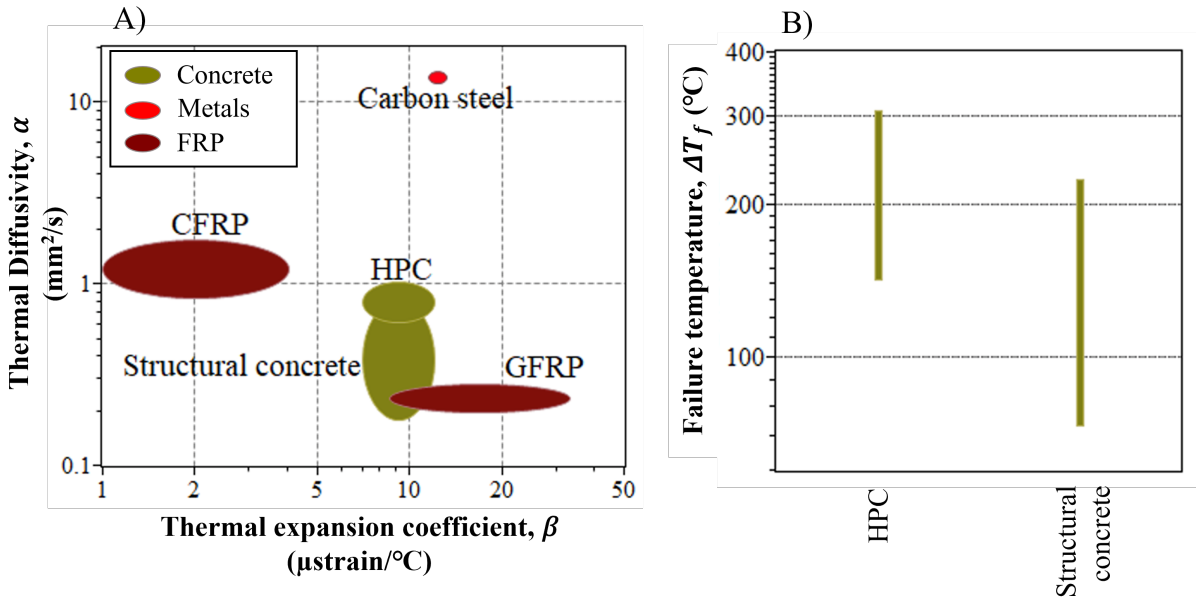


Figure 2.11: Properties of unreinforced concrete plotted on a logarithmic scale. (A) Thermal expansion coefficient and thermal diffusivity. Materials used for connectors are included (steel & fibre reinforce polymers.) (B) Failure temperature due to thermal expansion (see Section 2.2.4, Equation 2.4) Material data from ANSYS (2021).

Concrete can be reinforced with steel bars or fibres. Fibre reinforced concrete has greater impact resistance and tensile strength, and require a smaller thickness compared to concrete reinforced with steel; this is because textiles are not corrosive, and therefore there is no need to provide the appropriate cover which is the thickness driver in reinforced concrete construction. However, the strength and stiffness properties of fibre reinforced concrete were found to severely deteriorated at moderately low temperature ranges, as heat leads to rapid degradation in the bond between fibres and concrete (Nguyen et al. (2020)).

Concrete can be precast in monolithic panels that are supported on the main structure to create a non-load-bearing facade (supported) or can be stacked on top of each other to form a load-bearing facade (free-standing). Non-load-bearing panels are connected to the support structure

by cast-in or bolted connectors, made of reinforced concrete, steel or fibre-reinforced polymers (Sorensen et al. (2022)). If the connector is fixed to the top of the panel (tension bar in Fig. 2.12A) the concrete is under tension, whilst if the bracket is fixed to the bottom, the panel is in compression (corbel bracket in Fig. 2.12B). Usually supports are positioned at the bottom of the panel since concrete is better in compression. Restrains for out-of-plain load are provided (spacer bolt in Fig. 2.12A). Connectors, especially if metal and polymeric, are sensitive to heat, and if they fail then the whole concrete panel might detach and fall. Thermally induced spalling of concrete and the high temperature behaviour of the connectors are the main fire safety issues of concrete facades. While the spalling behaviour of concrete has been studied for years (Khoury (2000), Hertz (2003), Kodur and Banerji (2021)), the fire performance of the connectors is still unexplored.

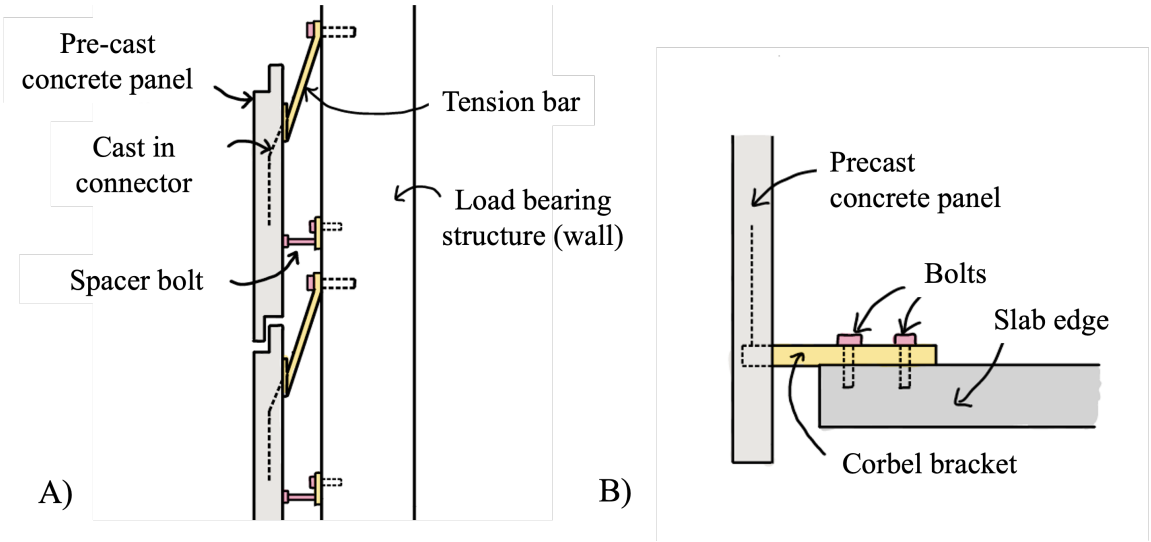


Figure 2.12: Concrete panels connected to the main structure: suspended with tension bar (A) and fixed at the bottom with corbel bracket (B). Metal bars and brackets (in yellow) and steel bolts (in red), if affected by heat will deform and lose their load-bearing capacities.

2.4.3 Metals

Metals can be shaped in various ways and are robust and impermeable to gas and vapour. Single metal panels have been extensively used in facades as they allow high level of pre-fabrication and mass production (Herzog et al. (2004)). Metals heat up rapidly and experience substantial thermal expansion, see Figure 2.13A.

Thermal expansion can lead to large stresses in the fixing and restrains and will be a problem for the stability of metals facades exposed to fire. Comparing the failure temperature due to thermal expansion of a fully restrained element (Fig. 2.13B) we can observe that titanium elements can sustain larger temperature changes, followed by cast iron and stainless steel. Aluminium, zinc, lead alloys and copper are clearly more sensitive to heat as they exhibit high values of both thermal diffusivity and thermal expansion and can reach failure at very low temperatures

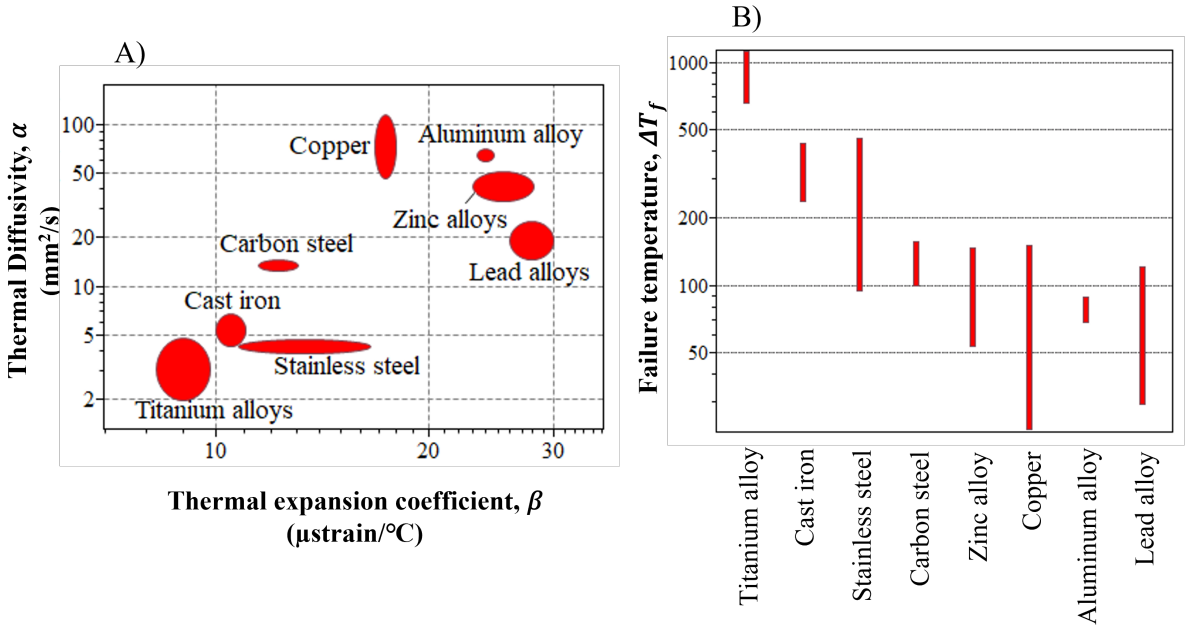


Figure 2.13: Properties of metals plotted on a logarithmic scale. (A) Thermal expansion coefficient and thermal diffusivity. (B) Failure temperature due to thermal expansion (see Section 2.2.4, Equation 2.4) Material data from ANSYS (2021).

(> 100°C). For some metals rapid thermal degradation can also be a problem (e.g., aluminium, zinc alloys).

Cladding panels are usually perforated or solid and approx. 2-3mm thick. They are connected to the facade via screws and bolts but can also be silicone bonded. The detailing of the joints between panels is important and can affect the fire performance – if large open joints are present (e.g., louvres) flames and smoke can easily penetrate through the gaps, whereas airtight joints can contain a fire.

2.4.4 Glass

Glass is a brittle material and is prone to fracture and consequently failure. Soda-lime-silica glass (SLS) can undergo different manufacturing processes. Float Annealed is the cheapest as it does not undergo any specific treatments, it has low bending strength and breaks into shards with sharp edges, see Figure 2.14. Heat-strengthened or heat-treated is 2x stronger than float glass and breaks into shards of smaller size. Fully tempered or toughened glass is 4x stronger than float glass and breaks into small cubes with smooth edged, therefore it is commonly referred to as safety glass (Herzog et al. (2004)).

Borosilicate glass (BS) is only used for specific applications where a fire-resistant design is paramount as its expensive and difficult to manufacture (Bedon et al. (2017)). BS glass has a lower thermal expansion coefficient (Fig.2.15A) and can withstand higher temperatures and thermal shock. Figure 2.15B shows the failure temperature of an idealized scenario where a

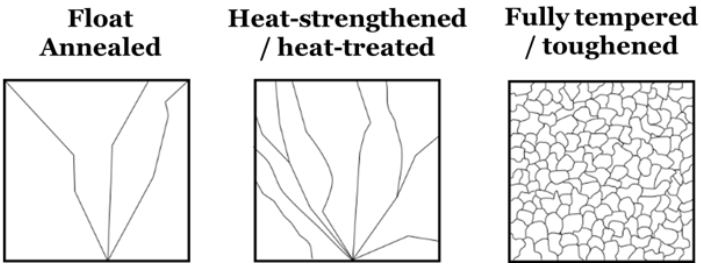


Figure 2.14: Fracture pattern of common construction glass: float annealed, heat-strengthened and fully tempered.

glass element is fully restrained and is heated uniformly, these values are plotted for comparison purpose. Glass has a low thermal diffusivity hence it will heat up in a very non-uniform manner and the thermal gradients developed within the glass will lead to failure at temperature much lower than reported in Fig. 2.15B.

For safety reasons the glazing units in buildings are usually laminated. Laminated glass consists of two or more glass sheets bonded by a polymer, typically polyvinyl butyral (PVB). When the glass cracks, the shards will stick to the visco-plastic interlayer and stay in position. The problem posed by laminated glass is the degradation of the bonding polymer which can results in delamination and possibly fall out of one of the glass sheets (Kozłowski et al. (2018), Bedon et al. (2018)). The effect of temperature on glass properties is still not that well defined especially when considering laminated glass. A comprehensive summary of recent experimental re-search on glass temperature dependant properties was carried out by Bedon et al. (2017).

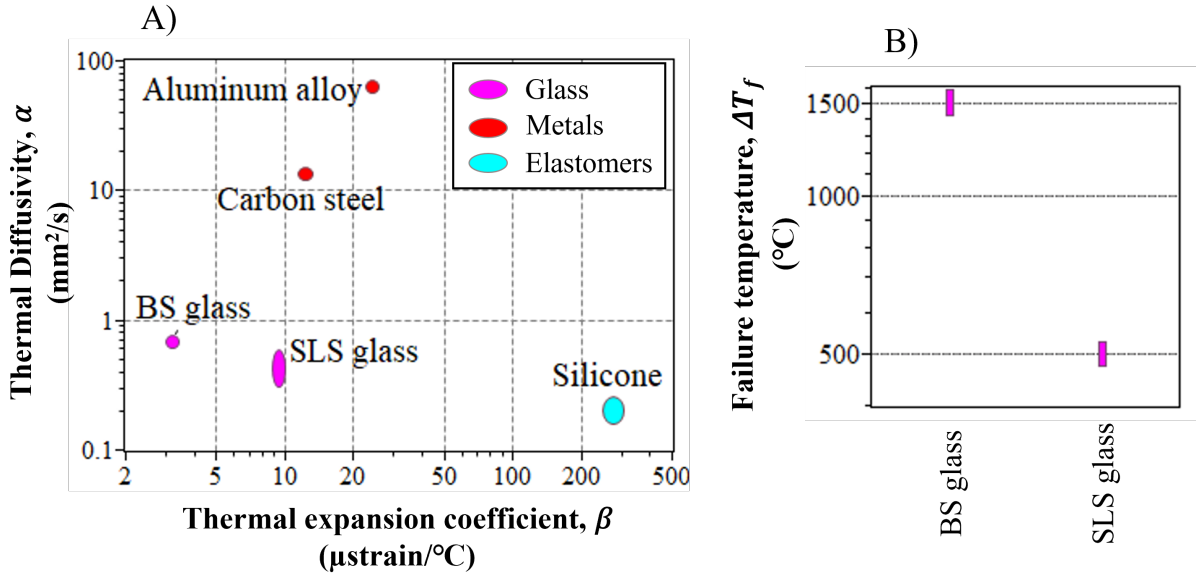


Figure 2.15: Properties of glass plotted on a logarithmic scale. (A) Thermal expansion coefficient and thermal diffusivity, material used to frame glass are also included (steel, aluminium & silicone). (B) Failure temperature due to thermal expansion (see Section 2.2.4, Equation 2.4) Material data from ANSYS (2021).

The failure mechanism of glass at elevated temperatures has been widely studied and the breakage of glass has been found to be strictly related to the restrain conditions and the shaded portion of the glass hidden behind a frame or gasket (Pagni and Joshi (1991), Joshi and Pagni (1994b), Joshi and Pagni (1994a), Wang et al. (2013), Wang and Hu (2019)). When heated the glass exposed to radiation and convection will heat up quickly while the shaded portion of the glass panel will remain at lower temperature. Glass is a poor conductor and heat will travel slowly from the hot section to the cooler one. The hotter section, usually the centre of the pane, will expand produce tensile stresses in the cooler shaded perimeter areas. Due to the low tensile strength of glass, cracks will initiate at the shaded area and propagate to the hotter area.

Differential expansion of the metal frame and of structural silicone could induce local stresses within the glass – see Fig. 2.15A. Silicone is typically used in curtain wall systems to keep glass in place. This elastomer has higher resistance to heat than other polymers, but its fire resistance should be carefully studied regardless. Its heat induced softening might lead to serious consequences, namely the fall-out of glass panels.

2.5 Combustible Facades Materials

Facades with combustible components have an additional level of complexity which arises from the need to include the ignition and burning behaviour of the flammable component in the analysis and discussion. Mechanical failure is not a critical issue compared to the risk of fire spread for such systems. Therefore, flammable facades are not discussed in detail as this would require a new framing of the problem (Bonner et al. (2020), McLaggan et al. (2021)). In this section we will briefly discuss membranes, timber and fibre reinforced cladding considering their mechanical behaviour when exposed to heat. Fire spread and flammability will not be discussed in detail as out of scope of the present work.

Textile membranes are mainly employed in stadiums and outdoor structures or added as an outer layer to glazed facades to provide shade (e.g., roller blinds). They have high tensile strength, high tear and impact resistance and can be used for long-span areas (Hu et al. (2020)). Common materials used are polyester yarns coated with polyvinylchloride (PVC) or glass fibre yarns coated with either polytetrafluorethylene (PTFE) or silicone. Whereas ethylene tetrafluoroethylene (ETFE) or PTFE foils are used as an alternative to glass. Foils can transmit 95% of light and have a great strength to weight ratio (Hu et al. (2017)). Textile membranes and foils exhibit a rapid decrease of mechanical properties with increasing temperature, however they do not normally pose a fire safety risk as they will rapidly burn or shrink away when exposed to hot gasses (Chilton (2013)). In the only reported large-scale fire experiment in literature investigating membrane facades by Blomqvist and Andersson (2012), falling burning debris was observed in test involving thicker PVC coated membranes ($\geq 1mm$), whilst glass fibre textile membranes coated with silicone retained their integrity during the test.

Timber is light weight and has good insulative properties and is therefore an ideal material for

use in facades. However, wood will ignite very rapidly in a fire scenario as discussed by Bartlett et al. (2019) . The size (i.e., thickness) of wood products is an important factor, as thick sections of wood will produce a char layer that will insulate and protect the deeper section, slowing down combustion. A significant body of work exists on the mechanical behaviour of timber columns, beams and slabs exposed to fire, however very little work has specifically focused on the fire mechanical performance of timber cladding panels and timber battens. Previous work by Osvald and Štefková (2020) has investigated the reduction of flexural strength of timber exposed to radiant heat. An experimental study by Koutaiba et al. (2017) compared the combustion of two different wood species – Birch and Okoume – when used as vertical cladding panels. The birch facade burnt faster, and parts of the panels fell off, which did not occur for the Okoume facade. This indicates that some wood species might be more appropriate for cladding than others.

There are many types of fibre reinforced polymer composites depending upon the choice of resin (epoxy, polyester, vinyl ester, etc.) and reinforcing fibre. The fire safety issue with these materials is that inorganic fibre (aramid, carbon, and glass) will soften with heat and the organic fibres will burn (e.g., wool, hemp), whilst the polymeric matrix will decompose at relatively low temperatures. Models of the fire damage at material level and for predicting mechanical properties at high temperature and post-fire can be helpful to understand the behaviour of composite facades and have been previously reviewed by Mouritz et al. (2009) and Kim et al. (2018). Research on Glass Fibre Reinforced Polymers (GFRP) sandwich panels by Pereira et al. (2016) investigated the influence of the core material on the fire performance of the panels. Failure was assumed when the mass loss of the core material produced large hollow spaces causing the external GFRP plate to be hanging unrestrained. Therefore, failure was found to correlate with the thermal decomposition temperature of the core materials. A series of bench-scale experiments were performed to investigate failure load and failure modes of sandwich panels made of epoxy reinforced with carbon fibres and a plastic foam core Schartel et al. (2019). The panels loaded in compression with a load lower than 50% of the static failure load demonstrated a visco-elastic failure mode. The panels loaded more than 50% of the failure load displayed a plastic hinge at failure.

2.5.1 Concrete Sandwich Panels

Sandwich panels are commonly used due to their lightness and good insulative properties. Pre-cast concrete sandwich panels are characterised by high thermal resistance provided by a layer of insulation sandwiched between two concrete layers of 7-10 cm thickness. These layers are fixed together with mechanical connectors made of concrete, metal, or fibre reinforced polymers. The connectors act as thermal bridges and therefore an efficient design is paramount. Metal truss, tube or plate provide composite action, i.e., the two concrete elements act as one, whereas pin connections do not (O'Hegarty and Kinnane (2020)). Most insulation will be flammable to a certain degree, mineral wool can be used as a non-combustible core material, however it has very little stiffness therefore the connectors need to be stronger and bigger, creating an important

thermal bridge (O'Hegarty et al. (2020)).

Thin high-performance concrete (HPC) plates used for sandwich panels were tested under extreme thermal loading by Hulin et al. (2016c). The specimen tested were unrestrained and unloaded to investigate the spalling behaviour. Thicker concrete plates (30mm) were found to perform better than thinner plates (20mm) and the use of polypropylene (PP) fibres was found to improve the spalling behaviour. The behaviour at elevated temperature of sandwich panels with point and mesh steel connectors were investigated experimentally by Hulin et al. (2016b) and numerically in Hulin et al. (2016a). When the panels are exposed to uniform heat following the standard fire curve CEN (2014)., large stresses develop around the shear connectors as these restrain the thermal bowing of the concrete plates (Hulin et al. (2016b), Hulin et al. (2016a)). The effect of a small thermal gradient across the thickness of concrete sandwich panel with diagonal shear connector was also investigated (Huang and Hamed (2019). When the panel is simply supported and free to elongate the lateral deflection due to thermal bowing was found to increase with the diameter of the steel bars used as connectors. When restrained on both sides, the panels were found to fail in buckling triggered by thermal bowing.

2.5.2 Metal Sandwich Panels

Metal composite sandwich panels are fabricated by bonding two thin metallic sheets to a structural core, obtaining stiff but light panels with enhanced insulative properties. Metals commonly used are steel and aluminium, whereas the core material is usually made of foamed plastics like polystyrene (PE), polyurethane (PUR) or polyisocyanurate (PIR) which are all combustible. Stone and mineral wool can be used as a non-combustible alternative. For sandwich panels heat induced delamination is critical, it occurs when the adhesive bonding the metal sheets with the core loses its cohesive properties causing the layers to detach from one another (Fig. 2.16). Once delamination occurs the panel will not retain much flexural strength. Delamination is particularly dangerous when sandwich panels are used for free-standing walls and suspended ceiling (Cooke (2004)).

The behaviour of a facade clad with steel sandwich panels and exposed to an internal fire was studied computationally by de Boer et al. (2019). The sandwich panel consisted of steel plates and a PIR core, supported by steel angle section bolted to steel columns of the main structure. The authors considered different failure criterion: failure of composite panel due to heat induced deflections (bowing), failure of the screw connection between the panel and angle section and failure of the bolt connection between the supporting steel angle and the main structure. In the simulations the authors found the screw to be the weakest link failing in shear. The shear load was caused by the thermal expansion of the sandwich panels. By increasing the diameter of the screws, failure was avoided. However, this study does not consider the complex behaviour of the PIR core and does not model delamination. The authors were not able to specify temperature dependant properties for the screws and bolts, therefore probably predicting longer failure times. These small elements when heated might fail more rapidly due to loss of strength and stiffness.



Figure 2.16: Delamination of steel sandwich panels after a fire test, with rockwool insulation (left) and PIR insulation (right), the PIR insulation has been completely consumed. Image from Pyl et al. (2012).

The fire performance of stand-alone steel/PIR sandwich panels has been investigated experimentally and numerically by Wang and Foster (2017). The authors investigated different panels thicknesses and joint orientations. Large gaps were found in the insulation at the joint between panels (tongue & groove joint) in all the tested panels and delamination was also observed. The authors found that the gap at the joint between two panels, when wide enough ($\geq 5mm$), facilitated the transfer of heat by convection and radiation across to the unexposed side. The joint gap even if small initially, could widen due to the opening of gaps in the insulation caused by ablation. The joint is therefore a weak link in this type of system and the authors proposed the use of intumescent paint at joints to increase resistance time of sandwich panels.

Aluminium sandwich panels are often used as they are more lightweight, however these panels are extremely vulnerable when exposed to fire as the aluminium sheet will conduct heat and degrade very rapidly. The fire resistance of the sandwich panel will mainly depend on the material used as a core and the correct detailing of fire barriers. Recent tragic events and published work by Dréan et al. (2019) and Guillaume et al. (2020) demonstrated that if the core used for the sandwich panel is made with highly flammable material it will burn away very rapidly and the panel will lose its integrity. The possibility of panels detaching while still integral due to failure of fixing needs to be investigated.

2.6 Comparison of Material Properties

This section brings together the data presented in previous plots (Figures 2.9, 2.11, 2.13 and 2.15) to allow a direct comparison of materials used in facade systems. To analyse the fire performance of typical components found in facades, we consider the two main causes of failure: material failure and failure due to thermal expansion. Looking at properties that relate to these two detrimental behaviours, we can identify the elements more vulnerable to fire. The fire behaviour of composite materials and flammable components such as insulation material

and other functional layers is not discussed. Only non-combustible materials are included in the comparison as the focus is on mechanical failure and, as explained earlier, for combustible materials mechanical failure is not a critical issue compared to the risk of fire spread.

2.6.1 Material Failure

When heated, all materials will experience degradation of their mechanical properties. Material failure due to heat-induced degradation are summarized in Table 2.2 for the non-combustible materials discussed in this work. Encompassing all the different and complex behaviours in Table 2.2 in a single parameter (e.g., failure temperature) used to compare between materials is not possible, mainly due to the fact that these behaviours depend on many parameters (e.g., restrains, loading, thickness of element, environmental conditions, heating conditions).

Table 2.2: Primary material failure in fire of non-combustible facade elements.

Facade material	Material failure in fire
stones and ceramics	fracture, spalling, scaling
concrete	spalling, delamination (sandwich panels only)
metals	softening, delamination (sandwich panels only)
glass	fracture, delamination (laminated glass only)

To compare between materials that have substantially different behaviours the maximum service temperature was studied. The maximum service temperature is the highest temperature at which the material can be used in a load-bearing component without oxidation, chemical change, or excessive creep becoming a problem (Ashby (2011)), meaning it is the critical temperature at which material strength starts to fall sharply. This is defined as $T_m/3$ for Metals and $T_m/2$ for Ceramics including concrete and glass, with T_m being the melting temperature. The maximum service temperature is a material property and is defined as a uniform temperature, therefore is independent of size and shape. The test performed to quantify this property does not consider the effect of thermal gradients or the effect of sudden temperature change.

Plotting the maximum service temperate in Figure 2.17, we observe that concrete, stone, and ceramics maintain their load-bearing capacities at temperatures above 500℃, with the exception of limestones which lose strength at lower temperatures. Stainless steel exhibits a service temperature of around 700℃. Cast iron and titanium also perform well and maintain most of their mechanical properties up to 400-500℃. Conversely, aluminium alloys, copper, lead and zinc alloys, experience important degradation at low temperatures, and therefore exhibit a max service temperature lower than 150℃. These heat-sensitive metals could lead to rapid failure in fire, especially when used in load-bearing elements (e.g., connections, supporting frames) and the risk of fall-out of panels or larger sections should be considered.

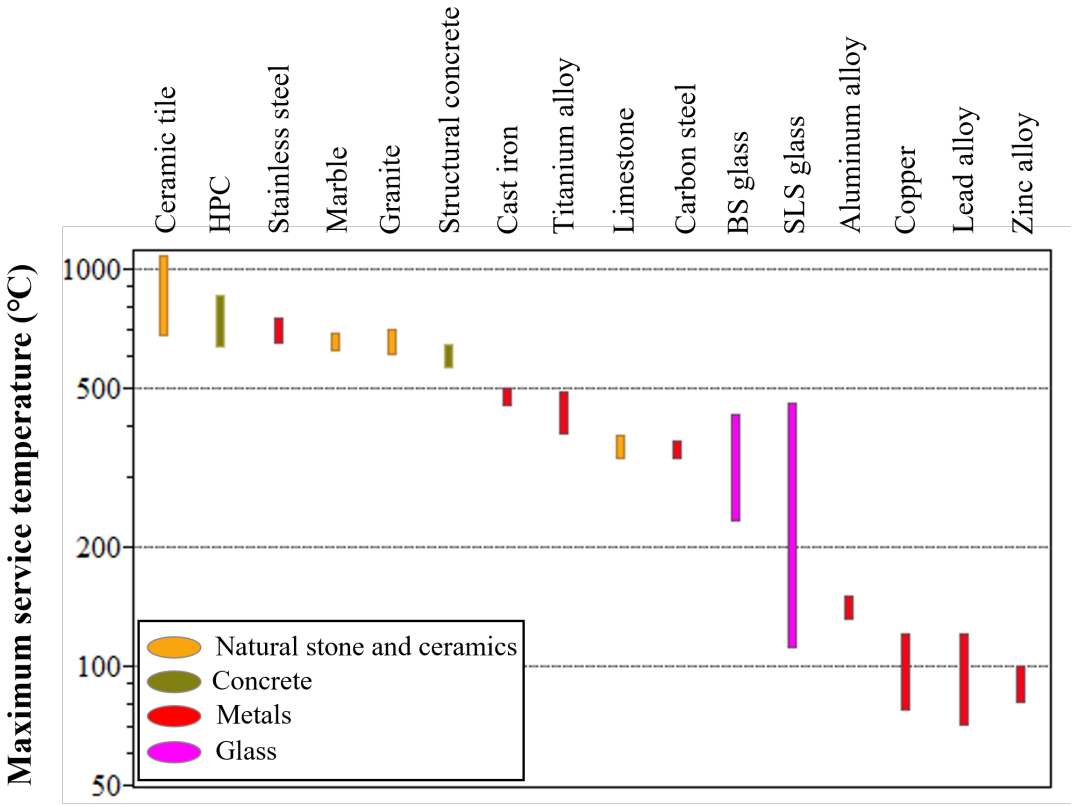


Figure 2.17: Maximum service temperature of non-combustible facade materials on logarithmic scale. Data from ANSYS (2021)

2.6.2 Thermal Expansion and Element Failure

To compare the risk of mechanical failure due to thermal expansion, three parameters are considered:

- *thermal diffusivity* - described in Section 2.2.1.
- *thermal expansion* - described in Section 2.2.3.
- *failure temperature due to thermal expansion* - described in Section 2.2.4.

These three parameters are plotted in Fig 2.18 and 2.19 for all the non-combustible materials discussed in this paper. From Figure 2.18 we observe how most concrete, stone, ceramics and glass products have relatively small values of thermal diffusivity and thermal expansion when compared to metals. These materials are therefore less reactive to heat as they will heat up at a slower rate and expand to a smaller degree. Some metals exhibit comparatively high values and therefore can be found on the upper right corner of the plot. Metals will heat up, expand rapidly, and will exhibit more uniform temperature while stone, ceramics, glass, and concrete will experience large thermal gradients.

Materials with large thermal expansion coefficients need to be considered with care, especially

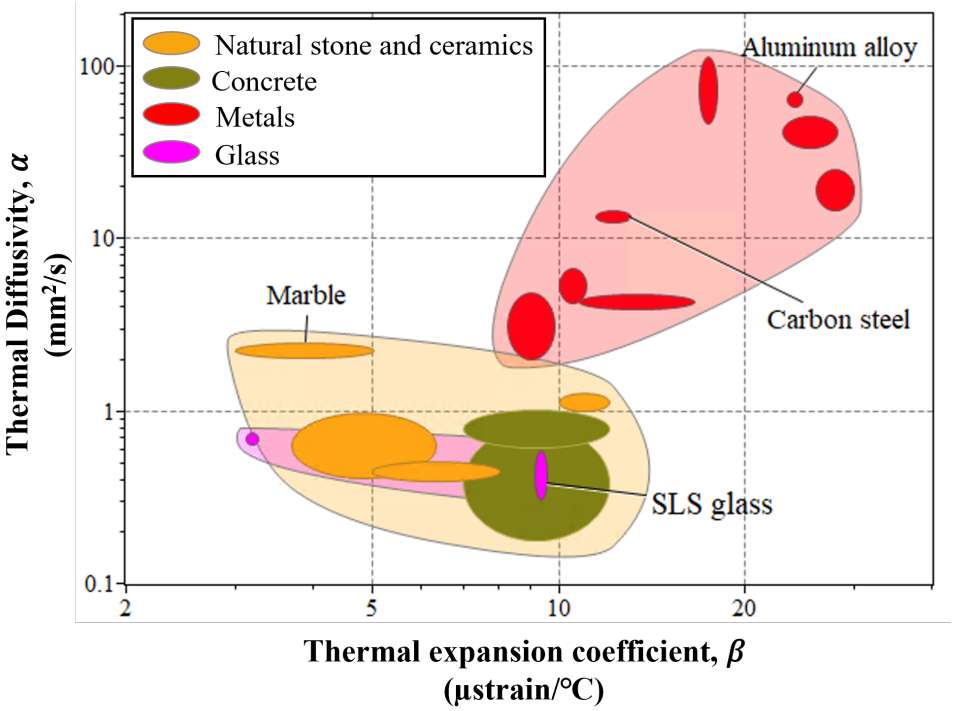


Figure 2.18: Thermal expansion and thermal diffusivity of non-combustible facade materials plotted on logarithmic scale. Data from ANSYS (2021).

when in contact with brittle materials that exhibit lower expansion. Particularly of concern is the interaction between aluminium framing elements and glass panels in curtain wall systems. These two materials are on opposite extremes on the graph: while glass will heat up and expand slowly, aluminium will rapidly react to heat. The expansions and deformation of the aluminium frame can lead to fracture or fall-out of the panel.

The failure temperature due to thermal expansion (Fig. 2.19) for a uniformly heated and perfectly restrained element can be used to draw some comparison between materials, for details on how we calculate this failure temperature refer to Section 2.2.4. Metals seem to fail more rapidly than other material, except for titanium alloys that can withstand temperature of nearly 1000°C due to their strength and low thermal expansion coefficient. BS glass can also endure substantial uniform temperature evolutions (above 1000°C) due to the development of very small thermal strains. Unreinforced concrete fails at low temperature due to its very low compressive strength.

It should be noted that material degradation is not considered and that ambient values are used when calculating the failure temperatures reported in Figure 2.19. In addition, stone, ceramics, concrete, and glass will experience large thermal gradients due to their low thermal diffusivity and therefore the assumption of uniform temperature is unrealistic. Nevertheless, the failure temperature reported here is useful for comparing the thermal expansion behaviour of facade element and its induced stresses.

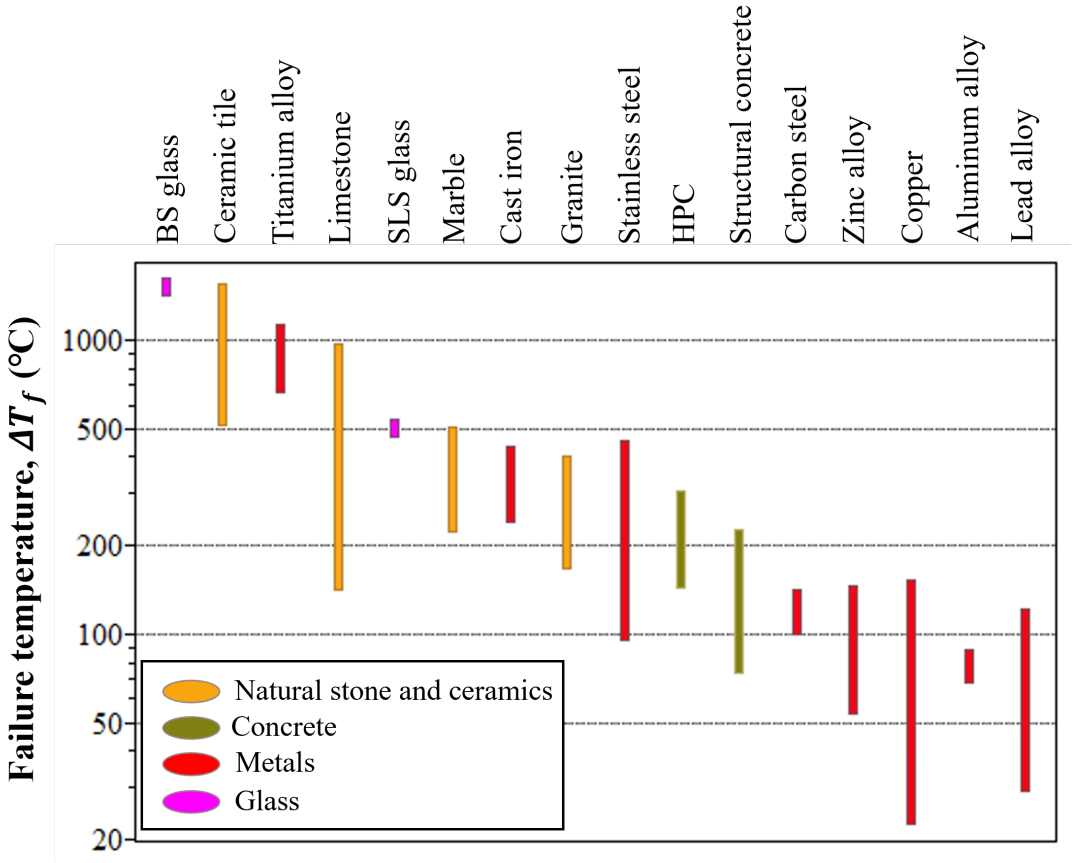


Figure 2.19: Failure temperature due to thermal expansion for fully restrained element with uniform temperature across its cross-section. For description of how the failure temperature is calculated see Section 2.2.4, Equation 2.4. Material data from ANSYS (2021)

2.7 Conclusions

This chapter provides a review of mechanical failure modes of facade systems exposed to fire and a comparison of mechanical and thermal properties of facade materials that influence such failures. Facade system failure can occur due to different mechanisms; mainly it will be induced by the thermal degradation of mechanical properties and thermal expansion. Mechanical failure can cause portions of the facade to fall out. Depending on its size, the falling part can become an obstacle to evacuation and firefighting activities or can have even greater consequences to safety. If the failure creates a new opening in the facade, flame spread outside the fire compartment can occur. In the most unfavourable of events, the entire system could collapse when the support structure is compromised.

Fire incidents where mechanical failure has been observed have highlighted the importance of investigating possible failure mechanism in order to prevent them during engineering design. However, overall, research on facade mechanical failure by fire is limited to a few laboratory and computational studies, even fewer if we consider different facade system separately. The current paper, in compiling the studies on this topic, reveals that there are large knowledge gaps and

unexplored areas.

Research investigating the fire performance of typical facade support systems, namely railings and light steel frames, and of typical facade connections is very limited. When the support system or the connections fail, large sections of the facade can detach and fall (i.e., an entire panel), therefore these elements need to be studied with priority. Past work has shown that metal frame systems risk failing in buckling or lateral torsion due to thermal gradients, especially when supporting an eccentric load, typical in facades. Hence, researchers and practising engineers should investigate failure mechanisms for facade frame systems with realistic loading and restrain conditions.

Currently, the effect on heat on the breaking load of dowel connections is unknown, these connections are typical of stone panels. Fall out of heavy stone panels should be prevented therefore understanding the effect of high temperature on the breaking load of dowel connections is paramount. The heat resistance of metal brackets used to support precast concrete panels is also largely unexplored and required attention from researchers.

Aluminium, copper, lead, and zinc were found to be quite vulnerable to fire when their mechanical and thermal properties were compared to other metals (e.g., large expansion coefficient coupled with high thermal diffusivity, low failure temperature). Nonetheless studies investigating the behaviour of facade built with such metal are lacking. The expansion of restrained metal panels will induce large stresses on the fixings and could lead to failure. Shear failure at the connection was reported in literature for steel sandwich panels, this failure mechanism should also be investigated for solid metal panels. Finally, the fire performance of modern curtain walls needs to be appropriately investigated as studies on such complex systems are lacking. Deformation of the metal frame and failure of the metal brackets are mechanisms that need to be explored. The influence of polymeric thermal breaks on the stability of the frame requires greater attention from researchers as can be a weak link in the system due to its rapid thermal degradation.

Given the possible consequences of facade failure, more experimental and numerical studies are needed to develop both fundamental understanding and provide design solutions to allow the construction of safer facades. There should be a global multidisciplinary effort and parties involved should include both expert in fire safety and facades. Only through collaborations between these two groups can the research be directed toward useful projects that explore facades in their end use form – with appropriate detailing and under realistic conditions.

Chapter 3

Development of Thermal Model for Curtain Wall Systems with Increasing Complexity

3.1 Introduction

Facade systems have become sophisticated and complex, consequently it has become challenging to quantify their fire behaviour (Bonner and Rein (2018)). One example of such complex facades are curtain walls which are typically used for modern high-rise buildings. These systmes are vulnerable and the heat from a fire could cause key elements to fail and, in a worst-case scenario, a large facade unit could detach and fall from the building as discussed in Chapter 1. If a facade unit fails it can create a new opening through which fresh air can enter the compartment and feed the fire. External flames can damage upper floors and lead to vertical flame spread (O'Connor (2008)). Despite this, the thermal and mechanical performance of curtain wall facades in a fire event is not regulated (Koffel et al. (2005)) and is still poorly understood.

While the fire performance of glass panels as a component of curtain wall facade systems has been explored over the years (Pagni and Joshi (1991), Debuyser et al. (2017), Bedon and Louter (2018), Kozłowski et al. (2018), Wang and Hu (2019)) very little work has focused on the behaviour of assemblies as a whole. This is because frames, spandrel panels and brackets are generally not considered as vulnerable to fire as the glass panels. This assumption, however, has not been confirmed. The metallic elements are thin and can therefore heat up rapidly, causing a reduction in stiffness and strength, which can lead to excessive deformation and load redistribution. Therefore, the accurate prediction of the thermal performance of all individual elements is an important step in the structural fire safety design of a curtain wall.

In order to design safe curtain walls, we need to understand the system behaviour in fire, and to

understand the system behaviour we need to be able to predict its thermal response. Curtain walls are made of several components connected together and the heat transfer across these components is very complex. Previous thermal 1D and 2D numerical models of a single glass panel exposed to fire (Bedon and Louter (2018), Kozłowski et al. (2018)) have been developed to predict the temperature developments. Laminated glass has also been modelled in 3D where the heating was assumed as predefined temperature on the surface (Wang and Hu (2019)). These models were validated against experiments but did not consider the frame system or the brackets supporting the glass panels. Heating of multi glass units by fire have not been modelled previously. An aluminium window frame with thermal breaks was simulated in a paper reconstructing the Grenfell Tower fire by Koohkan et al. (2021). The model was not verified with experimental data and the analysis was limited to one specific scenario. To the knowledge of the author, the thermal response of a curtain wall assembly exposed to fire has not been investigated systematically.

In this chapter we develop a heat transfer model to investigate the response of curtain wall assemblies to heat from a fire. We start by building a simple 0D model and we build up on the model to include more heat transfer mechanism and obtain more accurate predictions. The aim is to present a rigorous heat transfer methodology for use in the analysis of curtain walls and to identify what level of complexity is needed to obtain an "accurate enough" temperature distribution that can help us understand the failure mechanism of the system exposed to fire. First the methodology behind the thermal model is described. The heat transfer mechanisms are described in more detail for the 0D model in Section 3.4.1, 1D model in 3.4.2 and for the 2D and 3D models in 3.4.3 and 3.4.4. The boundary conditions are discussed in Sections 3.3. This is then followed by a discussion on differences, benefits and limitations of the models presented.

3.2 Curtain Wall Heat Transfer Methodology

3.2.1 Curtain Wall Components

In a curtain wall system, the main components are glass panels, metal frames and metal brackets. The panels are fixed to the frame via silicone gaskets and the frame is fixed to the main structure via metal brackets. The aluminium frame consists of both a structural frame and a pressure cap (shown in Figure 3.1 and 3.2). The structural frame is the load bearing component which supports the weight of the glass panel, whilst the pressure cap is connected to the structural frame via steel screws and/or a thermal break polimeric component. The pressure plate keeps the glass in position. Both pressure plate and the structural frame are usually made of extruded aluminium.

Direct contact between metals and glass can cause the glass to crack due to concentrated stress applied to the glass; therefore, a gasket or silicone sealant is always present between the two materials. Structural silicone has a very low thermal conductivity ($k = 0.35W/mK$) and therefore

it was assumed that no heat is transferred between the glass and the aluminium. Consequently, each component can be treated independently when considering the thermal response only.

Brackets are not discussed in this work as no data was available for the verification of these elements. The current fire safety strategy to limit fire spread relies on providing insulation all around the brackets and inserting fire stops in the gap between the edge of the floor slab and the facade (where the brackets are located). We assume brackets have been properly insulated and therefore they will not heat up as quickly as they are not directly exposed to the heat from the fire.

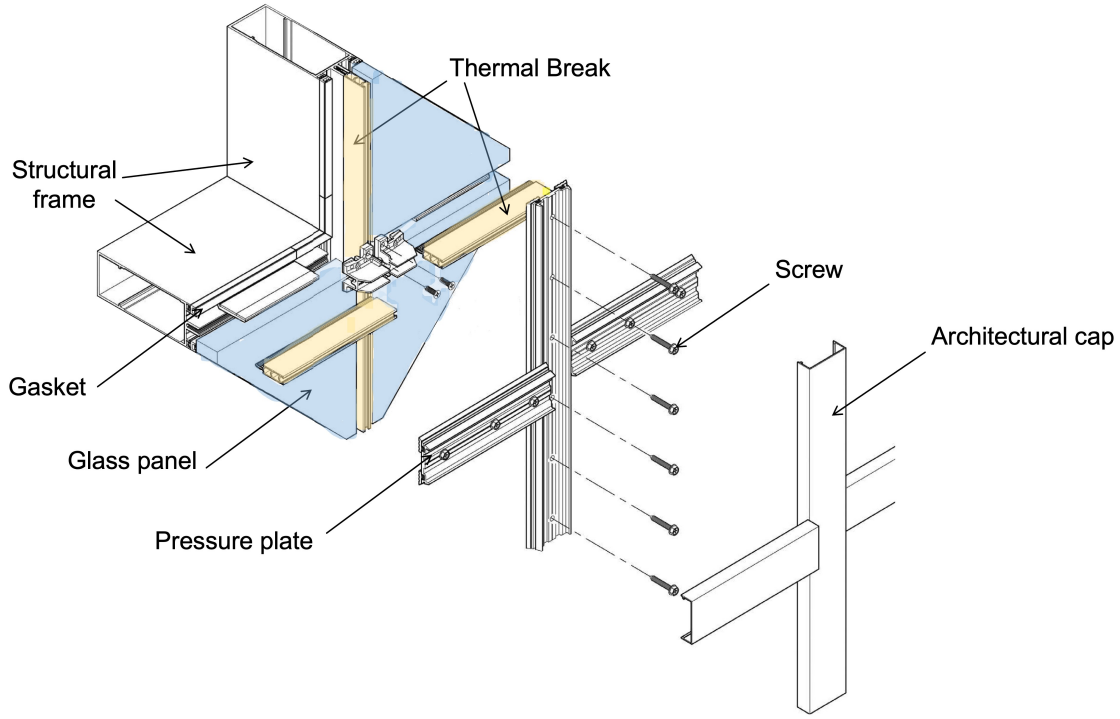


Figure 3.1: Exploded view of a curtain wall facade with glazed panels and supporting frame.

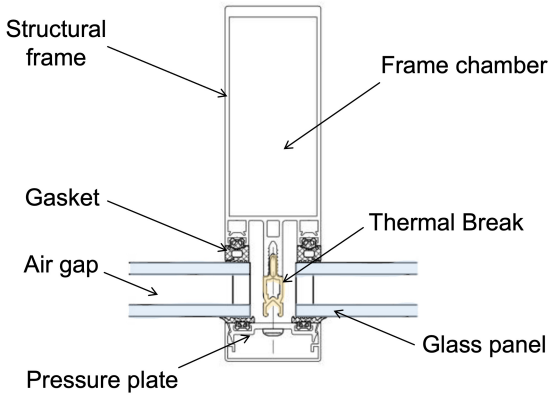


Figure 3.2: Section through a curtain wall framing system.

3.2.2 Heat Transfer Mechanisms for Glass Panels

Thermal radiation transfers via electromagnetic waves with a wavelength between 0.4 and 100 μm (Drysdale (2011)). When the waves hit the surface of an opaque medium the incident thermal radiation will be in part absorbed by the medium and in part reflected away from the medium. The absorbed radiation will affect the internal energy generating a temperature change. If the medium is semi-transparent, part of the incident radiation will be transmitted and will pass through the medium without affecting its temperature. The portion of irradiation absorbed, reflected or transmitted depends on the upper and lower surface conditions, wavelength of irradiation, composition and thickness of medium.

The absorptivity, transitivity and reflectivity of glass are functions of temperature and wavelength. For example, glass will transmit along its thickness (allow through without interaction) shorter wavelengths but will absorb or reflect longer wavelength. In addition, these phenomena are volumetric: they take place within the material and not at a surface level. Absorption, for example, leads to a decay of the incident radiation across the thickness of glass, this decay is exponential and is a function of the absorption coefficient. However, for our model we will assume that absorption, reflectance, transmittance and emission are all surface phenomenon. We will quantify these using the values deduced by Debuyser et al. (2017) for glass panels heated via a propane radiating panel at a constant heat flux $\approx 10W/m^2K$. The values are presented in Table 3.1.

$$\alpha + \rho + \tau = 1 \tag{3.1}$$

Table 3.1: Absorptance, transmittance and reflectance values for glass panels from Debuyser et al. (2017)

Glass thickness [mm]	Absorptance, α	Transmittance, τ	Reflectance, ρ
6	0.583	0.263	0.154
10	0.629	0.250	0.121
15	0.657	0.175	0.168

For panels with multiple glazing the radiation transmitted across the thickness of the first pane, closest to the flames, was defined as the boundary condition for second glass pane, further away from the flames. Glass units can be installed as a single pane (single glazed), however, to increase the insulating properties of the facade usually multi-pane glazing is used (double or triple glazing). The glass panels are separated by spacers to allow air in between, increasing the thermal and acoustic insulation exponentially. Spacers can be metallic, however, since metal reduces the insulating properties of the unit, less conductive materials like polymers are used. In the air gap between glass panels there is no convection as Equation 3.3 is satisfied. Heat will

be transferred via conduction, so the gap is modelled as a solid element with the temperature dependant material properties of air.

Between the glass panels, there is no convection as the gap is too small and the viscous forces exerted by the walls of the cavity are larger than the buoyant forces. Thus we model the transfer of heat within the air gap between glass panels by convection only. A portion of the heat in the form of radiation waves will also transmit through the first pane and reach the second pane, consequently when modelling the second pane we need to apply a radiative boundary condition on the surface of the glass ($\tau q^{''}(t)$) .

3.2.3 Heat Transfer in Frame chamber

An accurate prediction of the heat transfer across the frame requires the characterization of the frame chambers (typically one or two chambers). Once heated, the air in the chamber will start flowing due to buoyancy, hotter gases moving upwards. If the friction on the walls is greater than the buoyancy, the movement will be halted, and heat will be transferred via conduction and not convection. To know which heat transfer mode to consider in the frame chamber we need to perform a Rayleigh check, Equation 3.2 and 3.3 from Incropera and DeWit (2013). If Equation 3.3 is true, conduction will be dominant.

$$Ra = \frac{g\beta(T_1 - T_2)L^3}{\alpha\nu} \tag{3.2}$$

$$Ra < 10^4 \tag{3.3}$$

If convection is dominant, which is usually the case, we can utilize the correlations Equation 3.4 and 3.5 from Nogueira et al. (2011) to calculate the convective heat transfer coefficient within the rectangular chamber, where L and H are the cross-sectional dimension of the chamber. This heat transfer mode will cool down the frame, especially if cool air is able to enter the chamber.

$$1 < \frac{L}{H} < 2 \qquad Nu = 0.18\left(\frac{Pr}{0.2 + Pr}Ra_l\right)^{0.29} \tag{3.4}$$

$$2 < \frac{L}{H} < 8 \qquad Nu = 0.22\left(\frac{Pr}{0.2 + Pr}Ra_l\right)^{0.28} \tag{3.5}$$

with the lateral dimension H between 50–85 mm and the longitudinal dimension L between 50–225 from Paoletti and Nastri (2023) and since $L \geq H$:

$$1 < \frac{L}{H} < 4.5 \tag{3.6}$$

As the walls of the frame heat up, they will radiate heat across the chamber. Depending on the view factor between two points, heat will be transferred from the hotter walls to the cooler ones. This mechanism will cause a reduction in the thermal gradient across the frame and can be significant as the frame reaches high temperatures and radiation grow.

3.3 Boundary Conditions

Depending on where the fire is located, the facade will experience different boundary conditions. If the fire is burning inside the building, the internal surface of the facade will be heated. If the fire is external, e.g. an adjacent building on fire, the heated surface will be the external one. Boundary conditions for a compartment fire are shown in Figure 3.3 where two separate surfaces are identifiable, the fire exposed surface and the ambient exposed surface. The facade is being heated on the fire side and cooled on the ambient side. Parameters related to the fire side will be denoted with an f subscript whilst the ambient side with an a subscript and are discussed in the following sections.

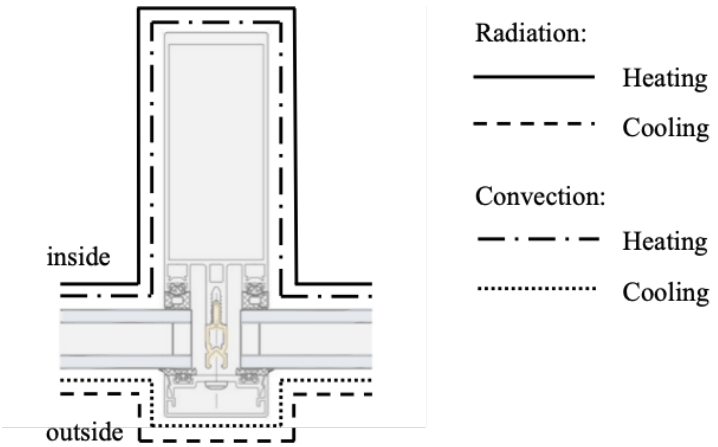


Figure 3.3: Boundary conditions for a facade heated internally (e.g. compartment fire)

3.3.1 Convective Heating

The convective heat transfer coefficient for boundary layer flows can be calculated using the correlations expressed in Equation 3.7 and 3.8 accounting for natural convection on a vertical wall of length, l, for laminar flow and turbulent flow respectively. The Grashof and Prandtl dimensionless parameters are evaluated assuming air at ambient pressure. The heat transfer convective coefficient is time dependant, as both the gas and the wall will get hotter as the fire progresses. A time dependant coefficient would be cumbersome to calculate and to use in our modelling activity, therefore, if we select the peak temperature of the gas within our fire compartment and the initial temperature of out wall, we can define a conservative value. An example calculation is given in Table 3.2 for a gas temperature of 500℃ and a 2 m wall.

$$10^4 < Gr \cdot Pr < 10^9 \qquad h_c = \frac{k}{l} 0.59 (Gr \cdot Pr)^{\frac{1}{4}} \tag{3.7}$$

$$Gr \cdot Pr > 10^9 \qquad h_c = \frac{k}{l} 0.13 (Gr \cdot Pr)^{\frac{1}{3}} \tag{3.8}$$

Table 3.2: Calculation of convective heat transfer coefficient for natural convection on vertical plate.

Parameter	Symbol	Unit	Value
Air Temperature	T_∞	℃	500.0
		K	773.2
Wall Temperature	T_s	℃	15.0
		K	288.2
Film Temperature	T_{film}	K	530.7
Air properties at 530K			
Expansion coefficient	β	$/K$	1.88×10^3
Thermal conductivity	k_{air}	W/mK	0.04262
Kinetic viscosity	v	m^2/s	4.29×10^{-5}
Prandtl number	Pr	–	0.6834
System Properties			
Gravitational acceleration	g	m/s^2	9.81
Length of vertical plate	l	m	2.0
Grashof number	Gr	–	3.91×10^{10}
Flow check	$Gr \cdot Pr$	–	2.67×10^{10}
Convective heat transfer coeff.	h_c	W/m^2K	**8.28**

The heat transfer coefficient described above can be used in cases where the fire is located at a distance from our facade and the flow along the facade is natural. However, most of the time a fire burning within a compartment will create a forced gas flow. For a fire impinging on a ceiling, the heat transfer coefficient was found to be in the order of $50\,W/m^2K$ by Lattimer (2016) and this can be taken as an upper bound.

$$q''_{c,f} = h_f (T_\infty - T_s) \tag{3.9}$$

3.3.2 Radiative Heating

The radiative component of heat from the fire can be defined as in Equation 3.10 if the temperature of the flame or the radiative surface, T_f is known. The radiation recieved by a surface will also depend on the view factor, which defines how much of the flames the surface can "see".

$$q''_{r,f} = \varepsilon\sigma(T_f^4 - T_s^4) \tag{3.10}$$

Alternatively a total heat flux can be defined as a boundary condition,combining both convective and radiative components. For example if a heat flux gauge was used to measure the heat flux incident on a surface, the data collected could be used to define a total heat flux boundary condition. Peak heat fluxes were measured on a flat wall heated by a square propane burner burning against the wall and these are shown in Figure 3.4. The values of peak heat flux on a wall surface as a function of heat release are useful and can be taken as a conservative approximation.

$$q''_{tot} = q''_c + q''_r \tag{3.11}$$

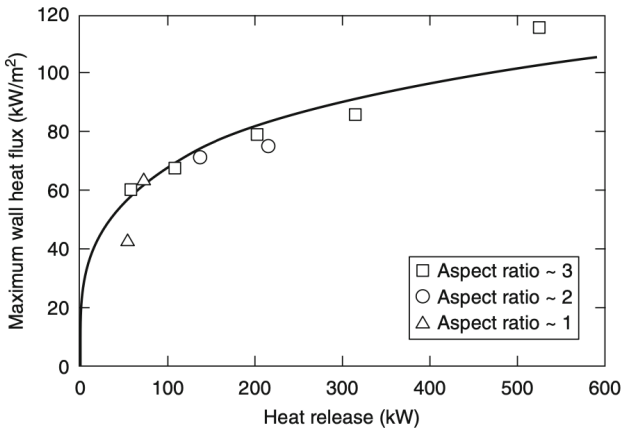


Figure 3.4: Peak heat flux measured against a wall from propane burner fires with varying heat released from Lattimer (2016)

3.3.3 Ambient Cooling

Cooling occurs on the surface of the facade on the ambient side. The surface is cooled by convection due to the flow of ambient air and radiation, as the facade radiates heat to the ambient environment. The temperature of the ambient air will vary depending on the time and location. If considering the temperature in the city of London we can select an ambient value of $T_a = 15$ ℃ as an average value. Equations 3.12 and 3.13 will apply here.

$$q''_{c,a} = h_a(T_s - T_a) \tag{3.12}$$

$$q''_{r,a} = \varepsilon\sigma(T_s^4 - T_a^4) \tag{3.13}$$

3.4 Models with Increasing Complexity

3.4.1 Lumped Capacitance - 0D Model

We have developed a simplified zero dimensional heat transfer model by treating each independent component (framing system and glass panel) as a lumped mass. A lumped capacitance assumption is considered appropriate when the resistance to convection and/or radiation at the boundary of the modelled solid is much greater than the resistance to conduction within the boundary of the solid. This condition is usually tested by evaluating if the Biot number, Bi, is below a certain threshold. We will use Equation 3.14 to check if the lumped capacitance assumption is appropriate, where the effective heat transfer coefficient, h_{eff}, considers both resistance from radiation, h_r, and convection, h_c, while L_c is the characteristic length corresponding to the maximum spatial temperature difference.

$$Bi = \frac{h_{eff}\, L_c}{k} < 0.1 \tag{3.14}$$

$$h_{eff} = h_c + h_r \tag{3.15}$$

The radiation heat transfer coefficient can be calculated knowing the average temperatures of the flame, T_f, of the solid surface, T_s, and the emissivity of the material, ε, as shown in Equation 3.16.

$$h_r = \varepsilon\sigma(T_s + T_f)(T_s^2 + T_f^2) \tag{3.16}$$

For typical curtain wall dimensions (L_c) and material components (k) we can calculate the maximum effective heat transfer coefficient for which a lumped capacitance model is appropriate. As seen in Table 3.3, for a steel or aluminium frame there will be situations where the lumped assumption will be valid but these need to be assessed each time as they depend on the amount of combined radiation and convection recieved by the facade. Wheresas for the glass panel a lumped model will not give accurate predictions when used in a fire scenario.

Table 3.3: Maximum effective heat transfer coefficient for lumped capacitance assumption to be valid (Bi=0.1) for different curtain wall components.

	k $[W/mK]$	L_c $[m]$	h_{eff} $[W/m^2K]$
Aluminium frame	190.00	0.050	380.0
Steel frame	53.00	0.050	106.0
Glass panel	1.05	0.006	17.5

Figure 3.5 shows the limit values of flame temperature and convective heat transfer coefficient for which the lumped mass assumption is valid for the main curtain wall components, e.g. aluminium frame, steel frame and glass panel. For the glass panel the lumped assumption has very limited applicability as in compartment fires the convective coefficient is usually $< 20W/m^2K$.

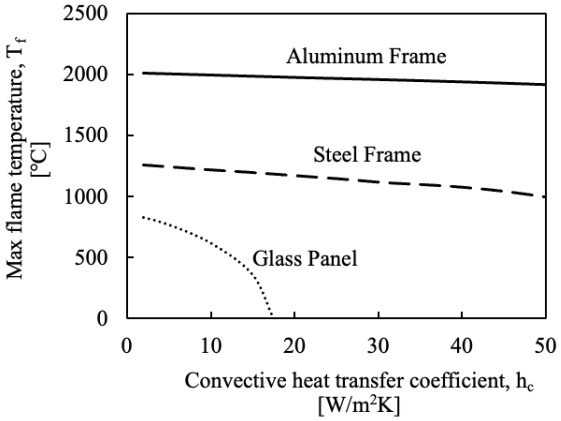


Figure 3.5: Maximum flame temperature for a given convective heat transfer coefficient for the lumped mass capacitance assumption to be valid for different curtain wall components.

When the aluminium frame (or any other curtain wall component) is modelled as a lumped mass, the frame is assumed to have a uniform temperature ($t = T_S$) and no thermal gradients. Therefore, radiation and convective transfer inside the frames chamber are not considered. The governing equation for transiet heating is presented below (Eq. 3.17) with a schematic of the model (Figure 3.6).

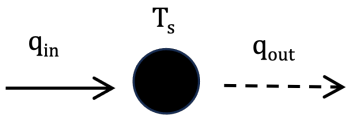


Figure 3.6: Zero dimensional model schematic.

$$\varepsilon\sigma(T_f^4 - T^4) + h_f(T_\infty - T) = \rho c L\frac{dT}{dt} + \varepsilon\sigma(T^4 - T_a^4) + h_a(T_a - T) \tag{3.17}$$

3.4.2 Lumped Capacitance Network - 1D Model

The 1D model is built by subdividing the frame in three lumped masses connected together. The first temperature T_1 represents the temperature of the structural frame, T_2 the temperature of the connector (bolt or thermal break) and T_3 the pressure plate and cap. A schematic of the model is shown in Figure 3.7.

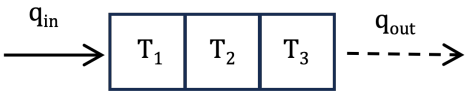


Figure 3.7: One dimensional model discretisation schematic.

The governing equations for transiet heating are presented below with Eq. 3.18 for node 1, Eq. 3.19 for node 2 and Eq. 3.20 for node 3.

$$\varepsilon\sigma(T_f^4 - T_1^4)A_r + h_f(T_\infty - T_1)A_r = \rho_1 c_1 V_1 \frac{dT_1}{dt} + \frac{k}{z}(T_2 - T_1) \tag{3.18}$$

$$\frac{k}{z}(T_2 - T_1) = \rho_2 c_2 V_2 \frac{dT_2}{dt} + \frac{k}{z}(T_2 - T_3) \tag{3.19}$$

$$\frac{k}{z}(T_2 - T_3) = \rho_3 c_3 V_3 \frac{dT_3}{dt} + \varepsilon\sigma(T_3^4 - T_a^4) + h_a(T_3 - T_a) \tag{3.20}$$

3.4.3 Finite Element - 2D Model

The 2D and 3D models developed are finite element models and can predict the temperature distributions within the framing elements and the glass panels. The model includes conduction across the components of the framing system, as well as radiation and convection across the frame chamber (see Section 3.2.3).

The transient heat equations (Equations 3.21- 3.26) are solved numerically via the finite element model LS-DYNA. An implicit solver in respect of time is used. Perfect contact is modelled between each component and thus there is no thermal resistance. This is achieved in the model by defining components with shared nodes at the interface. The bulk node feature (Shapiro (2012)) is used for convection and radiation in the frame chamber. The air convection within the chamber will cool down the frame whilst the radiation will facilitate the exchange of heat between the walls of the enclosure.

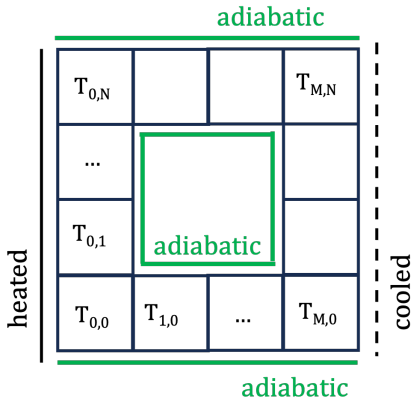


Figure 3.8: Two dimensional model discretisation schematic.

Heated surface

$$T_{0,n}^{t+1} = \frac{2\Delta t}{\rho c \Delta x}\left[\varepsilon\sigma(T_f^4 - T_{0,m}^4) + h_f(T_\infty - T_{0,m}) - \frac{k}{\Delta x}(T_{0,n} - T_{1,n})\right] \tag{3.21}$$

Internal nodes

$$T_{m,n}^{p+1} = Fo\left(T_{m+1,n}^{p} + T_{m-1,n}^{p} + T_{m,n+1}^{p} + T_{m,n-1}^{p}\right) + (1 - 4Fo)T_{m,n}^{p} \tag{3.22}$$

With Fo defined as the finite-difference form of the Fourier number:

$$Fo = \frac{\alpha \Delta t}{(\Delta x)^2} \tag{3.23}$$

Adiabatic Surface

$$\frac{\partial T}{\partial x} = \frac{T_{m,N+1} - T_{m,N}}{\Delta x} = 0 \tag{3.24}$$

$$T_{m,N}^{p+1} = Fo\left(T_{m+1,n}^{p} + T_{m-1,n}^{p} + T_{m,n-1}^{p}\right) + (1 - 3Fo)T_{m,n}^{p} \tag{3.25}$$

Cooled surface

$$T_{M,n}^{t+1} = \frac{2\Delta t}{\rho c \Delta x}\left[\frac{k}{\Delta x}(T_{M-1,n} - T_{M,n}) - \varepsilon\sigma(T_{M,n}^4 - T_a^4) - h_a(T_{M,n} - T_a)\right] \tag{3.26}$$

3.4.4 Finite Element - 3D Model

The 3D model considers heat transfer within the frame chamber via radiation and convection, radiation across glass panels and conduction across the gap between glass panels. The LS-DYNA bulk node feature (Shapiro (2012)) is used for convection and radiation in the frame chamber as described in Section 3.4.3.

The model schematc in shown in Figure 3.9, the governing equation for internal nodes is Equation 3.27. The heated, adiabatic and cooled surfaces are described by the same equations presented for the 2D model in the previous Section 3.4.3 (Eq. 3.21, 3.24, 3.26 respectively).

The transient heat equations are solved using an implicit solver in respect of time. Perfect contact between each component is achieved in the model by defining components with shared nodes at the interface. The frame modelled is 1 m in length and screws are added along the length of the frame at equal spacing.

Internal nodes

$$T_{m,n,q}^{p+1} = Fo\left(T_{m+1,n}^{p} + T_{m-1,n}^{p} + T_{m,n+1}^{p} + T_{m,n-1}^{p}\right) + (1 - 4Fo)T_{m,n}^{p} \tag{3.27}$$

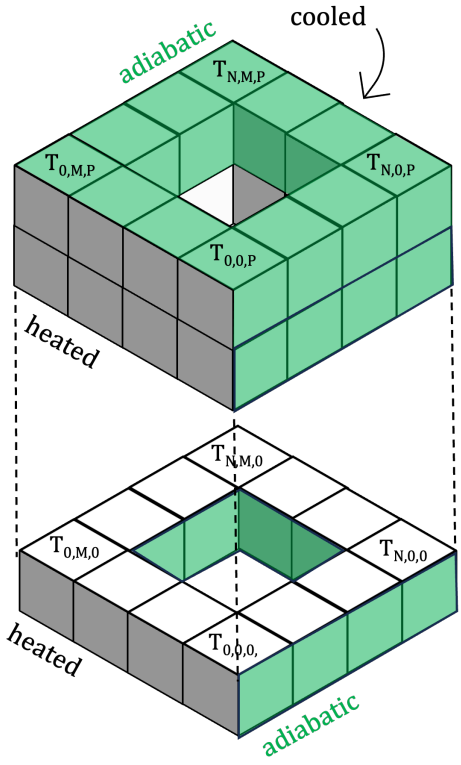


Figure 3.9: Three dimensional model mesh schematic.

3.5 Material Thermal Properties

The thermal properties for the aluminium frame are taken from EN 1999-1-2 (CEN (2007)), temperature dependant conductivity values for alloys 6xxx are used, whereas the density is assumed independent of temperature (2700 kg/m^3). The emissivity of aluminium was defined as an uncertain parameter ranging from 0.3 to 0.7. For the steel connector (bolt), conductivity and specific heat follow those for mild carbon steel from EN 1993-1-2 (CEN (2002)), the density of steel (7850 kg/m^3) was assumed to be independent of temperature. Where a thermal break is present this was assumed to be made of polyamide material with constant density (1400 kg/m^3), whilst thermal conductivity and specific heat temperature independent with ambient vallues of $0.3W/mK$ and 1470 J/kgK respectively. Polyamide melting temperature of 260°C was taken from BASF (2022). Temperature dependant thermal properties of glass were defined as in Cárdenas et al. (2016), namely specific heat and conductivity. Density of glass (2500 kg/m^3) was assumed temperature independent and for absorptance, transmittance and reflectance the values from Debuyser et al. (2017) were assumed. For air we defined temperature dependant thermal properties from Incropera and DeWit (2013). The properties of the gypsum board follow those discussed in Manzello et al. (2007), and the emissivity was taken as 0.8. The temperature dependant thermal conductivity and specific heat are shown in Figure. 3.10 for all materials considered.

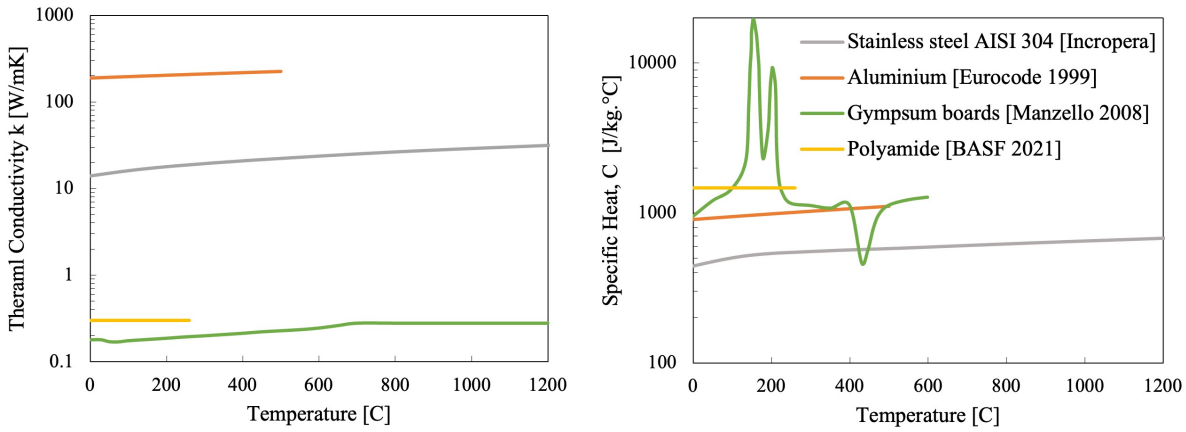


Figure 3.10: Thermal conductivity (left) and specific heat (right) for materials components a curtain wall frame. Thermal property plotted on logarithmic scale.

3.6 Model comparison

The models proposed here consider different heat transfer mechanisms as shown in Table 3.4. As expected, the level of complexity affects the simulation resources. The most complex model, the 3D model, requires up to five times more resources than the 2D model and 300 times more than the lumped mass 0D model.

Table 3.4: Comparison of model complexity.

	0D	1D	2D	3D
heat conduction	×	✓	✓	✓
heat transfer in chamber	×	×	✓	✓
non-uniform heating	×	×	×	✓
screw effect	×	×	×	✓
n of elements	1	3	6754	1113334
CPU time [s]	69	214	3982	20801

The 0D and 1D models assumes a constant temperature for each component and do not allow for the defintion of heat trasfer across the frame chamber. The 2D and 3D models allow for a non-uniform temperature distribution within a component. Thermal gradients across the supporting frame could define the possible structural consequences and need to be accurately predicted, therefore the 2D and 3D model are considered in the follwoing chapters. Additionally, the 3D model stands as the only model allowing the definition of non-uniform heating at its boundary and the only model that can capture the localized screw effect, as explored in Chapter 5.

Comparatively, the 2D model is easier to construct and quicker to run than the 3D model. It can be employed for scenarios where the heating is uniform and in unitized systems where screw connectors are not present. Unitized systems are increasingly prevalent in high-rise buildings

and are predicted to overtake the curtain wall market in the future. Therefore, the 2D model holds substantial applicability.

For the 2D and 3D model the commercially available multi-purpose finite element package LS-DYNA was selected as it has been extensively used for structures and fire (Rackauskaite et al. (2019)). The software is powerful in solving simultaneously heat transfer and non-linear problems. It has been validated for radiation in an enclosure, required for solving the radiation in the frame chambers, and for various other 3D scenarios.

Previous models for curtain wall systems assumed uniform temperatures and lacked validation through experimental data. An aluminium window frame was simulated by Guillaume et al. (2020) using a 3D model similar to the one proposed here. The frame modelled included polyamide thermal breaks and heat transfer across the frame chamber, however the model was not validated with experimental data. In the work of Badr et al. (2023) a 0D lumped model was used to predict the tempreature of the glass panel and the aluminium frame exposed to the temperature defined in a ISO standard fire.

3.7 Conclusions

In this chapter, we develop a thermal model of varying complexities to simulate the thermal response of a curtain wall framing system. Given that the system comprises various components, the heat transfer across it necessitates the definition of multiple heat transfer phenomena that interact, resulting in a non-linear problem. This work introduces a spectrum of models increasing in complexity and evaluates their performance.

The proposed models can be used flexibly depending on the fire scenario and the accuracy of the required predictions. The most complex model incorporates heat transfer through conduction across each component, convective and radiative heat transfer within the frame chamber, and considers convective and radiative boundary conditions.

Previous models for curtain wall systems assumed uniform temperatures and lacked validation through experimental data. The present models prediction are compared with experimental data in Chapter 4 and used to invetigate the thermal and structural response of a curtina wall exposed to fire in Chapter 5 and 6 respecitvely.

Chapter 4

Validation and Parameter Sensitivity Study of 2D and 3D Models

4.1 Introduction

Declaration note[1]

The Relay Building fire (Section 1.1.1) has demonstrated the fire hazard that curtain wall facades can pose to public safety and that such facades might require an added level of fire protection (passive or active), especially when used in high-rise buildings. In most western countries building regulations, the requirement for curtain walls in high-rise buildings is limited to the provision of c.a. 1 m spandrel panels assembled with elements of E 30 class of fire resistance, e.g. Repubblica Italiana (2022). This requirement is not included in the UK regulations, Ministry of Housing, Communities and Local Government (2019). Furthermore, both UK and European building regulations limit the use of combustible materials. Although these measures are useful in reducing the probability of fire propagation and falling facade elements, further studies should be conducted to verify their effectiveness in different fire scenarios as previous experiments have shown that these measures will not be effective in many cases Law and Kanellopoulos (2020).

To identify what fire protection is optimal and what changes can be made to the system to increase its fire resistance, the thermal and mechanical behaviour of curtain walls in fire needs to be understood. Analysis from first principles would allow the most suitable protection measures to be defined for each specific structure. However, understanding and predicting the fire behaviour of curtain walls is challenging because of the complexity of these facade systems Hu et al. (2016).

[1]This chapter is based partially on " F. Lugaresi, P. Kotsovinos, G. Rein (2021) *Computational study on the thermal response of curtain wall systems exposed to fire* , ***Proceedings of the 12th Asia-Oceania Symposium on Fire Science and Technology (AOSFST 2021)***. " *and partially on "F. Lugaresi, Sedlak, B., P. Kotsovinos, G. Rein (2023) Thermal response of a curtain wall framing system under fire conditions.* , ***Fire Safety Journal***. "

A few experimental and numerical studies have been conducted to assess the fire performance of curtain wall systems however measurements are limited to temperature of frame and glass, and in some cases, the deflection of the frame was also recorded in Sulik et al. (2016). Finite element models have been developed to predict the static and dynamic behaviour of curtain walls (Memari et al. (2007) & Aiello et al. (2018)). Recently Badr et al. (2023) developed a model to predict lateral deformations of glass facades during a fire. The latter model utilizes a lumped mass assumption for heat transfer, defining a uniform temperature for each of the main elements (glass panel and aluminium frame). A more advanced thermal model was developed for an aluminium window frame by Koohkan et al. (2021); however, the model was not verified with experimental data. To our knowledge, the thermal response of a curtain wall frame exposed to fire has not been systematically investigated.

This work therefore aims at rigorously investigating the 2D and 3D model introduced in 3. The frame is the most vulnerable component of the system as it is made with thin aluminium profiles, includes polymeric sections that degrade a low temperature, and is directly exposed to heat during a fire. It is also the most critical component, as it carries the load of the glass panels to the main structure. Two experiments are used to define the accuracy of the model predictions. In Section 4.5 a parametric study is carried out to identify the parameters that can be altered to improve the thermal performance .

4.2 Experimental Data in Literature

To assess the accuracy of the thermal model predictions, we searched the literature for available experimental data. A number of experimental studies have investigated the thermal performance of a curtain wall assembly in the last 25 years. These are summarized in Table 4.1 and ordered by date of publishing. Only studies which investigate typical curtain wall assemblies were included in the table. Most of the experiments conducted did not report all the required details; either the frame dimensions were missing, or the temperature was only recorded on the glass surface, or only on the frame surface. Most studied recorded the temperature at one location across the heating lenght, with only one study (Sędłak et al. (2021)) reporting temperture at two locations.

In the pioneer study by the UK Loss Prevention Council LPC (1999), a series of experiments were conducted to study the failure mechanics of a full-scale curtain wall facade. These experiments were later published in a different format in Morris and Jackman (2003), the latter entry is not included. A number of experimental studies have investigated the thermal performance of a curtain wall assembly heated uniformly in a furnace (Sędłak et al. (2013), Sulik et al. (2016), Kinowski et al. (2016)). During these experiments, temperature measurements were collected, and in some cases, the deflection of the frame was also recorded. More recently, an experiment by Srivastava et al. (2020) considered fire spread along a curtain wall with glass and aluminium composite panels and a curtain wall with masonry spandrel walls. The authors reported fall-out of intact glass panels due to the deformation of the aluminium frame.

LPC (1999) only study to measure the temperature on the brackets but the geometry and dimensions of the brackets is not reported. Deformations were measured LPC (1999) and Sulik et al. (2016). For all experiments the temperature was recorded on the unexposed side of the facade (ambient side), except for Manzello et al. (2007) where is was measured on both the exposed and unexposed surface of the glass panel, and for Nam et al. (2017) where only the temperature on the exposed side was recorded.

The experiments used different heat sources to model a compartment fire. Most experiments were conducted by fire labs which use standard furnace facilities to test the behaviour of building components. These furnace can create well defined boundaries that are easily reproduced in a model as the furnace leads to a uniform heating and a well controlled fire side gas temperature. Fire tests to certify systems are performed regularly but fire labs only collect very limited data, and reports shared with the public only contains a pass or a failure criterion. The experiments presented here were all run by the Polish Building Insitute (Instytut Techniki Budowlanej).

Peng and Zhaopeng (2016) measured the heat flux and velocities of a flame ejected from a window and impinging on a facade above and the reported value can also be used readily to define the heat transfer to the curtain wall, however the authors only measured temperatures on the glass panels while the temperature developments of the frame were not measured.

For our model verification we selected Nam et al. (2017), refered to Korean experiments hereafter, the partition wall experiment by Sędłak et al. (2021) and the curtain wall experiment by Sędłak et al. (2021). The latter two will be refered to as Polish experiments. The Korean experiment was chosed as the temperature development was recorded for both the glass and the frame. The frame had the simplest assembly - no insulation inserts or thermal break. This was also the only experiments that included repeats, as the same test was run three times. The heating boundary conditions in this experiment were non-uniform. The fire source, a small heptane pool fire, was well defined and the air temperature inside the compartment was measured at different location during the experiments, facilitating the definition of the convective boundary condition. Important to note that the temperatures were measured on the heated surface of the frame and the glass, this is the surface directly exposed to the fire.

The Polish experiment cosidered two different frame assemblies. Both assemblies included an insulation isert in the frame chamber and a thermal break, thus were useful in verifying the model prediction when such components are included. The heating boundary condition were uniform since the facades were tested in a furnace with uniform gas temperature. The partition wall experiment (Sędłak et al. (2021)) was the only experiment to included temperature measurments across the section of the frame and not just at one location either on the external or the internal surface of the facade, thus allowing a verification of the thermal gradients predicted within the frame.

Table 4.1: Summary of Experimental data on thermal response of curtain walls components heated by different fire sources. The curtain wall components considered are glazed panels, frame and brackets.

Paper	Heat source	Temperature-time measurements					
		Panels		Frame		Brackets	
		Material	Data	Material	Data	Material	Data
LPC (1999)	wood crib	double glazed	✓	aluminium/ steel	✓	aluminium / steel	✓
Manzello et al. (2007)	furniture	double glazed	✓	not defined		not defined	
Ni et al. (2012)	propane burner	double glazed	✓	aluminium		not defined	
Sędłak et al. (2013)	furnace	glazed	✓	aluminium with insulation	✓	not defined	
Sulik et al. (2016)	furnace	glazed		aluminium with insulation	✓	not defined	
Kinowski et al. (2016)	furnace	double glazed	✓	aluminium with insulation	✓	not defined	
Peng and Zhaopeng (2016)	wood crib	quadruple glazed	✓	steel		not defined	
Sędłak et al. (2017)	furnace	glazed		aluminium with insulation	✓	not defined	
Nam et al. (2017)	heptane pool	double glazed	✓	aluminium	✓	steel	
Sędłak et al. (2018)	furnace	triple glazed	✓	aluminium		steel	
Srivastava et al. (2020)	furniture	glazed		aluminium		not defined	
Sędłak et al. (2021)	furnace	glazed		aluminium with insulation	✓	not defined	

4.3 Korean Experiments

From the studies reported in Table 4.1 the experiments by Nam et al. (2017) was selected as first verification exercise and will be refered to as Korean experiment hereafter. The authors tested a curtain wall attached to the wall of a compartment of dimensions 3 m x 3.2 m x 2.4 m. The panels were double-glazed with 6 mm thick low-E glass and a 12 mm air gap in-between, supported by an aluminium frame 2 mm thick. No other information were reported nor a drawing of the section included, thus the shape and dimension of the frame had to be assumed. The frame was mechanically fixed using screws and bolts to a steel frame welded to the chambers outer wall.

Thermocouples were placed on the internal exposed surface of the aluminium frame and the glass panes. Temperature data from the thermocouples was collected from three repeated experiments of duration 100s. A pool fire of diameter D = 0.565 m was used to heat up the compartment. Heptane was used as fuel, and its mass loss due to combustion was recorded. From the mass measurements the mass loss rate was calculated as the derivative over time, $\dot{m}$. Taking the heat of combustion of heptane $\Delta H_c = 48059(kJ/kg)$ from Drysdale (2011) and accounting for incomplete combustion ($\chi = 0.9$) the heat release rate was calculated with Equation 4.1.

$$\dot{Q} = \chi \dot{m} \Delta H_c \tag{4.1}$$

The heat flux incident on the surface of the curtain wall can be approximated via the Shorki & Beyler method from Beyler (2016). In this method the heat flux is calculated assuming the flames have a cylindrical shape with a diameter equal to the diameter of the pool and with a height calculated using the Heskestad correlation. Knowing the flame height and the position of the fire relative to the target, a view factor F is calculated and multiplied by the effective emissive power E to obtain the incident radiation at the target, Equation 4.2.

$$\ddot{q_r} = F \cdot E \tag{4.2}$$

The correlation for effective emissive power proposed in the Shorki & Beyler method applies only for large pool fires ($D > 1\,m$). Therefore to obtain the emissive power E for a pool fire of $0.565m$ diameter we used data collected by Ji et al. (2021). The authors investigated the radiative flux from small heptane pool fires of radius ranging from 0.1 m to 0.4 m. The data reported included flame height and incident heat flux at 5 different locations near the flames. From these measurements the effective emissive power plotted in Figure 4.1 was calculated and by assuming a linear correlation the effective emissive power for a pool fire of $0.565m$ diameter was extrapolated. The radiative heat flux $\ddot{q_r}$ was tabulated and utilized as a boundary condition

in the simulations. The heat release rate, the flame height and the incident radiation at the two location of interest are plotted in Figure 4.2.

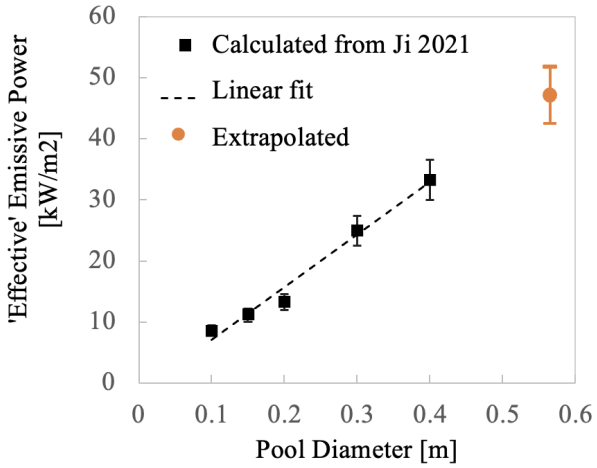


Figure 4.1: Emissive power as a function of the pool fire diameter. Experimental data from Ji et al. (2021).

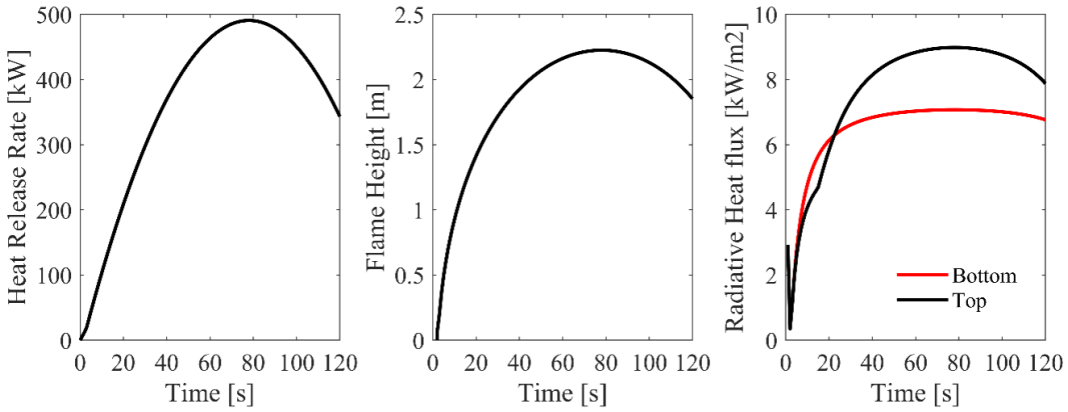


Figure 4.2: Heat release rate of heptane pool fire calculated from Korean experiment, flame height obtained from Heskestad correlation, and irradiation from pool fire at target location (bottom and top of curtain wall) calculated via Shorki & Beyler method for pool fires.

4.3.1 Comparison with Korean Experiments

The thermocouple readings from the Korean experiments are compared with model predictions for the aluminium frame in Figure 4.3 and for the glass panel in Figure 4.4. For both the aluminium frame and the glass panels the thermocouple were attached to the exposed surface (inside the fire compartment). The model's predictions cover a range of values, show as a shaded area, as we have included uncertain input parameters. Uncertain parameters are treated as random variables with a defined probability distribution and the uncertainty was propagated through a Monte Carlo simulation. The uncertain input parameters are the emissivity of the aluminium, the incident radiation from the pool fire and the convective heat transfer coefficient.

We selected only the parameters with larger and more established uncertainty. In future work, thermal properties of insulation materials and polymeric thermal breaks could also be defined as ranges and added to the uncertain parameters, as these materials can have large uncertainty in their properties. Whereas thermal properties for steel and aluminium are better defined and uniform and therefore not treated as uncertain.

The results show good alignment with the experiment for aluminium at the bottom location (red) whereas the top location (black) the model is under predicting the temperature experienced by the aluminium frame (Figure 4.3). This could be due to the fact that in the model we did not include any thermal breaks as these were not specified in the paper. Thermal breaks are polymeric sections usually made of polyamide. The presence of thermal breaks will create a resistance against the heat moving from the heated section of the frame to the unexposed section on the outside and this delay will be more visible where heating rates are higher as the heat transfer across the thermal break will lag behind. If such resistance is present the frame will see a faster increase in temperature as the heat cannot be dissipated to the ambient side of the facade and would explain the higher temperture recorded in the experiments for the top thermocouple. For glass the correlations between model predictions and experiments start to diminish rapidly after 60s (Figure 4.4). This could be due to the assumption that the radiative thermal properties, namely the absorbance and transmittance described in Section 3.2.2, are assumed constant value in the model. In fact, these properties are wavelength dependant and as the flames develop the value assumed might deviate from the real value.

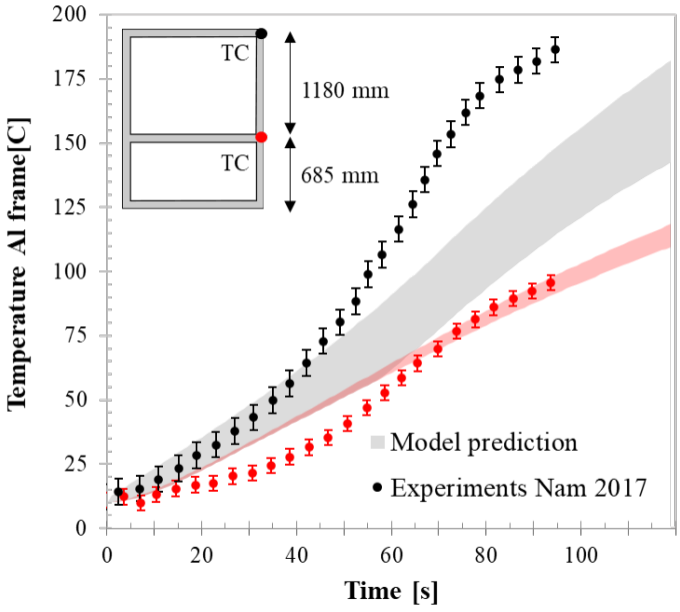


Figure 4.3: Temperature of exposed surface of the aluminium frame. Comparison of finite element model predictions and experimental data from Korean experiment. The thermocouple (TC) data from experiments was collected at two height on the frame, shown in the top left corner of the plot. Experimental data error bars include results from three repeats.

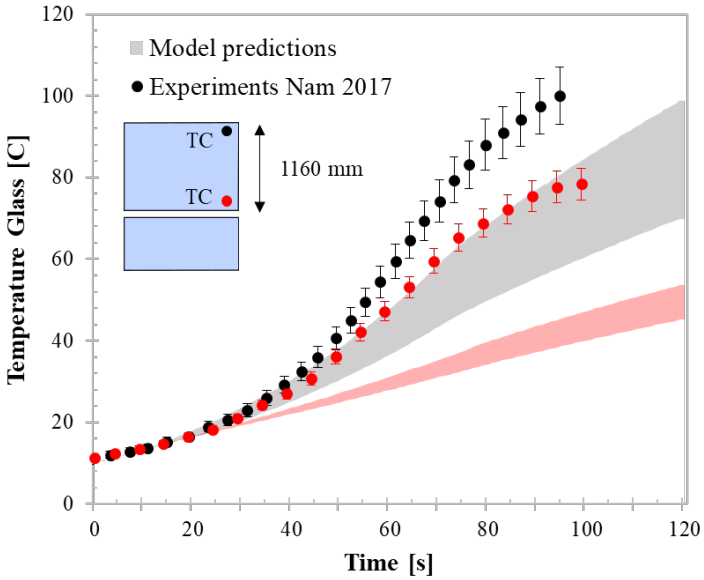


Figure 4.4: Temperature of exposed surface of the glass panel. Comparison of finite element model predictions with experimental data from Korean experiment. The thermocouple (TC) data from experiments was collected at two locations, shown in the top left corner of the plot. Experimental data error bars include results from three repeats.

The mismatch from the model prediction and the experimental data for glass and aluminium, could also come from the definition of the boundary conditions, as predicted values for both cases seem to be underpredicting the experimental measurments. Firstly, the methodology used for calculating the radiative heat flux is based on large and open pool fires whereas our fire has a diameter of 0.565 m and is burning inside a small compartment. This could lead to under predicting the heat flux as we are not considering the radiation from hot surfaces and hot gasses contained within the room. We also assumed the pool fire was placed at the centre of the room and therefore the distance to the target was taken as 1.5 m. However, the position of the pool fire is not accurately defined in the paper and therefore our assumption could be wrong. If the pool fire is closer to the curtain wall, we would be under predicting the heat flux and this would explain the temperature underprediction in Figure 4.3 & 4.4. Another error could come from how the convective heat transfer coefficient, h, was defined. The coefficient is transient but in our model we define a constant value.

Important to note that in the Korean experiments the temperatures were measured on the heated surface of the frame and the glass, and thus the thermocoupe were directly exposed to the fire. This adds a level of uncertinty to the thermocouple readings and does not allow any insight regarding the temperature distribution across the frame and the glass panels. Despite these limitations, the model still provides a reasonably adequate outcome from a practical engineering perspective.

4.4 Polish Experiments

The thermal response to fire of glazed frame systems has been investigated experimentally as part of two experimental programs that we will refer to as Partition Wall Experiments (Sędłak et al. (2021)) and Curtain Wall Experiment (Sędłak et al. (2013)). The Partition Wall Experiments involved the testing of different full-scale geometries of aluminium glazed partition wall to investigate their fire resistance. The partition walls were attached to a furnace and heated while temperature data was recorded. This is the only experiment that reports temperature evolution on both the exposed side (furnace side) and the unexposed side (ambient side) of the frame. The data is therefore very useful in our validation attempts as we can compare our predictions across the domain. Although the frame of a partition wall has a different geometry compared to a curtain wall frame, the systems share the main features. Both frames are made up of rectangular aluminium profiles connected via thermal breaks (Figure 4.5). Similarly, to a unitized system, the partition wall frame does not include any screws.

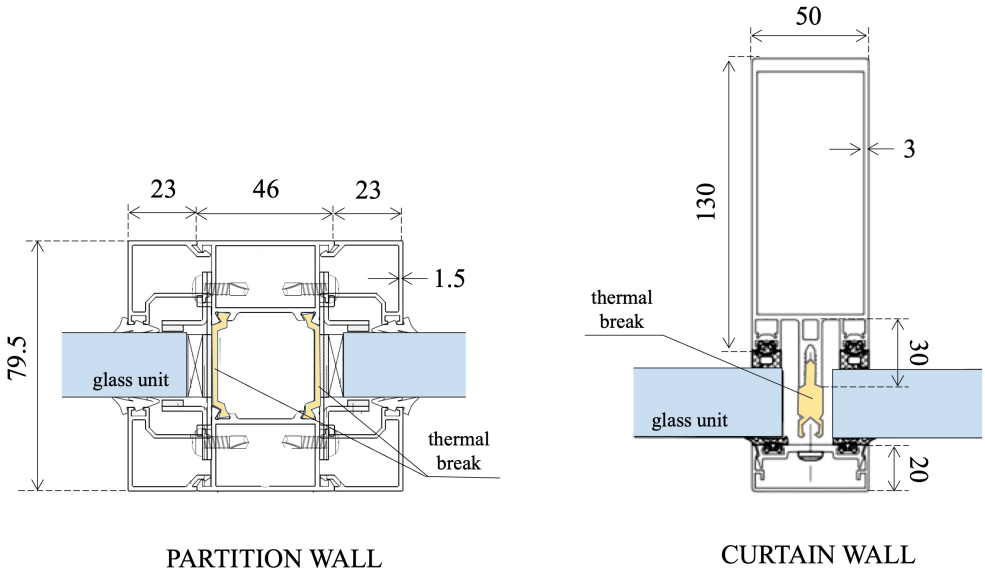


Figure 4.5: Cross section of mullion of partition wall (left) and curtain wall (right). Dimensions in mm. Glazing highlighted in blue and thermal break in yellow. Figure adapted from Sędłak et al. (2013) and Sędłak et al. (2021).

The Curtain wall experiment involved a stick system curtain wall heated via a furnace. For this experiment the same mock-up was tested twice, simulating first a compartment fire and subsequently an external fire. The temperature during heating was measured on the unexposed side only. The curtain wall mullion includes a thermal and screws spaced at 200 mm. These screws introduce a 3D component to the heat transfer and therefore a 3D model is required. Within the frame chambers an insulation insert is provided. The cross-section of both frame systems is shown in Figure 4.5.

The furnace temperature (Tf) can be assumed to be uniform and follows one of the standard

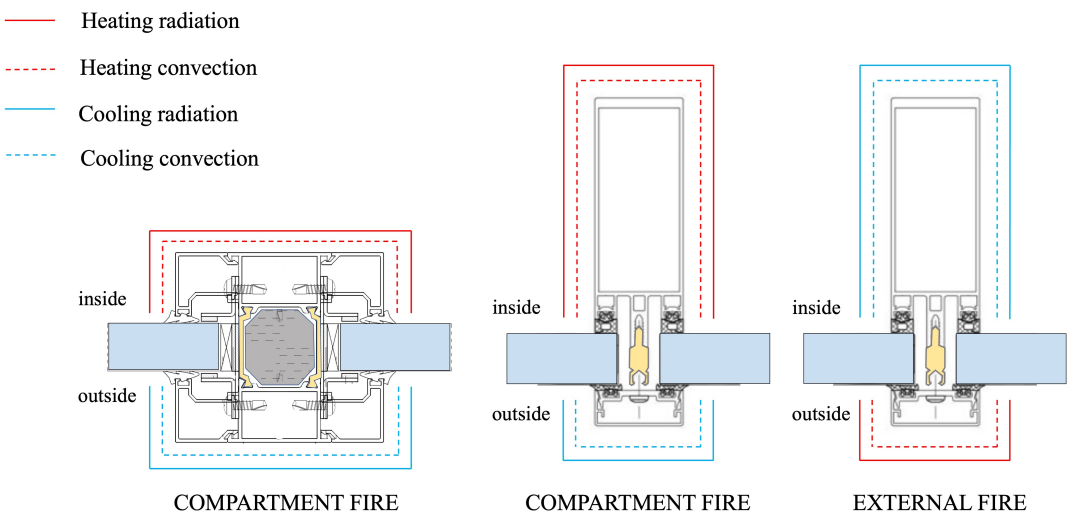


Figure 4.6: Boundary condition for the mullions of the partition wall (left) and curtain wall (centre and right) in the Polish experiments. The curtain wall was tested under a compartment fire and external fire regimen.

fire curves (standard fire or external fire from CEN (1991)) . On the fire side (inside the furnace) the frame will be heated by radiation from the furnace walls, and convection from the hot gasses. The emissivity of the furnace is assumed to be equal to 1, while the heat transfer coefficient inside the furnace is taken as $h_f = 25W/mK$. On the ambient side (outside the furnace) the frame is cooling down by radiation and convection to the ambient air ($T_a = 14$), and the convective coefficient is set as $h_a = 4W/mK$. The boundary conditions are shown in Figure 4.6.

For the partition a 2D assumption was made due to the cross-section being uniform in the longitudinal direction as well as the boundary conditions. For the curtain wall this assumption is not possible as the screws are spaced at 200 mm and add a 3D effect to the heat transfer. For the curtain wall a compartment fire or an external fire will lead to heat travelling in opposite direction leading to different temperature and gradients within the frame.

4.4.1 Partition wall

The thermocouple readings from the partition wall experiment are compared with model predictions for the aluminium mullion in Figure 4.7. The results show good alignment with the experiment on both the fire side (location P1) and the ambient side of the frame (location P2), temperature evolution generated by the model follow the same trend line as the experimental results. For the temperature predicted on the exposed side the correlations start to diminish after 28 min of heating (indicated with a vertical line in Figure 4.7). Around this time the temperature of the thermocouple located on the fire side (P1) experiences a steep increase which is probably due the flow of hot gasses inside the frame chamber. Once the section of the aluminium exposed to the furnace reaches the critical temperature of degradation of 600°C gaps will

be created allowing the hot gasses to enter the chamber. This hypothesis was further backed by the video recording of the test, as visible hot black smoke was seen seeping through the frame around that time. Although the degradation of the frame is captured by our model as shown in Figure 4.8, to model the infiltration of hot gassess a change in boundary conditions would be required, with convective heating specified on the internal surface of the frame chamber. This change of boundary conditions is not captured in our model and would explain the sudden jump of the temperature recorded by the thermocouple P1 after 28 minutes of heating.

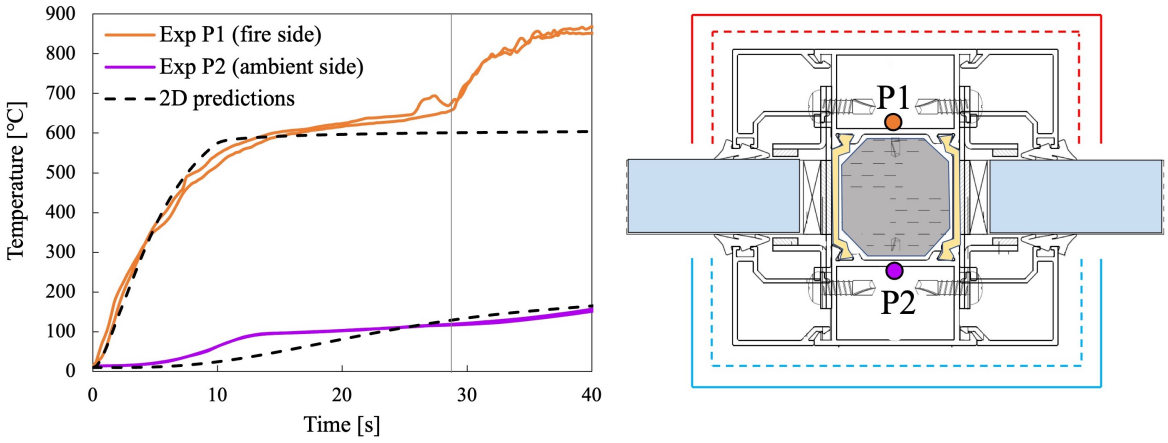


Figure 4.7: Predictions of frame temperature compared to data recorded during the Partition Wall experiment (left). Boundary conditions and position of thermocouples (right).

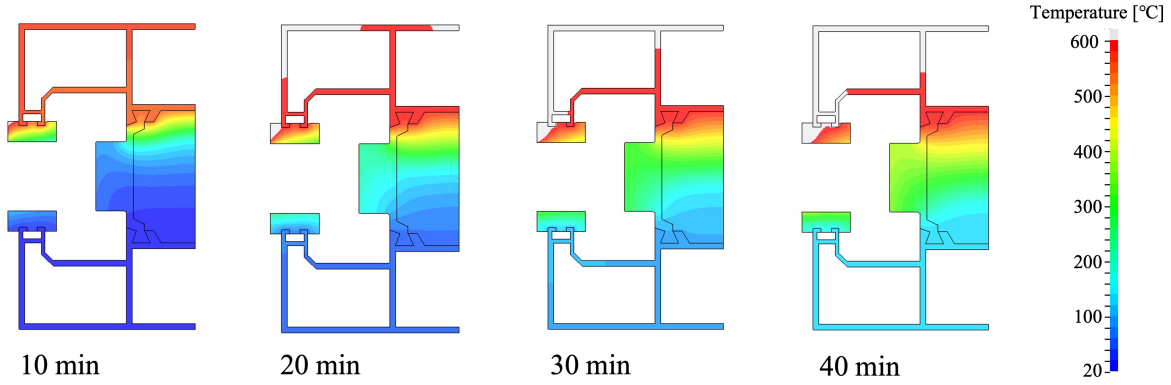


Figure 4.8: Frame temperature variation with time. The thermal degradation of the frame is visible on the exposed side (complete degradation assumed at 600°C). Only half of the partition wall frame is shown due to symmetry.

4.4.2 Curtain wall

The temperatures predicted by the 3D model are compared with the experimental results from the Curtain Wall experiment. In this experiment, two identical curtain wall assemblies were exposed to a compartment fire and an external fire. Figure 4.9 compares the simulation prediction for these two cases with the measured temperarture of the aluminium mullion for each

experiments. The experimental data for the compartment fire shows a very steep increase in the temperature of aluminium after approximately 10 min of heating. The sharp temperature increase was not reproduced by our model. At that time, it is believed that the gaskets sealing the joints between the glass and the aluminium frame lost their integrity. In video recordings of the tests, the gaskets was observed burning and falling off the facade after just a few minutes of heating, whilst visible hot black smoke was seen seeping through the frame. As discussed for the partition wall experiment, the creation of gaps due to the loss of the gasket allowed hot gases to escape from the furnace and reach the external side of the facade. In this scenario the thermocouple would recieve heat from the hot gassess explaining the sudden jump.

Similarly for the external fire, after approximately 30 minutes of heating the thermocouple start recording unstable temperatures (Fig. 4.9), and the predictions deviate from the experimental curves. This mismatch could be due once again to the breach of the sealing which allowed gases to escape from the furnace. The change in boundary conditions is not captures in our model and would expain why the prediciton give accurate results for the first 20/30 minutes of heating and then start diverging.

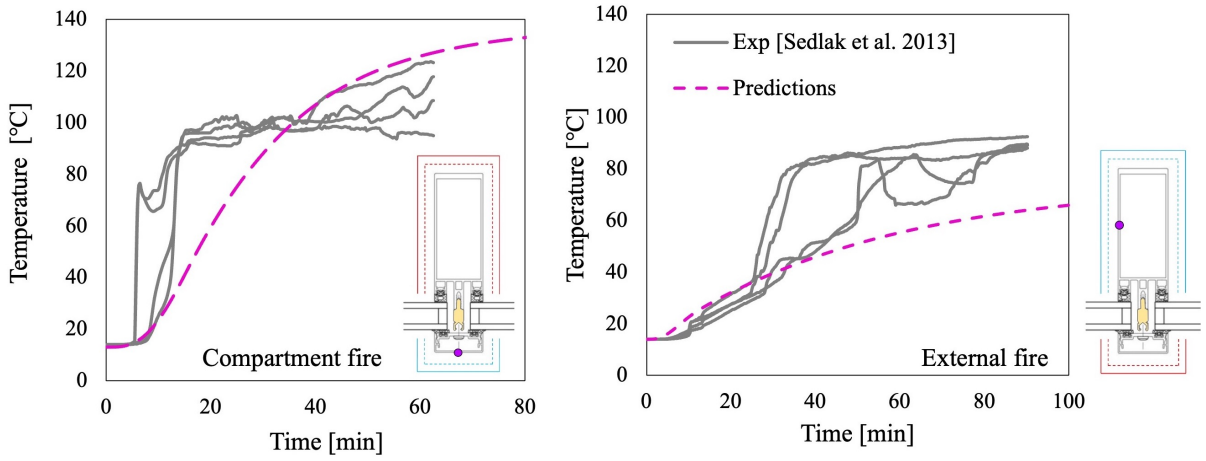


Figure 4.9: Predictions of temperature of frame in compartment fire (left) and external fire (right) in comparison to experiments. The boundary conditions and thermocouple locations for each scenario are sketched.

Gaskets are combustible and can ignite; however, make up a very small percentage of the overall mass and should not lead to severe negative effects in a fire scenario. These elements melt at very low temperature (130 - 270°C) creating passage of hot smoke and gasses. Although their failure is not as critical as the failure of the thermal break, since gaskets do not influence the mechnical response of the frame, the loss of the gaskets might lead to failure of the glass panel as local stresses are created when contact between the aluminium and the glass is made. Most importantly, the influence of gaskets and their integrity on the heating of the frame system has been found to be relevant, and therfore they should be considered carefully when modelling both the thermal and mechanical response of the frame system.

Temperature distibution of the curtain wall frame predicted by our model is shown in Figure 4.10 for the compartment fire. The onset of thermal degradation is placed between 10 minutes (frame temperature ≈ 500 ℃ in Fig. 4.10) and 20 minutes. After 20 minutes most of the structural frame will have reached the critical temperature for thermal degradation (again shown in Fig. 4.10). This prediction alings well with the temperatures reported in the experiments, as the sudden jump in the thermocouple readings is observed around 10 minutes. The consumption of the structural frame, the load bearing element of the system, is a critical event not only for the thermal response of the system as it leads to a change the boundary conditions, but most importantly it is critical for the mechanical response, as the stability of the system is not guaranteed once the frame is consumed.

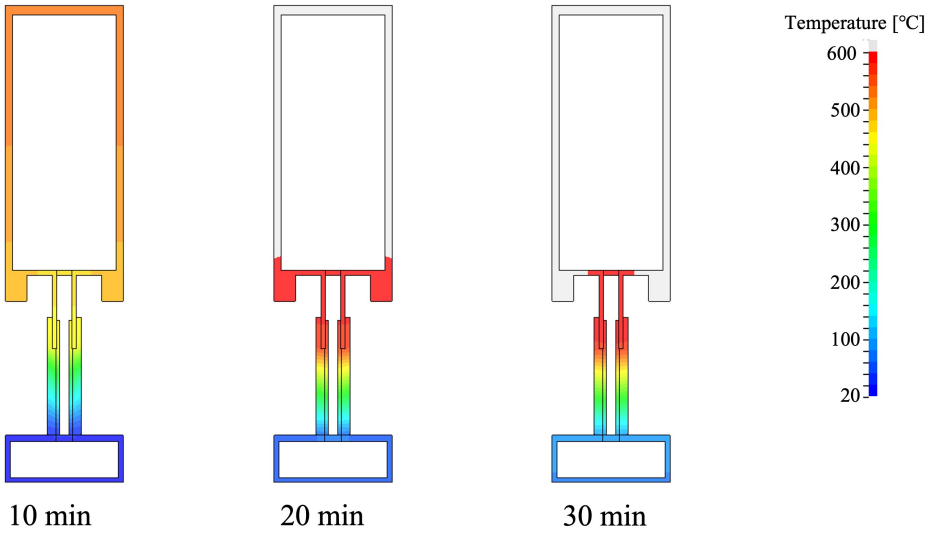


Figure 4.10: Frame temperature distribution after 10, 20 and 30 minutes of heating during the compartment fire exposure. The thermal degradation of the frame is visible on the exposed side (complete degradation assumed at 600℃). The steel screw is not shown.

4.4.2.1 The Screw Effect

As described in Section 3.2.3, the pressure cap is connected to the structural frame via steel screws and a thermal break. The thermal break is continous whereas the steel screws are spaced along the lenght of the extruded elements. In Figure 4.11 the prediction of the 2D model with a steel screw connector only, 2D model with a thermal break connector only, and the 3D model with both steel screw and thermal break, are compared with the experimental data from the compartment fire experiment. The 3D model includes a continous thermal break and stainless steel screws spaced at 200mm along the frame lenght. The 2D model with the steel screw is over predicting the temperature of the pressure cap, while the 2D model with the connector modelled as a polimeric thermal break is under-predicting. The 3D model, which includes both the steel screw and the thermal break, exhibits a better match with the experimental data which hihglights the need to include both connectors to predict the correct thermal behavious in the assembly.

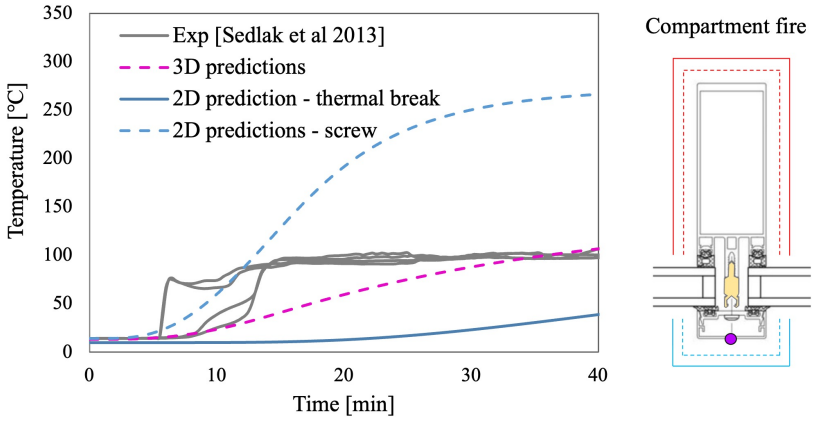


Figure 4.11: Predictions of 2D model with steel screw, 2D model with thermal break, and 3D model with screw and thermal break verified against data from Curtain wall experiment for the compartment fire test. Boundary conditions and location of temperature shown on the right.

This effect of the screw on the heat flow across the frame is shown in Figure 4.12. The steel screw is acting as a heat sink, taking the heat away from the heated structural frame. The heat, once it has reached the pressure plate, will have a wider surface for cooling. The pressure plate is located on the ambient side of the curtain wall and will be exposed to ambient air. Therefore the screw needs to be considered as without it the heat would not be able to move thorugh to the pressure plate and the temperature predicted within the frame wouls be much higher.

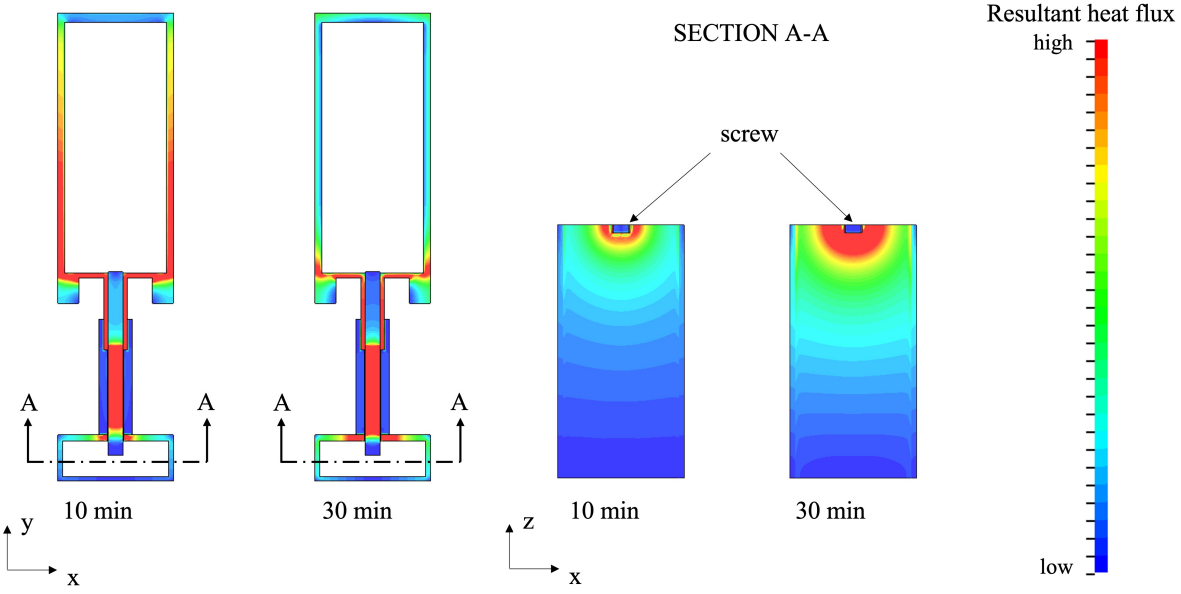


Figure 4.12: Resultant heat flux in frame and along the pressure plate (shown in section A-A) for 3D model after 10 and 30 minutes of heating. Heat flux values are simplified as high and low as reporting the actual vaules is superfluous.

4.5 Parametric Study

To investigate which material and heating parameters have the greatest effect on the thermal response of the frame we performed a sensitivity study. The input parameters investigated are listed in Table 4.2 and their base input value is reported. We consider how each of these parameters effects two different model outputs. The first output that we consider is the time it takes for the exposed side of the frame to reach 500 ℃, t_{500}. The second output parameter that we consider is the maximum temperature experience by the unexposed side of the frame after 40 minutes of heating, T_{max}.

Table 4.2: Values of input parameters investigated in the sensitivity study.

Parameter	Base value	Definition
k_{fr}	190	thermal conductivity of frame
c_{fr}	903	specific heat of frame
ε_{fr}	0.7	emissivity of frame
k_{th}	0.3	thermal conductivity of thermal break
c_{th}	1470	specific heat of thermal break
k_i	0.18	thermal conductivity of insulation
c_i	950	specific heat of insulation
T_a	10	temperature on the ambient side
h_a	4	heat transfer coefficient on the ambient side
$T_{\infty,f}$	1200	gas temperature on the fire side
T_f	1200	flame temperature on the fire side
h_f	25	heat transfer coefficient on the fire side
h_{ch}	4	heat transfer coefficient in the frame chamber

We chose these output functions as they represent to critical scenarios: t_{500} is a proxy for how fast the heated section of the frame will heat up and by altering this parameter we can hope to reduce the time to failure of the frame. T_{max} is crucial if we are interested in reducing the amount of heat travelling to the ambient side.

One-at-a-time analysis is the technique to quantify the sensitivity levels of different parameters. Two one-at-a-time (OAT) analysis approaches are used here: scatter-plot and sensitivity coefficient (Yuan et al. (2019)). Scatter plot is a graphical sensitivity analysis approach, which can reveal how the output changes (increases or decreases) with the parameter of interest while the other parameters fixed at their base values. Figure 4.13 is the result of scatter plot analysis. Every line displays how the simulated predictions changes with the variation of a unique. For the convenience of comparison, the variation of different parameters has been normalized and presented as a percentage change in respect of the base value.

The sensitivity coefficient is the derivative of output (y) with respect to the parameter of interest (X). Since the parameters compared here have different units, the dimensionless sensitivity

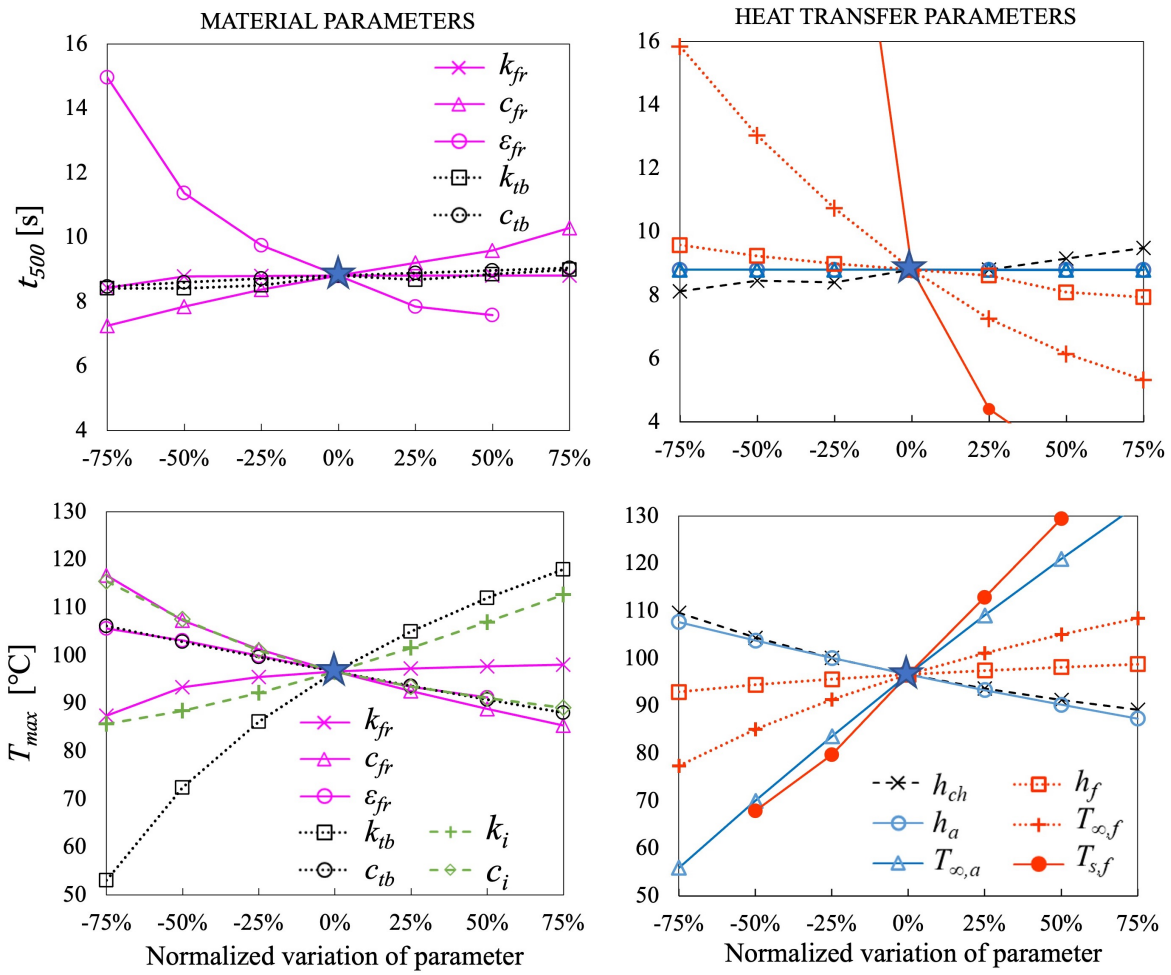


Figure 4.13: Scatter plot of one-at-a-time sensitivity study of material (left) and heat transfer input parameters (right). Results for output function t_{500} (top) and T_{max} (bottom). Material parameters colour coded for components: pink - structural frame, black - thermal break, green - insulation. Heat tranfer parameter colour coded: red - fire side, blue - ambient side.

coefficients $\bar{S}$ is calculated by Eq.4.3 and plotted in Figure 4.14.

$$\bar{S} = \frac{y(X_0 + \Delta X) - y(X_0)}{\Delta X} \frac{X_0}{y(X_0)} \tag{4.3}$$

By comparing the sensitivity coefficients, we can define the parameter that can be changed during the design to have the greatest impact on the heating of the system. For example, changing the material used for the frame will have the greatest effect on the temperature experienced on the exposed side (see c_{fr} and ε_{fr}). However, to reduce the heat transfer to the unexposed side, we need to change the thermal break (k_{tb}) or insulation material (k_i).

The temperature on the fire side ($T_{\infty,f}$ and $T_{s,f}$) can be decreased with measures such as sprinklers and window drenchers; however, the effect of active protection is beyond the scope

of this study and will not be discussed further. Such measures would be highly effective. As shown in Figure 4.14, the heating of the frame is extremely sensitive to the temperature of the fire, particularly when considering the heating of the exposed side.

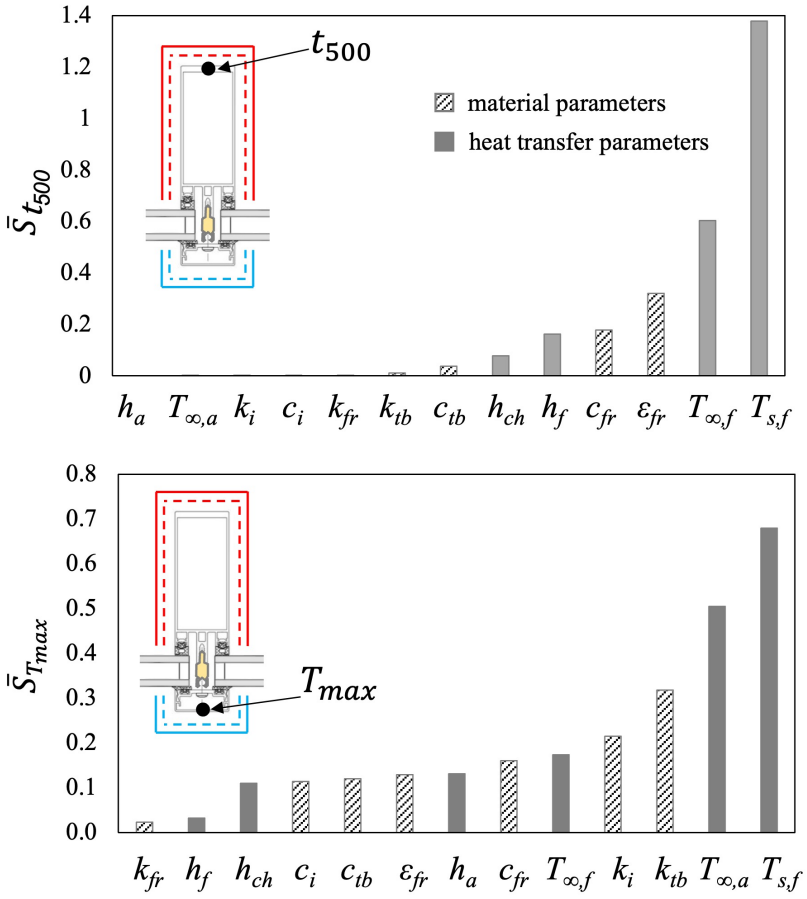


Figure 4.14: Sensitivity coefficient for material and heat transfer input parameters. Results for output function t_{500}(above) and T_{max} (below). Sensitivity coefficient plotted in increasing order.

4.6 Conclusions

Structural frame and the pressure cap are essential components for ensuring the stability of glass panels. Two typical systems are considered: a stick system and a unitized system. The role of the screw connector is explored with regard to the thermal response. We compared the model's predictions against experimental data from a partition wall experiment and a curtain wall experiment, and highlighted the mechanisms that our model does not include, which could lead to a mismatch with the experimental data.

The results of the validation study indicate that the 2D model is able to capture the thermal response of a heated frame and is able to capture all the physical phenomana that define the thermal response of the frame. The temperature gradient across the frame was predicted within acceptable level of accuracy. This is expected as the model considered were the most detailed model proposed in Chapter 3. The results show that the physical phenomena simulated by

the model show good agreement with the experimental result. More experimental evidence is necessary for further development and improvements of the model and the models predictions.

The results of the sensitivity study indicate that changing the frame material and reducing the fire intensity will affect the temperature experience on the fire side of the facade. Whilst the temperature on the ambient side (not exposed to heating) is mostly sensitive to changes to the thermal break material.

The model presented can be used as a tool to advance our understanding of curtain wall frame fire behaviour and can be coupled with a model of the frame displacements to predict structural failure. Such tools can aid in the development of more effective fire strategies and resilient facade systems, ultimately enhancing public safety and minimizing economic losses due to fire incidents.

Chapter 5

Thermal Failure Criteria of Curtain Wall Framing System Exposed to Fire

5.1 Introduction

Declaration note [1]

The evaluation of the fire performance of curtain walls is typically based on fire testing, where the facade is heated in a furnace and its resistance is measured as the time to failure. The mechanical behaviour of the facade is rarely taken in consideration in experiments that focus mostly on the thermal response, and where it is considered is usually limited to the behaviour of the glazed elements and the prediction of glass breakage. The only more relevant study considering the mechanics of failure of the whole facade assembly dates back to LPC (1999).

Considering the complexity in understating the failure behaviour of the whole facade we have decided to use here a simple thermal failure criteria for the framing system. Critical member temperature failure criteria are considered for each frame material. This chapter investigates the effects of different frame material, different levels of protection, and the addition of a thermal break.

An extruded frame representative of a generic curtain wall frame element (mullion or transom) is modelled using the general finite element software LS- DYNA. The 3D thermal model is described in Chapter 3. The fire exposures investigated include ISO- 834 standard fire, the ISO external fire and the Eurocode parametric temperature curves. The temperature development across the frame and the thermal gradients are analysed for each case to identify the thermal response of

[1] This chapter is based partially on " F. Lugaresi, P. Kotsovinos, G. Rein (2021) *Computational study on the thermal response of curtain wall systems exposed to fire* , ***Proceedings of the 12th Asia-Oceania Symposium on Fire Science and Technology (AOSFST 2021)***. " *and partially on "F. Lugaresi, Sedlak, B., P. Kotsovinos, G. Rein (2023) Thermal response of a curtain wall framing system under fire conditions.* , ***Fire Safety Journal***. "

the frame which can be used in structural models to predict the mechanical behaviour.

Experiments are difficult to set up and require large resources. Most experimental studies involve a single or small number of experiments, and each experimental investigates a single specific scenario. With a computational model many different scenarios can be studied as running the model requires less resources.

5.2 Behaviour of Curtain Wall Support Structure

The dead load of a curtain wall is carried down to the foundations through the main structure. To reduce the weight of the facade and to avoid overloading the main structure, engineers employ aluminium alloys for the frame element. Aluminium is a relatively cheap and lightweight material, with a lower strengths and stiffness than structural steel. Aluminium is also very good at conducting heat and experiences large thermal strains. When heated it losses strength and stiffness rapidly (Figure 5.1). For these reasons aluminium elements are very sensitive to heat and are prone to deformation and failure when involved in fire. In a similar manner, steel will also lose stiffness and strength when heated (Figure 5.1) however this will happen at higher temperatures.

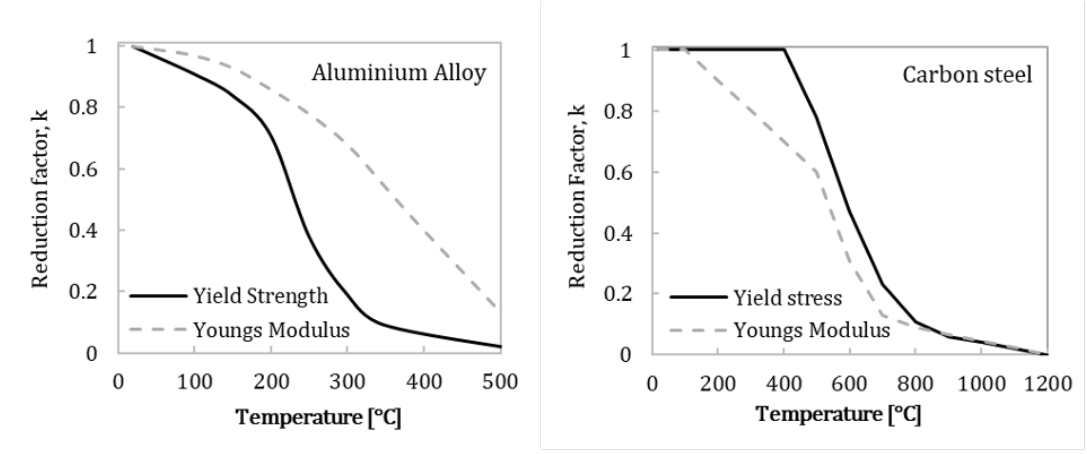


Figure 5.1: Strenght and stifness reduation for aluminium (left) and carbon steel (right) due to high temperature. From Eurocodes CEN (2002) and CEN (2007)

Frequently the frame elements are composed of an outer and inner aluminium profile connected by a polymer section referred to as a thermal break. Thermal breaks are plastic low conduction insertions designed to create some resistance against the transfer of heat across the aluminium profiles and minimize heat losses during cold months. These small elements must be considered carefully as they will melt at lower temperatures than the otherwise aluminium element, accelerating failure. An aluminium window frame was simulated by Guillaume et al. (2020) in their reconstruction of the Grenfell Tower fire. The frame modelled included polyamide thermal breaks with a melting temperature of 200°C. In their simulations the glass windows cracked before frame failure, however once the frame failed, the cracked window was shown to fall-out.

The failure considered in this chapter for the aluminium frame is the complete thermal degradation. The point of complete thermal degradation is taken as the temperature at which phase change occurs and the aluminium elements melts away. This is the upper boundary when considering the failure time as other failure modes will occur earlier and this is the last event as it involves the frame loss of integrity. If the element that reaches complete thermal degradation is the structural frame, the glass panels, if still in place, will fall out. In addition, when gaps are created in the frame due to degradation of the frame, internal flame spread could be facilitated along the voids on the system Koffel et al. (2005).

5.3 Results

5.3.1 Influence of insulation insert and thermal break

In this section, the influence of insulation inserts and thermal breaks on the thermal performance of the frame is evaluated. The frame assemblied investigated are shown in Figure 5.2. In some cases, insulation might be inserted in the frame chamber of the aluminium frame to improve the thermal and fire performance of the frame. To model an insulation material within the frame chamber, perfect contact is assumed between the aluminium frame and the insulation, and temperature dependant thermal properties for the gypsum plasterboard are taken from Manzello et al. (2008). In addition, the connection between the inner structural aluminium frame and the outer pressure cap can be made via a thermal break. Thermal breaks are made of plastics with low thermal conductivity, designed to create some resistance against the transfer of heat across the aluminium profiles.

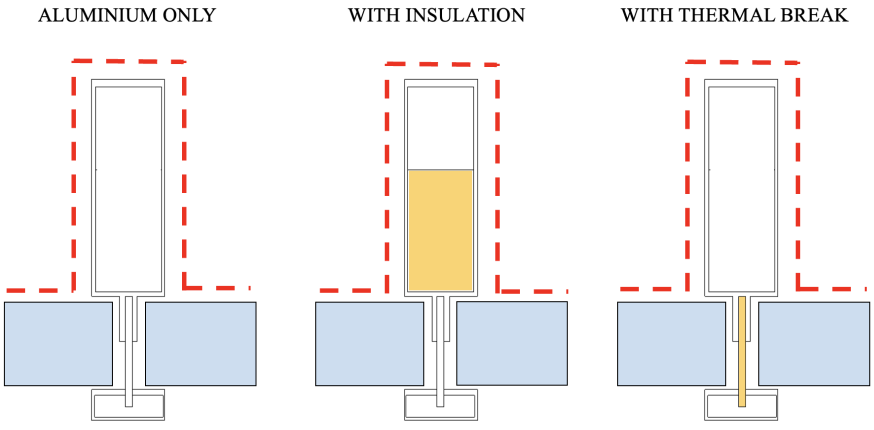


Figure 5.2: Section of frame system investigated. Form left to right: aluminium frame, aluminium frame with half of the frame chamber filled up with insulation, aluminium frame with a thermal break as connector element between external and internal sections. Red dashed line indicates heated surface.

The results from our simulation in Figures 5.3 and 5.4 show that the structural frame (T_1 and T_2) will experience a larger gradient when the insulation is present whilst the gradinet will be

minimized when the thermal break is present. The insulation will be obstructing the radiation inside the frame chamber and absorbing the heat from the hotter walls, slowing down the heat trasnfer from the heated sections of the frame to the cooler side (T_2). The temperature predicted in location 2 for the case with insulation is thus lower compared to a case without insulation (aluminium only). The exposed section of the frame will reach 650℃, the melting temperature of aluminium, in less than 10 minutes for both frames with and without insulation. Without the insulation inserts the aluminium frame will start melting a few minutes earlier compared to a frame with insulation inserts. The aluminium pressure cap never reached the melting point and levels off at around 400℃. The temperature difference between the frame with and without insulation at the pressure cap is negligible.

When a thermal break is present the structural frame will reach thermal degradation faster than the other cases whilst the pressure cap on the ambient side of the facade will be heating very slowly. After 11 minutes the structural frame will have completely degraded (T_1 and T_2 have reached 650 ℃), while the pressure cap will be experiencing a temperature of only 70℃ (T_3). This is important to note since during fire tests for curtain wall facades the temperature is always measured on the ambient side (e.g., on the pressure cap) and therefore will be much lower than the temperature experienced by the actual aluminium frame. A temperature difference in excess of 300℃ between the pressure cap of the frame with thermal break and without thermal break is predicted. When the thermal break is present a large gradient will develop across the thermal break (between T_2 and T_3) and the gradient across the structural aluminium frame will become negligible (see 5.4).

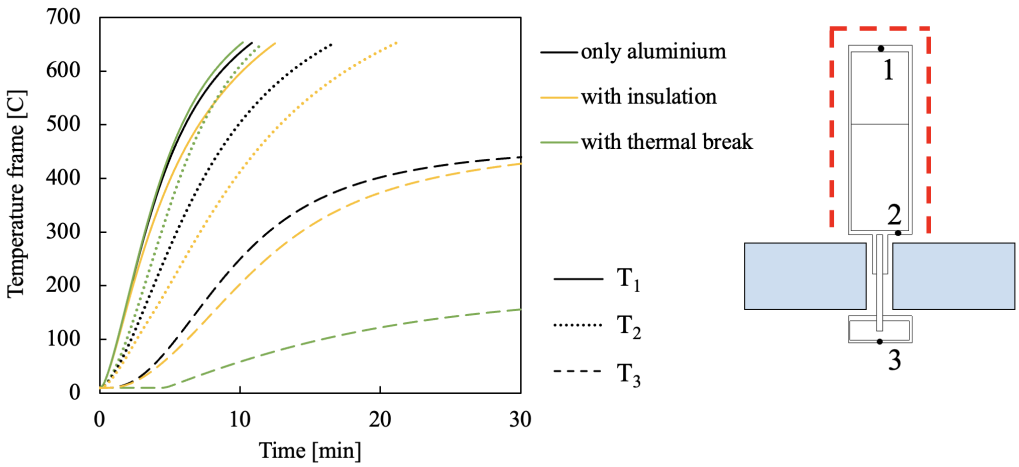


Figure 5.3: Temperature development in aluminium frame, aluminium frame with insulation insert and aluminium frame with polymeric thermal break exposed to a ISO standard fire (left). Section of the frame with temperature location and heated surface (right).

In Table 5.1 the time to thermal degradation of the aluminium frame for each different case is compared. Thermal degradation of the frame is defined as the time when the aluminium frame has experienced a temperature of 650 ℃. From the simulation it can be deduced that the frame

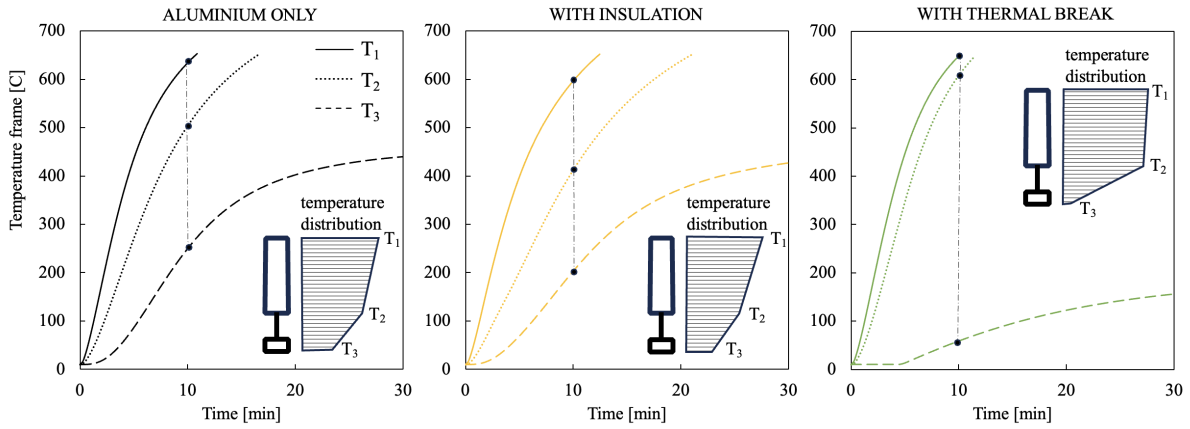


Figure 5.4: Temperature development and distribution in aluminium frame (left) , aluminium frame with insulation insert (middle) and aluminium frame with polymeric thermal break (right) exposed to a standard fire (ISO).

with thermal break will degrade quicker, followed by the frame with aluminium only. The frame with an insulation inserts will take longer to completely degrade. Important to note how for all three set ups the frame will melt very rapidly, after only 10 to 20 minutes of heating.

Table 5.1: Time to thermal degradation of aluminium frame, defined as the time when the cooler section of the frame not directly exposed to the hot temperature (T_2) reaches the melting temperature of aluminium.

Scenario	Time to degradation t_{deg}(min)
aluminium only	17
with insulation	21
with thermal break	12

In Figure 5.5 the temperature gradients, Δx, in the aluminium frame are compared. Δx is defined in Equation 5.1 as the difference between the temperature T_1 on the exposed side of the aluminium frame and T_2 on the unexposed side divided by the distance Δx. Thermal gradients are considered as they will have a strong influence in the structural response of the frame. Thermal gradients can cause the frame to deflect and bow, and excessive deflection could lead to fall out of the glass panel. When the insulation insert is present the frame will experience a larger gradient and therefore the possibility that the frame will deflect is increased by inserting an insulation insert. On the other hand, the insulation itself might be providing some stiffness to the frame. When a thermal break is present the thermal gradient is reduced as the heat is trapped on one side of the frame.

$$\Delta T = \frac{T_1 - T_2}{\Delta x} \tag{5.1}$$

Thermal gradients across the frame will define the possible structural consequences and need to be accurately predicted. For all cases investigated the thermal gradients across the frame were substantial with peak temperature differences of 100 ℃ to 200 ℃. This suggests that a curtain wall frame in a fire scenario is likely to bow, potentially creating gaps allowing flames and smoke to spread to upper floors, or in some scenarios pushing the glass panel out of the frame.

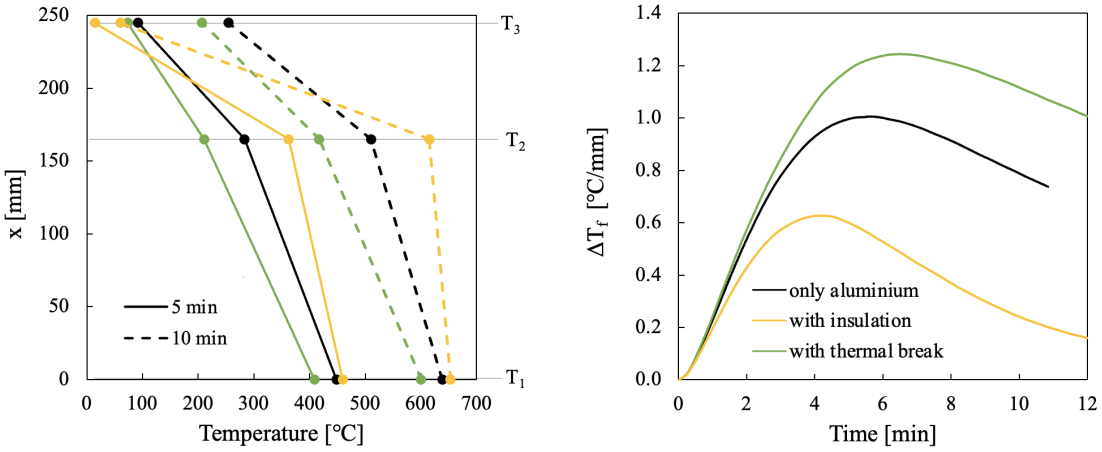


Figure 5.5: Temperature distribution after 5 and 10 minutes of heating (left) and linear thermal gradient across structural frame during heating (right). Values reported for a aluminium frame, an aluminium frame with an insulation insert and an aluminium frame with polymeric thermal break exposed to a ISO standard fire.

5.3.2 Thermally protected Frame

As discussed in Section 4.5 , if we want to modify the system to increase its fire performance, the most effective modifications will require either changing the material of the structural frame or reducing the fire temperature. As mentioned previously, we will not consider measures to control and reduce the intensity of the fire (e.g. sprinklers); however, we can control the heat received by the frame by adding some extra layers that shield it from the flames.

A typical curtain wall aluminum frame system was modelled, including a polymeric thermal break, insulation inserts, and steel screw connector. The simulation results indicate that failure due to thermal degradation of the aluminum frame is very rapid, occurring within the first 15 min of fire exposure for the ISO-834 standard fire. The thermal response of the standard frame was compared with that of a thermally protected frame. The frame was protected by applying a 10 mm gypsum board, essentially encapsulating the aluminium frame. The properties of the gypsum board follow those discussed in Section 3.5. The results shown in Figure 5.6 show the delayed heating for the encapsulated frame which does not reach thermal degradation during the 40 minutes of heating simulated here.

5.3.3 Steel Frame

The temperature evolution of a frame assembled with different materials, namely carbon steel and stainless steel is also investigated. The simulation predictions are shown in Figures 5.7 and

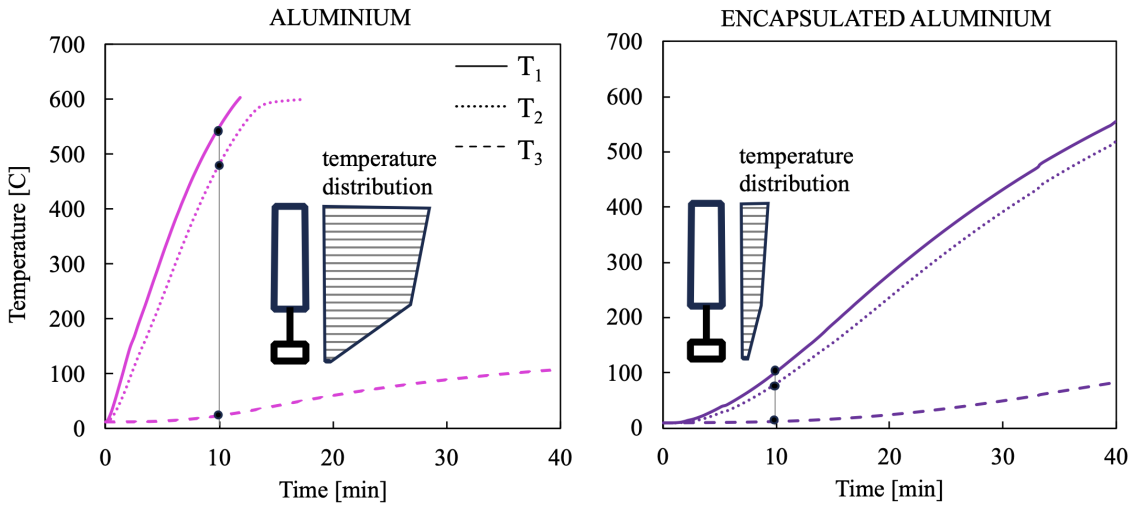


Figure 5.6: Temperature development and distribution of aluminium frame (left) and encapsulated aluminium frame (right) exposed to a standard fire (ISO).

5.8. The properties for stainless steel were defined in Section 3.5, for carbon steel we follow the properties indicated in Eurocode 3, CEN (2002). Both frames have a similar thermal response, with the stainless steel frame lagging behing slightly (Fig. 5.7). The pressure plate start heating up with a delay of 20 minutes and only experiences a slight temperature increase during heating. The stainless steel frame presents a quasi linear temperature distrubution (Fig. 5.8) as the connector is defined as a stainless steel bolt and thus the frame is virtually homogeneous.

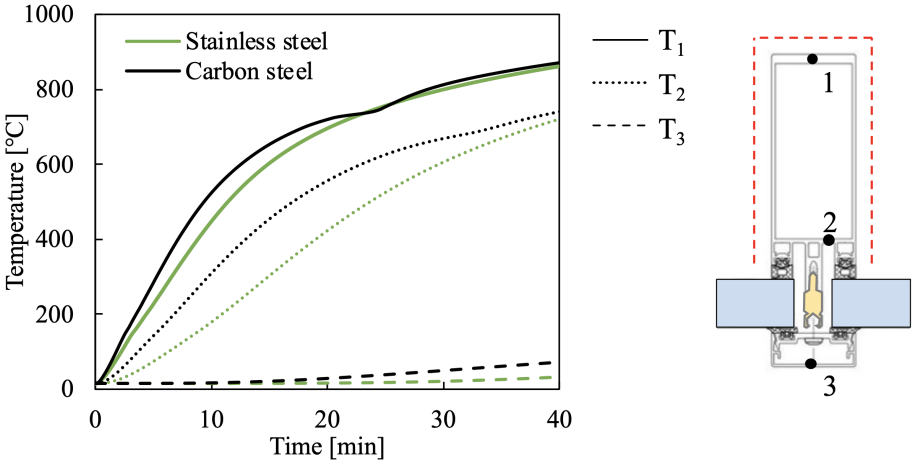


Figure 5.7: Temperature development for stainless steel frame and carbon steel frame exposed to a ISO standard fire. Temperature presented refer to location 1, 2 and 3 shown in sketch.

Carbon and stainless steel have high critical degradation temperatures, and their thermal degradation was not predicted. This indicates that curtain wall systems with steel profiles resist longer and provide a safer alternative to typical aluminium frames. However, materials are chosen not

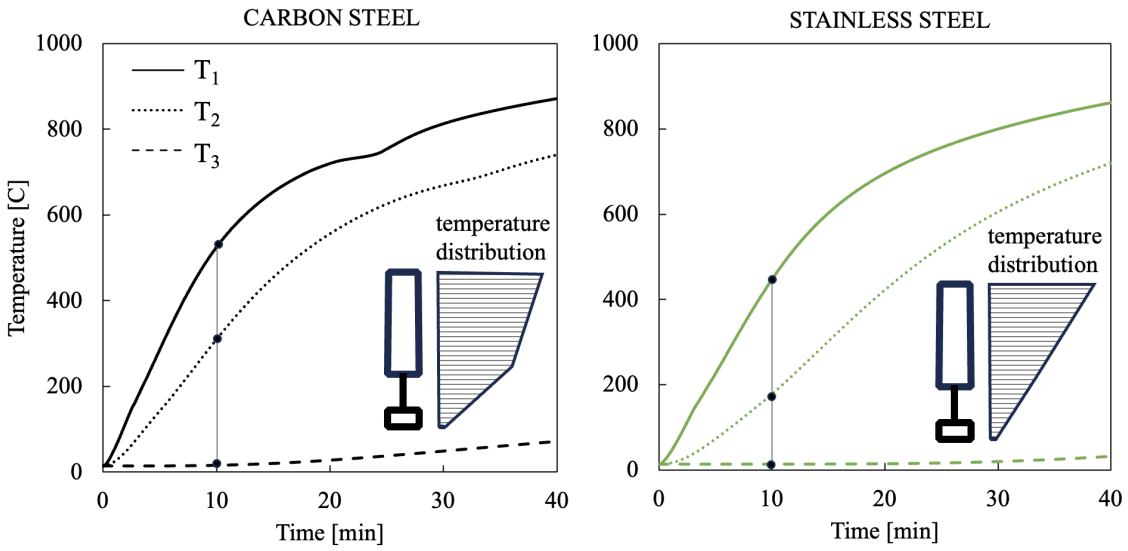


Figure 5.8: Temperature development of stainless steel frame (left) and carbon steel frame (right) exposed to a standard fire (ISO). Thermal gradients across the frame after 10 minutes of heating are show in sketches.

only for their heat transfer properties, and therefore might not be easily swapped, as there are other constraints that facade designers need address.

5.3.4 Fire scenarios

In all previous simulations we considered the ISO standard fire curve, here we investigate different fire scenarios and their effect on the thermal response of the frame system. Gas temperatures for the fire scenarios considered are shown in Figure 5.9; the external temperture-time curve and the Eurocode parametric short-cool (SC) and long-hot fires (LC). The ISO standard fire curve is also included for comparison.

The temperature of the frame system for each fire scenario investigated in this section are shown in Figure 5.10. For the parametric LC curve the frame heats up following the same trend as the ISO standard fire curve but with a slight delay, the structural frame starts degrading after 13 minutes (T_1) but only reaches complete degradation after 21 minutes (T_2), whilst the thermal break will fail first after only 15 minutes. For the SH scenario, degradation of the structural frame is very rapidly, just after 9 minutes of heating, this is the time it takes for T_2 to reach compete degradation. In the External fire scenario, the frame is heated on the external side of the building, as shown in the sketch, so the heat flow is in the opposite direction compared to the previous cases. For the external fire curve again the onset of failure is very rapid, and the element that fails first is the thermal break just after 8 minutes.

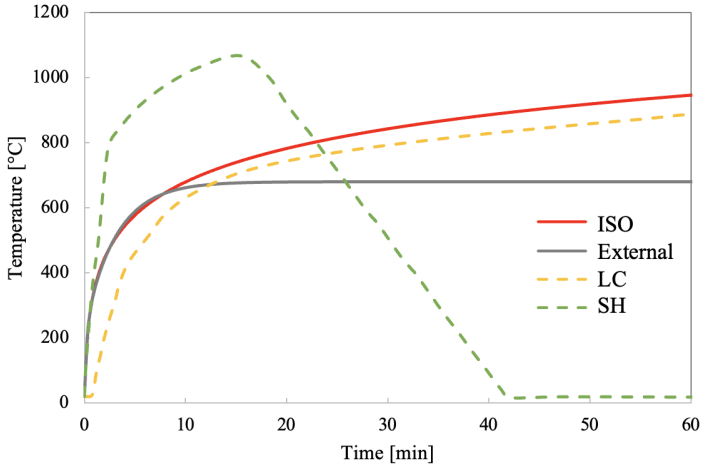


Figure 5.9: Gas temperatures for the considered fire scenarios. Standard fire curve (ISO), external fire curve, short-cool (SC) and log-hot(LH).

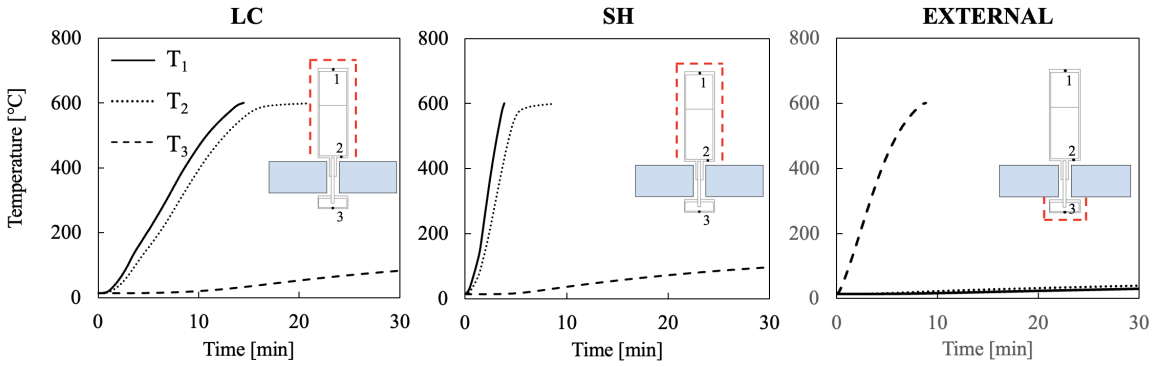


Figure 5.10: Temperature development of aluminum frame exposed to different fires. Temprature presented at three locations, T_1 and T_2 on two opposite sides of the structural frame, and T_3 on the external pressure late. For eah scenario the heated surface is shown in sketch by the red dashed line.

5.4 Discussion

The temperatures recorded at the pressure plate and at the structural frame for the different frame systems exposed to the standard fire curve are shown in Figures 5.11, whilst the temperature distibution across the system and the gradinet across the structural frame are shown in 5.12 for comparison. Considering 5.11, the stainless steel frame experiences very little heating at the pressure plate. The aluminium frame heats quicker than the other systes and whilst the frame reaches complete degradation in just over 17 minutes, the pressure plate during the simulated heating phase experiences a maxumu temperature $\approx$ 100 °C. When considering the temperature experienced by the pressure plate, the most effective measure is to utilise a stainless-steel frame. Considering the temperature of the exposed side, the addition of thermal protection has the largest impact on the temperature of the frame. When thermal protection was present, the

aluminium did not reach the critical degradation temperature during the heating phase.

The model predictions can be simplified into two independent linear gradients, as illustrated in Figure 5.12. The largest thermal gradient occur between the internal structural frame and the external pressure cap due to the presence of the thermal break ($120 \leq x \leq 185$). However the gradient of interest when considering the mechnical response is the gradient across the structural frame ($0 \leq x \leq 120$) and this will cause thermaml bowing. Thus the gradient across the frame is also plotted as a function of time (left of Figure 5.12). Gradients across the structural frame are largest for stainless steel frames and smallest the aluminium frame when encapsulation is present. The gradient peak occurs earlier for the aluminium frame, follwed by the carbon steel and the stainless steel frames. The encapsulated frame does not show a distinct peak as the gradient plateaus quite quickly.

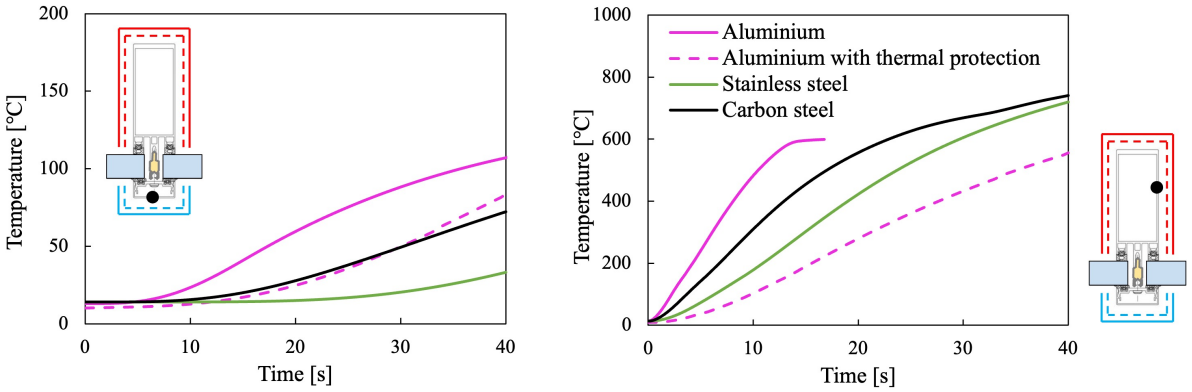


Figure 5.11: Temperature of pressure plate (left) and structural frame (right) of curtain wall systems with thermal protection and different materials. Location of temperature prediction marked by black dot in sketch.

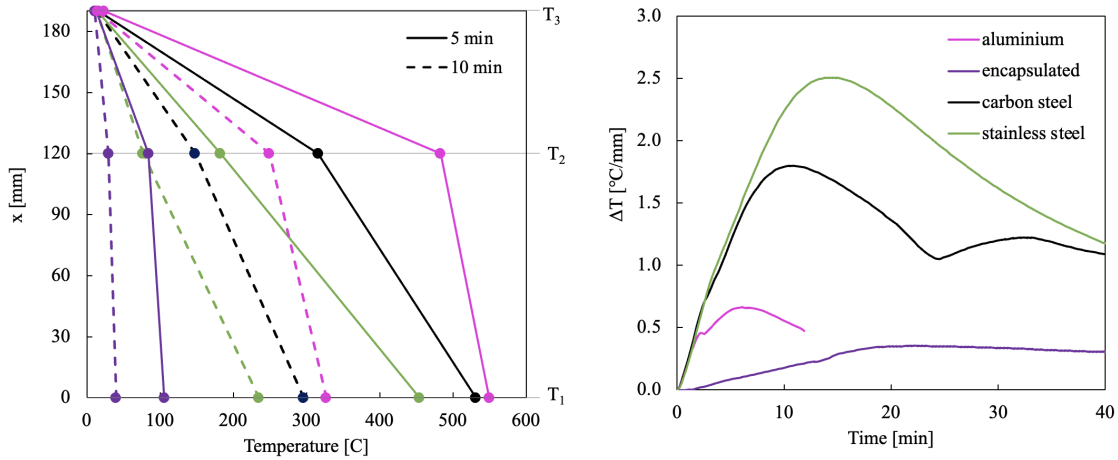


Figure 5.12: Temperature distribution after 5 and 10 minutes of heating (left) and linear thermal gradient across structural frame during heating (right). Values reported for a simple aluminium frame, an encapsulated aluminium frame, a stainless steel and a carbon steel frame exposed to a standard fire (ISO).

The failure time for all cases explored in this chapter are summarized in Table 5.2. Upon considering the different frame system and fire scenarios, it can be concluded that for the aluminium frames, where the thermal break is present, this element consistently fails after the structural frame has failed, except for the external fire scenario where it fails first. Overall, the aluminum frame exhibits a very rapid response to heating and degrades extremely quickly. In contrast, steel frames were found to fail at the thermal break. The stainless steel frame and the encapsulated aluminium frame demonstrate much better performance in this context, especially when solely considering thermal behavior, as failure was found to occur after 30 minutes and 39 minuted respectively. For the carbon and stainless steel frames and the encapsulated aluminium frame, the frame did not reach complete thermal degradation during the simulated heating (40 min).

Table 5.2: Comparison of failure time for all cases. Failure is considered as complete thermal degradation.

	Failure frame [min]	Failure thermal break [min]
Frame System		
aluminium	17	-
aluminium with thermal insulation	21	-
aluminium with thermal break	12	13
stainless steel	40+	30
carbon steel	40+	23
encapsulation	40+	39
Fire scenario		
short and hot	9	7
long and cold	21	15
external fire	40+	8

5.5 Conclusions

In this Chapter the model was used to investigate the response for an aluminium frame heated via a standard temperature time curve with and without thermal insulation and also to investigate a system with carbon steel and a stainless-steel frame. The results indicate that thermally protecting the frame or utilising a steel frame prevents rapid thermal degradation of the frame but might lead to other failure mechanism due to loss of integrity of the thermal break.

The model was used first to investigate the response for three aluminum frame assemblies heated via a standard temperature time curve. For a frame with aluminium only (no insulation and no thermal break) our model predicted thermal degradation after only 17 minutes of heating and the development of large thermal gradients (a max temperature difference between opposite side of the frame of 165 ℃). If an insulation insert was included, the thermal degradation of the frame was delayed (+4 minutes) however the frame experienced larger thermal gradients. When a thermal break was included in the assembly, thermal degradation of the frame was accelerated (-5 minutes) but the frame experienced smaller thermal gradients. For the latter

case, at the time of complete degradation of the frame (11 minutes) the predicted temperature at the pressure cap was only 70 ℃. This is important to note since in fire tests for curtain wall facades the temperature is always measured on the ambient side, on the pressure cap, and therefore these results suggest the temperatures reported may be much lower than the true temperatures experienced by the aluminium frame. For all cases investigated, the thermal gradients across the frame were substantial with peak temperature differences of 100 ℃ to 200 ℃. The largest thermal gradient occur between the internal structural frame and the external pressure cap due to the presence of the thermal break. When considering the structural frame the gradients are small, and this would suggest that thermal bowing will not be a problem.

Chapter 6

Mechanical Failure Criteria of Curtain Wall Framing System Exposed to Fire

6.1 Introduction

During a fire, the mechanical behaviour of a curtain wall depends on the interactions between the different elements, as well as the loads and restraint conditions of these elements. Therefore, the facade assembly, including support structure, fixings, and connections needs to be considered to accurately predict fire behaviour. Researchers and industry experts agree on this approach (Bonner and Rein (2018) and Hu et al. (2016)) but despite this a very limited number of studies consider the whole assembly.

Fire tests are run routinely in fire labs where failure is usually defined by loss of integrity (Kinowski et al. (2016) and Sulik et al. (2016)).These test can be useful as they define a minimum legal level of safety required for facades used in tall buildings, however they do not offer much insight on the failure modes or the actual fire performance in a realistic fire scenario. The data available therefore does not allow for reasonable conclusions about the fire performance of a full scale installation.

In this chapter, we aim to study the behaviour of the frame elements within the context of the facade system and point out to possible failure mechanisms. When modelling a complex structure with sophisticated computational tools which have many variables and input parameters, linking a cause to an effect can be impossible. For example mid span deflection of a beam can be caused by either a thermal gradient, or buckling due to restrained expansion, or compression due to the expansion of an adjacent element with a higher stiffness. Therefore the mechanical behaviour of the curtain wall framing elements is investigated here with a simple model where all the variables can be controlled. A model of similar nature was developed for the failure of non-tempered glass panel (Sabsabi et al. (2021)) and can be used in conjunction to the calculations proposed here to predict the sequence of failure events in a facade system.

Each basic facade unit is made up of a glass panel, two horizontal framing elements (transoms) and two vertical elements (mullions), such a unit acts as a single independent assembly as it is either hanged or supported from the main structure, the only interaction between units occurs if one element deforms or deflects enough to come in contact with the adjacent unit (Aiello et al. (2018)). Extensive displacement of the frame elements, due to thermal expansion and loss of stiffness, could cause the facade to bulk outward moving away from the main structure. In this scenario the compression keeping the firestop in position would be lost provoking the fallout of the firestop. Once the firestop is no longer in position, smoke and flames can penetrate adjacent compartments.

The level of interactions between components is investigated as this can lead to different responses. The failure mechanism considered are compression and buckling due to thermal expansion of the metal elements. Thermal strains developed due to the heating of the frame will lead to some stress if the expansion is restrained or to displacements if unrestrained (Usmani et al. (2001) & Bisby (2016)). Extensive displacement of the frame elements, due to thermal expansion and loss of stiffness, could cause the façade to bulk outward moving away from the main structure. In this scenario the compression keeping the firestop in position would be lost provoking the fallout of the firestop. Once the firestop is no longer in position, smoke and flames can penetrate adjacent compartments.

As an example calculation we demonstrate in this Chapter how we can predict the failure of the framing elements of a generic curtain wall system exposed to fire. The aim of this study was to quantify the structural behaviour of the curtain wall load-bearing frame elements constructed with aluminium and steel of different grades. Aluminium is the material commonly used for these systems whilst stainless steel is considered here as it has an enhanced fire behaviour compared to carbon steel (Gardner and Ng (2006)) and coupled with its corrosive resistance makes it a preferred option for external elements. All other variables, such as frame geometry, frame dimensions, and fire scenario remained the same, as this also allows comparison with results from previous chapters.

6.2 Modelling the Mechanical Response

6.2.1 Boundary Conditions

The mullion frame considered in this analysis is the same as in Chapter 5 and is based on the stick system frame tested by Sędłak et al. (2017). It is a frame representative of a generic curtain wall system supporting a glass panel of 3200 mm × 1680 mm. It was tested do obtain a 60 minute resistance ration. The layout and elevation of the loading of the frame are shown in Fig. 6.1. In this chapter the fire behaviour of the load-bearing frame elements is investigated when exposed to the ISO fire curve. The fire curve was selected as this is an onerous heating scenario and what most structures are designed against. The heat transfer is modelled in 2D following the methodology in Chapter 3, Section 3.4.3.

A member analysis is performed and each member is considered separately, namely the transom and the mullion. The interaction between members is modelled via a spring stiffness. The translation of the members is restraint in the axial direction by defining a spring stiffness. The connection between mullions and transoms is modelled as a pin connection which allows rotations therefore the stiffness acts only in the axial direction against translations. The glass panels restrain the frame elements in-plane and consequently buckling is considered only to occur about the strong axis.

The restrained conditions are modelled as a spring where stiffness of 100% of the mullion stiffness (EA/L) represents a pinned condition, and 0% a simply supported case. Here 100% ,50% , 25% and 5% are considered.

6.2.2 Ambient Loading

The only loads considered are dead loads - the weight of the glass panel and the self weight of the frame. The glass panel is supported by two setting blocks and therefore is applied at two discrete position on the horizontal transom creating branding moments within the frame.

The dead load of the facade is carried by the mullion and transferred to the main structure through the brackets. The unit is essentially hanging from the main structure and the mullion is in tension. The mullion is carrying the load of the transom and the glass panel and it self weight. At ambient the vertical mullion is under a tension force P. The force P equals to the dead load of the glass, the transom elements and the self load of the mullion combined. As this element is hanging it acts as a tensile element and no moments will develop.

The glass is supported on two setting bloc which transfer the panels load G to the horizontal transom. The transom acts as a simply supported beam and therefore moments will develop. Member loading is sketched in Figure 6.1.

To obtain the stresses due to bending of the transom, the second moment of inertia needs to be calculated. As the load-bearing part of the framing system is the rectangular structural frame, the connector and pressure plate can be ignored and Equation 6.1, for a hollow rectangular beam can be utilised.

$$I_y = \frac{WH^3 - wh^3}{12} \tag{6.1}$$

$$I_z = \frac{HW^3 - hw^3}{12} \tag{6.2}$$

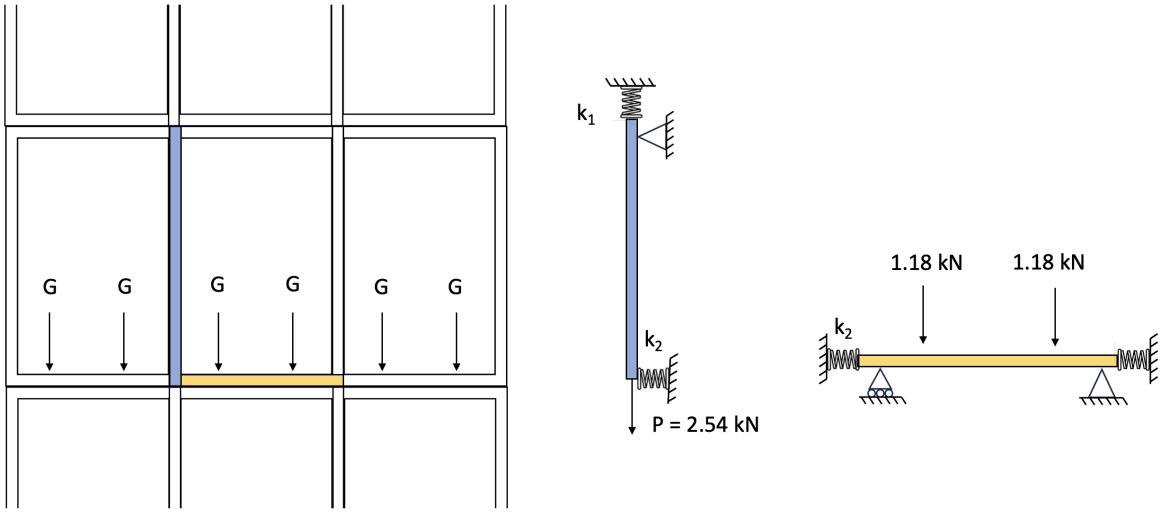


Figure 6.1: Elevation of frame system with glass panel dead load G (left) mullion member axial load P (middle) and restrain conditions (right).

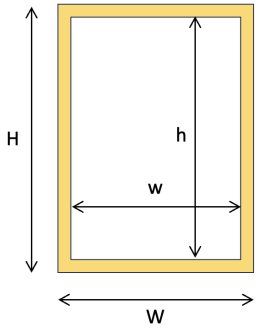


Figure 6.2: Dimension of the rectangular structural frame.

6.2.3 Mechanical Failure

Longitudinal expansion of mullion will lead to a certain degree of stresses depending on the restrain conditions - these stresses could lead to failure. Different levels of restraint are considered and include k_t = 5%, 25%, 50%, and 100 % (i.e. pinned) of beam axial stiffness (EA/L). The mullion is usually joined to the adjoining mullion via a spigot connection which has a stiffness comparable to the mullion but also allows some degree of translations.

Two failure modes are considered for an element subject to uniform heating. Failure due to compression, calculated via the compression axial stress developed by thermal expansion Equation 6.3, and failure due to buckling defined by the critical buckling temperature calculated via Euler's buckling load Equation 6.4.

$$\sigma_{th} = \frac{E\alpha\Delta T}{1 + \frac{EA}{k_t L}} \tag{6.3}$$

$$\Delta T_{cr} = \frac{\pi^2}{\alpha\lambda^2}\left(1 + \frac{EA}{k_t L}\right) \tag{6.4}$$

As shown in Figure 6.3, for mullion elements with a slenderness ratio around $\lambda = 70$, buckling occurs at temperature in the range of what it experienced by the frame elements whilst for the transom elements with a slenderness ration approximately $\lambda = 40$ buckling, occurs at elevated temperatures ($>$ 800℃) and consequently is not discussed here.

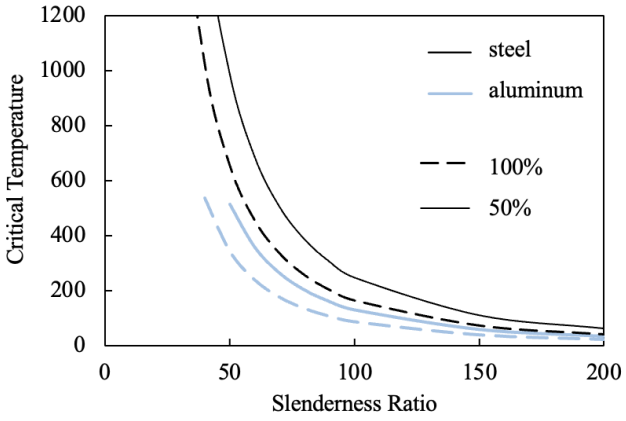


Figure 6.3: Critical buckling temperature as a function of slenderness ration for aluminium and steel elements.

Transoms are free to rotate at their ends and thermal gradients, T_y, will lead to curvature, ϕ, of the element with no stress development. The curvature and deflections however could leads to local stresses applied to the glass panel and therefore need to be defined. The deformations of the frame can be compared to the maximum allowed deformations. The mid span deflection, Equation 6.5, will be the greatest and will be analysed here.

$$y_m(\phi) = \frac{2l}{\pi}\sqrt{\varepsilon_\phi + \frac{\varepsilon_\phi^2}{2}} \tag{6.5}$$

$$\varepsilon_\phi = \alpha T_y \tag{6.6}$$

The deflection failure criteria is considered in this chapter. High deflections might lead to damage

to the fire stopping material or compartmentation leading to faster heating or further fire spread, these effects are not addressed here. At ambient a deflection failure criteria of L/500 is usually utilized for the horizontal transom elements, here we consider a failure of L/200 to account for the loss of stiffness of the heated frame and the glass. L is taken as the element length. The less stiff elements can accommodate more deflections without the development of large strains.

6.3 Results and Discussion

6.3.1 Mechanical Failure of Mullion

For the heating conditions analysed, the mullion geometry and materials considered, thermal expansion dominates over thermal bowing as seen in Figure 6.4. The thermal strains that lead to thermal bowing, ε_ϕ, are very small since the thermal gradients building up within the frames are moderate. Both thermal expansion and thermal bowing will produce mid span deflection, however usually thermal expansion produces a deflections in the opposite direction to the thermal bowing deflections. As the ε_ϕ due to the thermal gradient is negligable (close to zero) we will ignore the effect of thermal bowing and only conisder the axial thermal strain ε_{th}.

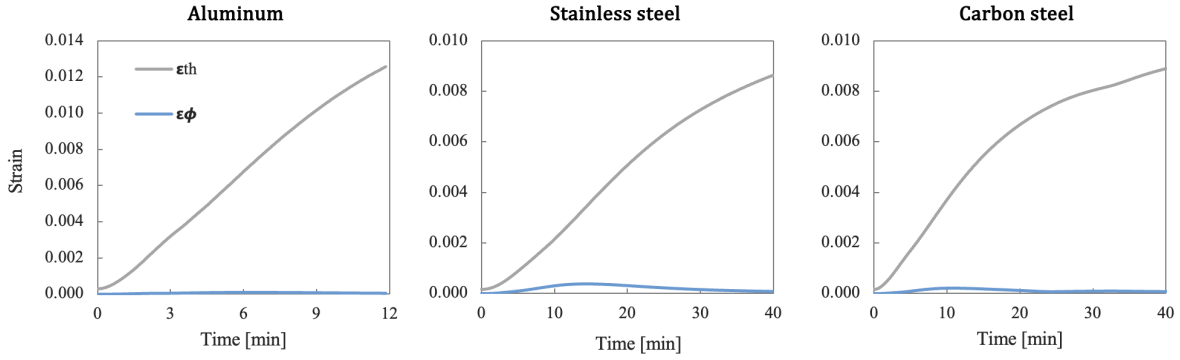


Figure 6.4: Thermal strain due to uniform temperature rise, ε_{th}, and curvature due to thermal gradients, ε_ϕ, for aluminium, stainless steel and carbon steel mullion exposed to ISO temperature-time curve.

6.3.1.1 Aluminium Mullions

For the aluminium mullion, failure occurs when the compressive stress developed, σ_{th}, is greater than the frame strength, f_y, or when the frame reaches the critical buckling temperature ΔT_{cr}. The stifness and strenght of the heated frame are shown in Figure 6.5 for a range of restrain conditions (stifness). The critical bukling temperature is also shown. For spring stiffness equal to 100 % of the mullion stiffness, buckling due to thermal expansion is the primary failure mode, for the other stiffness values (50%, 25 % and 5 % the mullion stiffness) failure is due to the compression stress within the frame surpassing the members strength. Stress developed in the mullion restrained at 5 % are very low, however the degradation of aluminium around 400 is substantially laving it with less than 80% of its original strength and causing the mullion to fail under low stress.

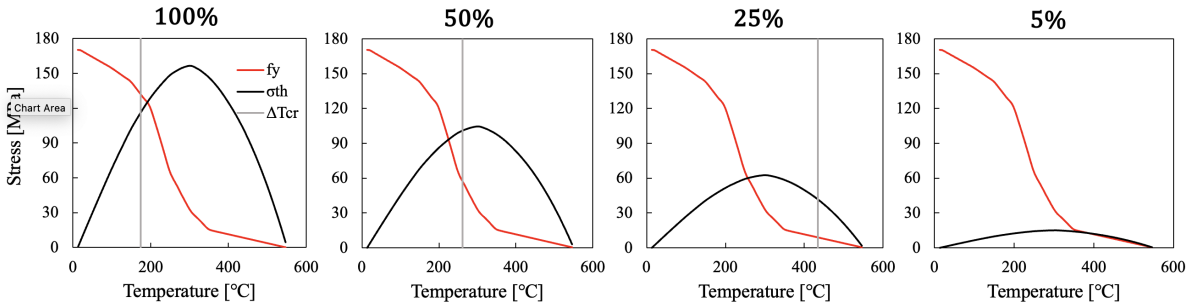


Figure 6.5: The effect of the spring stiffness on the thermal stress developed in an aluminium mullion framing member. For each spring stiffness the critical buckling temperature is shown as a grey line and the compressive stress due to thermal expansion as a black curve. The strength of the member is degrading as it is heated and is shown as a red curve.

When considering encapsulation of the frame, the response is only delayed in time as it takes longer to heat the mullion, as shown in Figure 6.6. Failure in the encapsulated frame occurs after 20 minutes of heating compared to the exposed frame which fails in 5 minutes. This indicated that if suppression of the fire or self extinguishment was to occur within the first 20 minutes of the fire, the encapsulated mullion would not fail.

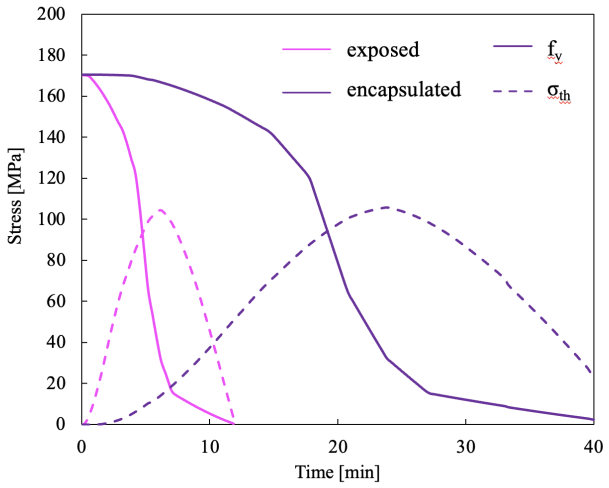


Figure 6.6: The effect of encapsulation on the strenght (f_y) and stress ()σ_{th}) of the loadbearing mullion exposed to uniform heating following the ISO fire curve. Compared to the exposed frame failure is delayed.

6.3.1.2 Steel Mullion

For stainless steel, the degradation of the 0.2% proof strength is taken as the yield strength (CEN (2006)) and the ultimate tensile strength is also plotted for comparison. The stress development due to thermal expansion are calculated and used to predict failure. The proof strength is used in literature Kucukler et al. (2020) . The Failure can either occur when the thermal stress σ_{th} is greater than the frame strength f_y or when the frame reaches the critical buckling temperature ΔT_{cr}. In all cases failure is due to the compressive stress within the frame surpassing the

members strength except for the 5% spring stiffness case where failure does not occur during the simulated heating phase (40 minutes).

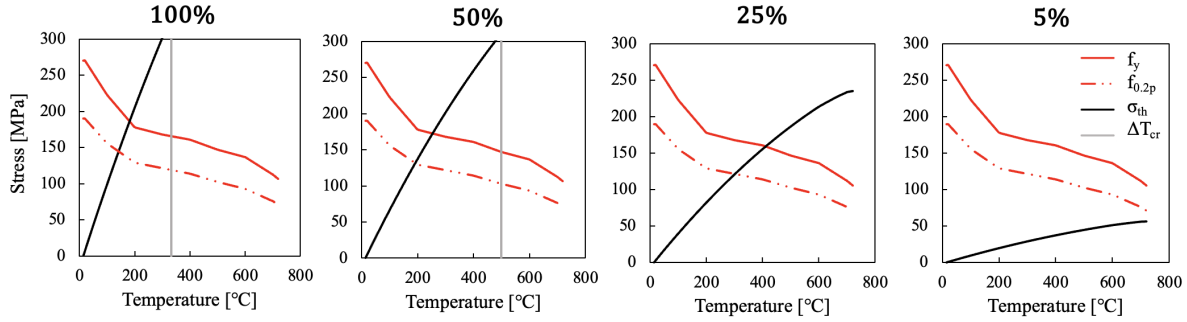


Figure 6.7: The effect of the spring stiffness on the thermal stress developed in an stainless steel mullion framing member. Critical buckling temperature for the 100 % and 50% spring stiffness is shown as a grey line, for other stiffness values the critical buckling temperature was greater than the temperature experienced by the frame (above 800 °C). The ultimate tensile strength and the 0.2% proof strength reduce as the frame is heated (red lines).

For carbon steel both grade S275 and S355 are considered. The 100% and 50% stiffness cases, failure mode will depend on the a steel used, with the S275 failing due to the axial load while the S355 fails in buckling, indicating the failure mode can be different for different strengh grades. For stiffness below 25% failure due to thermal expansion does not occur during the simulated heating phase (40 minutes). Carbon steel with weak retain conditions will fail at higher temperatures due to thermal degradation and not due to the thermal expansion.

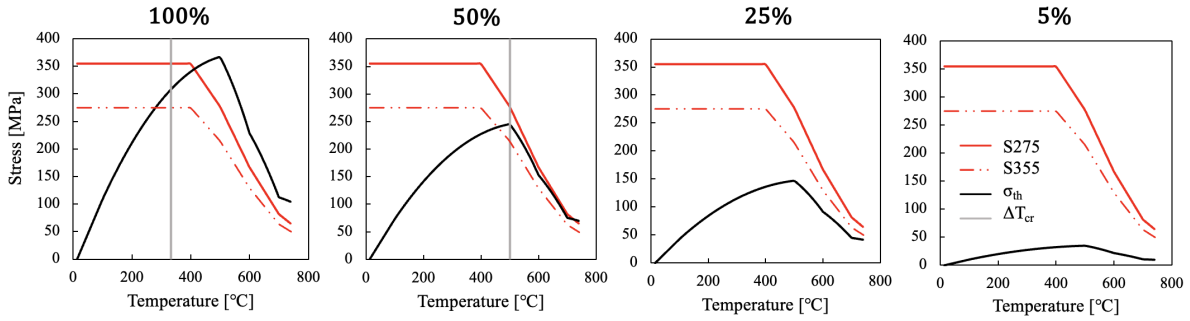


Figure 6.8: The effect of the spring stiffness on the thermal stress developed in an carbon steel mullion framing member. Critical buckling temperature for the 100 % and 50% spring stiffness are shown as a grey line, for other stiffness values the critical buckling temperature was grater than the range considered (above 800 °C). The strength reduces as the frame is heated and the degradation is plotted for S355 and S275 steel.

6.3.1.3 Failure

A comparison of the failure temperature within the heated mullions for the uniform fires exposure and the time to reach failure are shown in Fig. 6.9. Failure is given as a failure time and a failure temperature, the latter allows direct comparison with the results from Chapter 5 where failure was taken as the time to complete thermal degradation. For higher stiffness values (100% and

50%) the stainless steel mullion fails at the lowest temperature due to axial compression whilst for lower stiffnesses (5% and 25%) aluminium fails at lower temperature. Carbon steel performs best both if considering failure temperature or time.

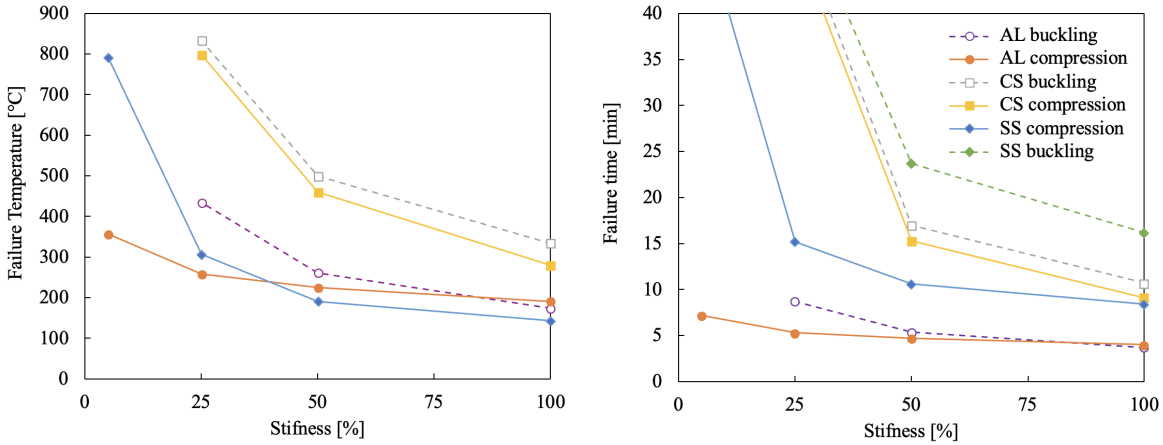


Figure 6.9: Failure time (left) and failure temperature (right) for the mullion element in aluminium (AL), stainless steel (SS) and carbon steel (CS). Two failure modes analysed for each case: compression and buckling.

6.3.2 Mechanical Failure of Transom

The thermal expansion will lead to the transom trying to straighten itself and counterbalance the bending due to ambient loading. Compressive force due to thermal expansion will be added to the compression due to bending in the top part of the element while the tension in the bottom of the transom will dampen the compression developing due to thermal expansion. As the transom is shorter and has a low slenderness ration buckling does not occur, and all failure reported in Figure 6.10 are due to axial compression in the upper part of the rectangle cross-section. The aluminium fails at lower temperatures and in less time than the steel transom.

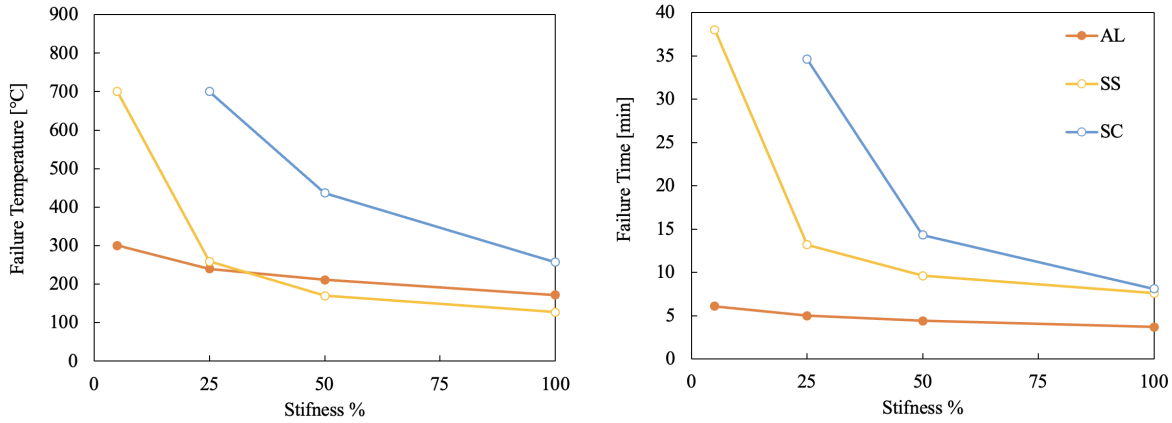


Figure 6.10: Failure time (left) and failure temperature (right) for the transom element with varying level of restrain (5-100% member stifness).

The midspan displacement of the transom due to the thermal gradient is shown in Figure 6.11. This displacement will cause the transom to bow outwards when heated internally and cause the facade to detach from the main structure. Based on the failure criteria of L/200, failure occurs only for the stainless steel element at a temperature of 130 ℃ and after 8 minutes of heating. This behaviour is in line with the results from Chapter 5 where the larger thermal gradients were seen to develop in the stainless steel members.

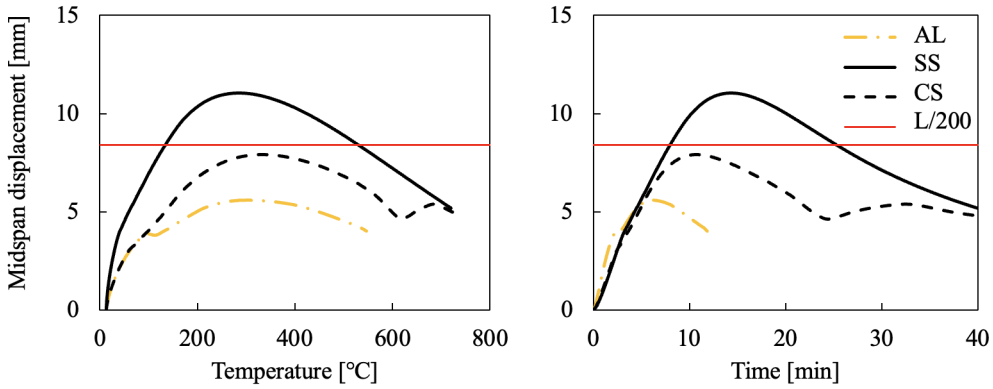


Figure 6.11: Midspan deflection due to thermal gradient of transom member. Evolution with temperature (left) and time (right).

6.3.3 Behaviour of Glass in Fire

The fire behaviour of glass as an independent component has been described in Section 2.4.4. At ambient conditions, glass is a linear elastic material and is brittle in tension. This means that, differently from steel and concrete, once it reaches its elastic deformability limit it will fail and break. The behaviour of glass at elevated temperatures has been widely studied and the breakage of glass has been found to be strictly related to the restrain conditions and the shaded portion of the glass (behind a frame or gasket). When heated the glass exposed to radiation and convection will heat up quickly while the shaded portion of the glass panel will remain at lower temperature. Glass is a poor conductor and therefore the heat will travel slowly from the hot section to the cooler one. The hotter section, usually the centre of the pane, will expand and the compression forces will produce tensile stresses in the cooler shaded perimeter areas. In this scenario, glass will break rapidly; due to the low tensile strength of glass cracks will initiate at the shaded area and propagate to the cooler area. The maximum allowable temperature difference for treated glass are listed in Table 6.1

Table 6.1: Allowable temperature difference ΔT for glass [prEN thstr:2004].

Glass type	Limit values (℃)
float	25-40
heat-strengthened	100
tempered	200

The tensile stresses that will cause breakage are directly proportionate to the temperature difference of the cooler perimeter and hotter central sections of the class (Joshi and Pagni (1994b)). Therefore, the temperature difference that will cause breakage can be defined as:

$$\beta \Delta T = \frac{\sigma_b}{E} \tag{6.7}$$

with β the linear thermal expansion coefficient, ΔT the temperature difference between the hotter and the cooler section of the glass panel, σ_b the glass breaking stress and E the Young's modulus.

6.4 Conclusions

In Chapter 5, limiting temperature criteria is used in the assessment of a curtain wall frame subjected to fire, however, this criteria is not always accurate. In this chapter, the frame structure has been analysed in the terms of development of stresses and deflections. The effect of uniform fire exposure on load-bearing capacity, buckling and mid-span deflection of a curtain wall frame structure have been investigated. Corresponding element temperatures at failure have been compared for each failure criteria.

A generic frame was analysed to determine the failure mode and time, under uniform heating . Aluminium framing system typical of curtain walls have been shown to fail at very low temperature and very rapidly when heated. The failure behaviour of the mullion was dependent on the level of restrain. For spring stiffness below 5% failure was due to axial compression, while for higher stiffness levels buckling was the mode of failure. Failure occurs as early as member temperature of 170℃ for 100% beam stiffness, whilst it only occurs around 400℃ for the 5% beam stiffness. For all cases the faliure temperature was lower that the failure temperature considered in Chapter 5, e.g. temperature for complete thermal degradation.

All transom elements fail due to axial compression, buckling does not occur as the member is shorter and stockier than the mullion. Transom members fail at slightly lower temperature than mullions as their cross section size is smaller and the element is therefore weaker. In the scenario considered, the whole facade is heated uniformly as the temperature of a compartment fire are assumed to be uniform along the height of the facade. However, in a realistic fire, the temperature will be lower at the bottom and increase with height as hot gasses collect under the ceiling. In addition, the transom will also be partially shaded/protected by fire stopping material which is placed at level with the transom and the main structure slab, therefore although failure of the transom occurs at lower temperatures they might not heat up as quickly as the exposed mullion.

The stainless steel transom were found to reach the deflection failure criteria very rapidly, with failure occurring at member temperature of 137 ℃ and just after 8 minutes of heating. Carbon steel and aluminium elements did not reach the deflection limit. This indicated that although stainless steel frames are generally considered to have a better performance compared to alu-

minium frames, the thermal gradients lead to larger bowing. The failure mode for stainless steel components is due to deflection and not stresses. Carbon steel performs better in all scenarios however it is not readily available for curtain wall framing.

The results indicates that the primary failure mode depends on the restrain condition. The higher restrain condition (100% stiffness) corresponds to the worst case as the failure temperature and failure time are lower for all cases. Moreover the failure mode depends on the frame material selected; aluminium was found to fail in buckling or compression, carbon steel in compression and not failing at all for low levels of lateral restrain, and stainless steel failing either in compression or due to large midspan deflection caused by the thermal gradient.

Chapter 7

Conclusions

7.1 Outcome of presented research

This thesis explores a critical aspect of facade systems: their mechanical behaviour and vulnerability in fires, covering failure modes and the thermal and mechanical properties of materials that impact these failures. This is crucial as mechanical failures during a fire event can pose substantial threats to public safety, including potential harm to passers-by, evacuees, and firefighting personnel. Current regulations predominantly focus on aspects such as fire spread and flammability, overlooking the possibility of mechanical failure that could lead to severe consequences during a fire event.

Facade system do not undergo the same scrupulous design process that the main building structure goes through. The failure of a structural element might pose a risk to the stability of the whole building and failure of a section of the main structure could initiate a collapse mechanism. Whereas failure of a section of a facade, even if large, would not interfere with the stability of a building. However as shown in the recent Relay building fire in London (Chapter 1) the failure of a facade component is a life threat. In addition, if the facade is compromised, the fire is able to spread to the upper floors breaching compartmentation.

Chapter 2 discussed the interdependence of elements within the facade system. The failure of any component, from stone panels to metal brackets or connections, can trigger cascading consequences, potentially exacerbating fire spread and structural integrity. This highlights the need for a comprehensive understanding of the system's behavior under fire conditions. Moreover, the literature review emphasizes the complexity of curtain wall facades, especially in predicting their behavior during fires. The comparison of mechanical and thermal properties of materials that influence mechanical failure in a fire scenario have shown that metals have higher thermal inertia and lower failure temperature as expansion of restrained metal panels will induce large stresses on the fixings. Aluminium was found to be quite vulnerable to fire compared to other metals (e.g., large expansion coefficient coupled with high thermal diffusivity, low failure tem-

perature) thus indicate that typical curtain wall framing system constructed with aluminium are weak when exposed to fire. Nonetheless studies investigating the behaviour of facade built with such metal are lacking.

The thermal models developed in Chapter 3 are a tool that can be used to analyse the behaviour of curtain wall assemblies under heat exposure. Although previous work had been done to quantify the thermal response of a curtain wall framing system, previous models made the assumption that the frame experiences a uniform temperature. The simpler 0D and 1D models do not allow for predictions of gradients across the section of the facade but were utilized for comparison with the higher complexity models. The 2D and 3D consider heat transfer across the structural frame, the connector (screw and thermal break) and the external pressure plate, and also consider heat transfer within the frame chamber. The 2D and 3D models predictions have been compared to experimental measurements and found to calculate accurate temperature developments within the frame elements (Chapter 4). The sensitivity study in Chapter 3 revealed that the emissivity and specific heat of the frame material have the greatest impact on the peak temperature experience by the structural frame, whilst the conductivity of the thermal break had the greatest impact on the temperature of the pressure plate. The boundary conditions on the fire side were also shown to have a major impact on the temperature developments of the frame.

The model was used to perform a parametric study on different materials, such as aluminium, stainless steel, and carbon steel. In Chapter 5 the thermal response of the different frames were compared and failure was assumed to occur when the frame would lose its integrity. Aluminum was found to fail very rapidly while steel frames were found to resist 40 minutes of heating under the fire scenario considered. Encapsulating the aluminum frame (e.g. adding thermal protection around the frame) was shown to be effective in reducing the peak temperature in the aluminium frame and the system resisted 40 minutes of heating. The temperature distribution across the frame cross-section was analysed for all cases, systems with thermal breaks did not develop large gradients across the structural frame. Stainless steel systems were found to develop the larger gradients across the structural frame.

The mechanical response of aluminium and steel curtain wall frames is taken in consideration in Chapter 6 and the results offer insights into their respective behaviour under fire conditions. For instance, while stainless steel frames might exhibit better overall performance, they can experience larger thermal gradients leading to significant bowing, thereby posing unique challenges. Large deflections of the frame can induce local stresses on the glass panels and accelerate failure. Thermal bowing can lead to the creation of large gaps between the facade and the structural slab facilitating the spread of flames and smoke to adjacent floors. These thermal model predictions were used in the mechanical failure calculation of failure time and failure temperature.

Chapters 5 and 6 investigate the effects of different materials, fire protection measures, and the impact of various frame structures, providing invaluable insights into failure mechanisms,

such as buckling, compression, and deflection. Different level of complexities were utilized when modelling the thermal and the mechanical response of curtain wall systems exposed to fire. The complexity levels are shown in Figure 7.1.

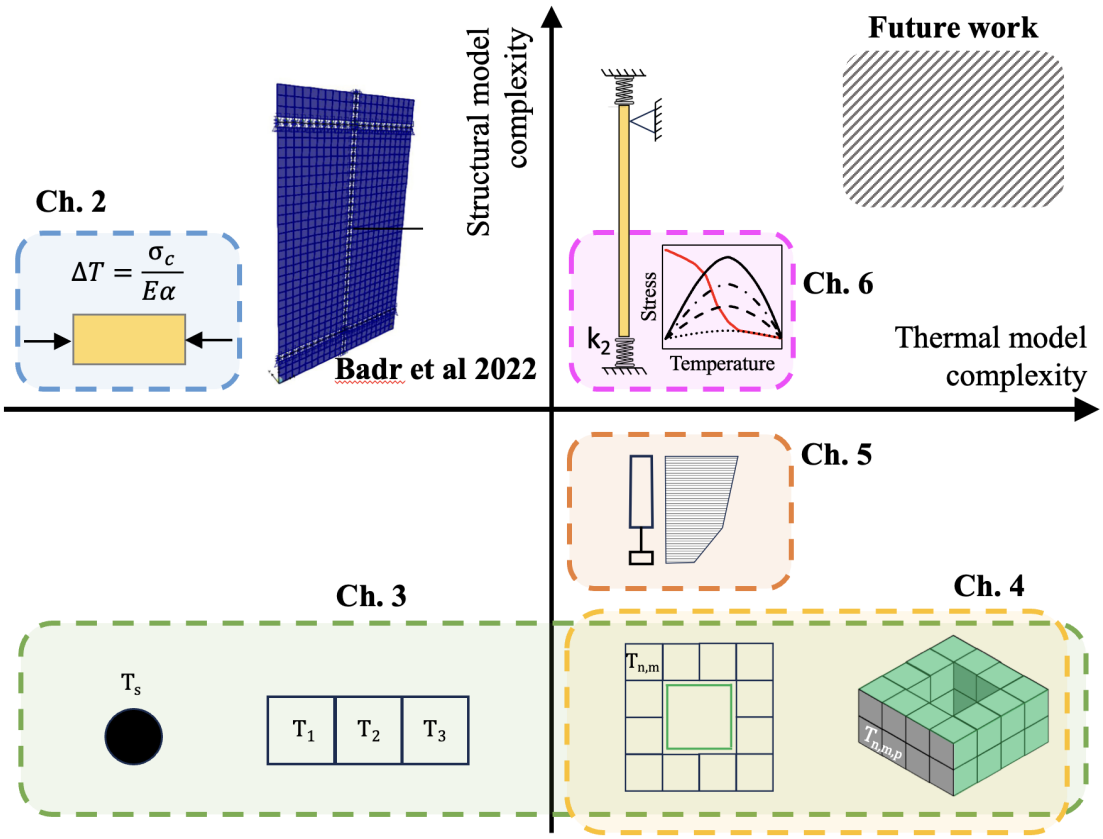


Figure 7.1: Diagram illustrating the complexity levels of the models employed in the chapters of this thesis.

7.2 Future Work

Facades should be investigated both experimentally and computationally with appropriate detailing and under realistic conditions. Failure mechanisms for facade frame systems with realistic loading and restrain conditions could be explored experimentally. Small scale experiment would be needed to define the behaviour of loaded frame element (mullion and transom) when heated. These elements should include all components like thermal breaks, screws and gaskets. Data recorded should include strain and deformations to allow a detailed understating of the system mechanical response. This data could be also useful to allow the verification of model predictions. Large-scale experiments employing facade mock-ups under non-uniform, localized heating would allow for the study of interactions between elements. In these tests, measurements should be taken of temperature of the frame and brackets on the exposed and unexposed side. Heat fluxes and velocities would be useful to help define the thermal boundary conditions. In addition, deformations and strains should be recorded to allow understand of mechanical response

of the assembly.

The analysis here presented should be extended by modelling the curtain wall framing system in 2D utilizing Finite Element Models like LS-DYNA. These would allow the study of the composite action of the metal frame and the glass panels as well as allowing the analysis of non-uniform heating conditions. Fire scenarios such as localized and travelling fires should be studied to understand the changes in failure modes. This could be ulteriorly extended by developing studies exploring the behaviour of entire facade assemblies, encompassing support structures, fixings, and connections between units.

7.3 Conclusions

Collaborative efforts between fire safety experts and facade engineers are required. Through this collaboration and a deeper exploration of these systems' behaviour, we can advance towards more informed regulations and safer facade designs, reducing potential risks during fire incidents.

Overall, the research underscores the need for a holistic approach in evaluating facade systems' fire performance. By examining both thermal and mechanical aspects comprehensively, this work serves as a guide for future studies.

Bibliography

Aiello, C., Caterino, N., Maddaloni, G., Bonati, A., Franco, A., Occhiuzzi, A., 2018. Experimental and numerical investigation of cyclic response of a glass curtain wall for seismic performance assessment. Construction and Building Materials 187, 596–609.

ANSYS, 2021. Ansys granta edupack software. Inc., Cambridge, UK. Accessed: 2022-11-12.

Ashby, M.F., 2011. Chapter 4 - material property charts, in: Ashby, M.F. (Ed.), Materials Selection in Mechanical Design (Fourth Edition). fourth edition ed.. Butterworth-Heinemann, Oxford, pp. 57–96.

Badr, M., Youssef, M.A., El-Fitiany, S., Vedrtnam, A., 2023. Structural performance of single-skin glass façade systems exposed to fire. Journal of Structural Fire Engineering 14, 321–343.

Bartlett, A.I., Hadden, R.M., Bisby, L.A., 2019. A review of factors affecting the burning behaviour of wood for application to tall timber construction. Fire Technology 55, 1–49.

BASF, 2022. Ultramid® a3hg5 - product datasheet. https://documents.basf.com/69c69fee302f17cb39e1326e3fe8572e7e6ba14b/Ultramid_A3HG5_en_SI.product_datasheet.pdf. [Online, Accessed: 2023-12-12].

Bedon, C., Louter, C., 2018. Thermo-mechanical numerical modelling of structural glass under fire-preliminary considerations and comparisons, in: Challenging Glass Conference Proceedings, pp. 513–524.

Bedon, C., Zhang, X., Santos, F., Honfi, D., Kozłowski, M., Arrigoni, M., Figuli, L., Lange, D., 2018. Performance of structural glass facades under extreme loads – design methods, existing research, current issues and trends. Construction and Building Materials 163, 921–937.

Bedon, C., et al., 2017. Structural glass systems under fire: overview of design issues, experimental research, and developments. Advances in Civil Engineering 2017.

Beyler, C.L., 2016. Fire hazard calculations for large, open hydrocarbon fires. SFPE handbook of fire protection engineering , 2591–2663.

Bisby, L.A., 2016. Structural Mechanics. Springer New York, New York, NY. pp. 255–276.

Blomqvist, P., Andersson, P., 2012. A study of fire performance of textile membranes used as building components. Fire and Materials 36, 648–660.

Bonner, M., 2020. A top-down approach to understand the fire performance of building facades using standard test data. Imperial College London.

Bonner, M., Rein, G., 2018. Flammability and multi-objective performance of building façades: Towards optimum design. International Journal of High-Rise Buildings 7, 363–374.

Bonner, M., Wegrzynski, W., Papis, B.K., Rein, G., 2020. Kresnik: A top-down, statistical approach to understand the fire performance of building facades using standard test data. Building and Environment 169, 106540.

BRE, 1992. Summary of fires investigated: April 1991 to march 1992, cr176/92 .

Callister, W.D., Rethwisch, D.G., 2018. Materials Science and Engineering: An Introduction. 10 ed., Wiley, Hoboken. Original Date: 2000.

Cárdenas, B., León, N., Pye, J., García, H.D., 2016. Design and modeling of a high temperature solar thermal energy storage unit based on molten soda lime silica glass. Solar Energy 126, 32–43.

Carter, S., 2022. Horrible fire in aldgate. emergency crews in attendance. https://twitter.com/SpencerSCarter/status/1500881316534960132. [Online, Accessed: 2023-12-12].

CEN, 1991. EN 1991, Part 1-2: Actions on Structures—Actions on Structures Exposed to Fire. European Committee for Standardization, Brussels, Belgium.

CEN, 2002. EN 1993-1-2: Eurocode 3 - Design of steel structures, Part 1-2 – Structural fire design. European Committee for Standardization, Brussels, Belgium.

CEN, 2006. EN 1993-1-4: Eurocode 3 - Design of steel structures - Part 1-4: General rules - Supplementary rules for stainless steels. European Committee for Standardization, Brussels, Belgium.

CEN, 2007. EN 1999-1-2: Eurocode 9 —design of aluminium structures—Part 1-2: structural fire design. European Committee for Standardization, Brussels, Belgium.

CEN, 2014. ISO 834-11:2014. Fire resistant tests. Elements of building construction - Specific requirements for the assessment of fire protection to structural steel elements.

Chilton, J., 2013. Lightweight envelopes: ethylene tetra-fluoro-ethylene foil in architecture. Proceedings of the Institution of Civil Engineers - Construction Materials 166, 343–357.

Chin, I.R., 2000. Common causes of failures of stone claddings on buildings, in: Dimension stone cladding: design, construction, evaluation, and repair. ASTM International.

Colwell, S., Baker, T., 2013. Fire performance of external thermal insulation for walls of multi-storey buildings:(br 135).

Cooke, G.M.E., 2004. Stability of lightweight structural sandwich panels exposed to fire. Fire and Materials 28, 299–308.

CTBUH, 2023. Council on tall buildings and urban habitat database, the relay building. https://www.skyscrapercenter.com/building/one-commercial-street/18787. [Online, Accessed: 2023-12-12].

de Boer, J., Hofmeyer, H., Maljaars, J., van Herpen, R., 2019. Two-way coupled cfd fire and thermomechanical fe analyses of a self-supporting sandwich panel façade system. Fire Safety Journal 105, 154–168.

Debuyser, M., Sjöström, J., Lange, D., Honfi, D., Sonck, D., Belis, J., 2017. Behaviour of monolithic and laminated glass exposed to radiant heating. Construction and Building Materials 130, 212–229.

Drysdale, D., 2011. An introduction to fire dynamics. John wiley & sons.

Dréan, V., Girardin, B., Guillaume, E., Fateh, T., 2019. Numerical simulation of the fire behaviour of façade equipped with aluminium composite material-based claddings—model validation at intermediate scale. Fire and Materials 43, 839–856.

Gardner, L., Ng, K., 2006. Temperature development in structural stainless steel sections exposed to fire. Fire Safety Journal 41, 185–203.

Guillaume, E., Dréan, V., Girardin, B., Koohkan, M., Fateh, T., 2020. Reconstruction of grenfell tower fire. part 2: A numerical investigation of the fire propagation and behaviour from the initial apartment to the façade. Fire and Materials 44, 15–34.

Gunalan, S., Kolarkar, P., Mahendran, M., 2013. Experimental study of load bearing cold-formed steel wall systems under fire conditions. Thin-Walled Structures 65, 72–92.

Gunalan, S., Mahendran, M., 2013a. Development of improved fire design rules for cold-formed steel wall systems. Journal of Constructional Steel Research 88, 339–362.

Gunalan, S., Mahendran, M., 2013b. Finite element modelling of load bearing cold-formed steel wall systems under fire conditions. Engineering Structures 56, 1007–1027.

Gunalan, S., Mahendran, M., 2014. Fire performance of cold-formed steel wall panels and prediction of their fire resistance rating. Fire Safety Journal 64, 61–80.

Hajpál, M., Török, Á., 2004. Mineralogical and colour changes of quartz sandstones by heat. Environmental Geology 46, 311–322.

Harmathy, T.Z., 1965. Ten rules of fire endurance rating. Fire Technology 1, 93–102.

Hertz, K., 2003. Limits of spalling of fire-exposed concrete. Fire Safety Journal 38, 103–116.

Herzog, T., Krippner, R., Lang, W., 2004. Facade construction manual. DETAIL-Institut für internationale Architektur-Dokumentation GmbH & Co. KG.

Hu, J., Chen, W., Qu, Y., Yang, D., 2020. Safety and serviceability of membrane buildings: A critical review on architectural, material and structural performance. Engineering Structures 210, 110292.

Hu, J., Chen, W., Zhao, B., Yang, D., 2017. Buildings with etfe foils: A review on material properties, architectural performance and structural behavior. Construction and Building Materials 131, 411–422.

Hu, L., Milke, J., Merci, B., 2016. Special issue on fire safety of high-rise buildings. Fire Technology 53, 1–3.

Huang, B., Fu, S., Lu, W., Günay, S., 2020. Experimental investigation of the breaking load of a dowel-pinned connection in granite cladding. Engineering Structures 215, 110642.

Huang, Q., Hamed, E., 2019. Nonlinear finite element analysis of composite precast concrete sandwich panels made with diagonal frp bar connectors. Composite Structures 212, 304–316.

Hulin, T., Hodicky, K., Schmidt, J.W., 2016a. Sandwich panels with high performance concrete thin plates at elevated temperatures: numerical studies. Materials and Structures 49, 3177–3193.

Hulin, T., Hodicky, K., Schmidt, J.W., Stang, H., 2016b. Experimental investigations of sandwich panels using high performance concrete thin plates exposed to fire. Materials and Structures 49, 3879–3891.

Hulin, T., Maluk, C., Bisby, L., Hodicky, K., Schmidt, J.W., Stang, H., 2016c. Experimental studies on the fire behaviour of high performance concrete thin plates. Fire Technology 52, 683–705.

Incropera, F.P., DeWit, D., 2013. Fundamentals of Heat and Mass Transfer. J. Wiley & Sons.

Ji, J., Ge, F., Qiu, T., 2021. Experimental and theoretical research on flame emissivity and radiative heat flux from heptane pool fires. Proceedings of the Combustion Institute 38, 4877–4885.

Joshi, A., Pagni, P.J., 1994a. Fire-induced thermal fields in window glass. ii—experiments. Fire Safety Journal 22, 45–65.

Joshi, A., Pagni, P.J., 1994b. Fire-induced thermal fields in window glass. i—theory. Fire Safety Journal 22, 25–43.

Keerthan, P., Mahendran, M., 2012. Numerical modelling of non-load-bearing light gauge cold-formed steel frame walls under fire conditions. Journal of Fire Sciences 30, 375–403.

Khoo Sheng Yeong, B., 2023. Multiphysics simulations of fire inside the cavity of a facade .

Khoury, G., 2000. Effect of fire on concrete and concrete structures. Progress in Structural Engineering and Materials 2, 429 – 447.

Kim, N., Dutta, S., Bhattacharyya, D., 2018. A review of flammability of natural fibre reinforced polymeric composites. Composites Science and Technology 162, 64–78.

Kinowski, J., Sędłak, B., Sulik, P., 2017. External wall claddings-study on impact of fixing methods in case of fire. IFireSS 2017, 2nd.

Kinowski, J., Sędłak, B., Sulik, P., 2016. Large glazing in curtain walls – study on impact of fixing methods on fire resistance. MATEC Web of Conferences 46, 05004.

Kodur, V., Banerji, S., 2021. Modeling the fire-induced spalling in concrete structures incorporating hydro-thermo-mechanical stresses. Cement and Concrete Composites 117, 103902.

Koffel, E.W., Memari, A.M., Rittenhouse, T., 2005. Structural practices — curtainwalls in modern buildings. Available at: https://structuremag.peppermint.warszawa.pl/?p=6958.

Kolarkar, P.N., 2011. Structural and thermal performance of cold-formed steel stud wall systems under fire conditions. Ph.D. thesis. Queensland University of Technology.

Koohkan, M., Dréan, V., Girardin, B., Guillaume, E., Fateh, T., Duponchel, X., 2021. Reconstruction of the grenfell tower fire — thermomechanical analysis of window failure during the grenfell tower disaster. Fire Technology 57, 69–100.

Koutaiba, E.M., Dhima, D., Duny, M., Garo, J., Wang, H.Y., Jullien, Q., 2017. Experimental study on vertical wooden façade combustion. Procedia Engineering 210, 520–527.

Kozłowski, M., Bedon, C., Honfi, D., 2018. Numerical analysis and 1d/2d sensitivity study for monolithic and laminated structural glass elements under thermal exposure. Materials 11.

Kucukler, M., Xing, Z., Gardner, L., 2020. Behaviour and design of stainless steel i-section columns in fire. Journal of Constructional Steel Research 165, 105890.

Lattimer, B.Y., 2016. Heat transfer from fires to surfaces. SFPE handbook of fire protection engineering , 745–798.

Law, A., Kanellopoulos, G., 2020. The rise and fall of the uk's spandrel panel. Fire safety journal 115, 103170.

Livkiss, K., Svensson, S., Husted, B., van Hees, P., 2018. Flame heights and heat transfer in facade system ventilation cavities. Fire Technology 54, 689–713.

Lodge, M., Terry, K., 2022. Huge fire breaks out in high rise block of offices and flats in east london as more than 125 firefighters and 20 fire engines tackle the blaze and take one rescued woman to hospital. https://www.dailymail.co.uk/news/article-10586639/

Huge-fire-breaks-high-rise-office-block-near-Londons-Aldgate-East.html. [Online, Accessed: 2023-12-12].

London Fire Brigades, 2022. Fire at block of flats and offices - whitechapel. https://www.london-fire.gov.uk/incidents/2022/march/fire-at-block-of-flats-whitechapel/. [Online, Accessed: 2023-12-12].

LPC, 1999. Fire spread in multi-storey buildings with glazed curtain wall façades. LPR 11:1999.

Lugaresi, F., Kotsovinos, P., Rein, G., 2021. Computational study on the thermal response of curtain wall systems exposed to fire, in: Proceedings of the 12th Asia-Oceania Symposium on Fire Science and Technology (AOSFST 2021).

Lugaresi, F., Rein, G., 2022. Technical note on the relay building fire. Available at: https://doi.org/10.5281/zenodo.6473162.

Manzello, S.L., Gann, R.G., Kukuck, S.R., Prasad, K.R., Jones, W.W., 2007. An experimental determination of a real fire performance of a non-load bearing glass wall assembly. Fire Technology 43, 77–89.

Manzello, S.L., Park, S.H., Mizukami, T., Bentz, D., 2008. Measurement of thermal properties of gypsum board at elevated temperatures, in: Proceedings of the 5th International Conference on Structures in Fire. Nanyang Technological University, Singapore, pp. 28–30.

McLaggan, M., Hidalgo, J., Osorio, A., Heitzmann, M., Carrascal, J., Lange, D., Maluk, C., Torero, J., 2021. Towards a better understanding of fire performance assessment of façade systems: Current situation and a proposed new assessment framework. Construction and Building Materials 300, 124301.

Memari, A., Shirazi, A., Kremer, P., 2007. Static finite element analysis of architectural glass curtain walls under in-plane loads and corresponding full-scale test. Structural Engineering and Mechanics 25, 365–382.

Ministry of Housing, Communities and Local Government, 2019. The Building Regulations 2010 - Fire Safety - Approved Document B. Accessed at: https://www.gov.uk/government/publications/fire-safety-approved-document-b.

Morris, B., Jackman, L., 2003. An examination of fire spread in multi-storey buildings via glazed curtain wall façades. Structural Engineer 81, 22 – 26.

Mouritz, A., Feih, S., Kandare, E., Mathys, Z., Gibson, A., Jardin, P., Case, S.W., Lattimer, B., 2009. Review of fire structural modelling of polymer composites. Composites Part A: Applied Science and Manufacturing 40, 1800–1814.

Nam, J., Jeong, M.G., Ryou, H.S., Kim, J.T., Nam, J.S., Kim, D.J., Cho, S.W., 2017. Validation of a numerical model for curtain walls with mvhs during free burning. Fire Safety Journal 94, 45–53.

Nguyen, K.T., Navaratnam, S., Mendis, P., Zhang, K., Barnett, J., Wang, H., 2020. Fire safety of composites in prefabricated buildings: From fibre reinforced polymer to textile reinforced concrete. Composites Part B: Engineering 187, 107815.

Nguyen, K.T., Weerasinghe, P., Mendis, P., Ngo, T., 2016. Performance of modern building façades in fire: a comprehensive review. Electronic Journal of Structural Engineering 16, 69–87.

Ni, Z., Lu, S., Peng, L., 2012. Experimental study on fire performance of double-skin glass facades. Journal of Fire Sciences 30, 457–472.

Nogueira, R., Martins, M., Ampessan, F., 2011. Natural convection in rectangular cavities with different aspect ratios. Revista de Engenharia Térmica 10, 44–49.

O'Connor, D.J., 2008 2.

O'Connor, D.J., 2016. The Building Envelope: Fire Spread, Construction Features and Loss Examples. Springer New York, New York, NY. pp. 3242–3282.

O'Hegarty, R., Kinnane, O., 2020. Review of precast concrete sandwich panels and their innovations. Construction and Building Materials 233, 117145.

O'Hegarty, R., Reilly, A., West, R., Kinnane, O., 2020. Thermal investigation of thin precast concrete sandwich panels. Journal of Building Engineering 27, 100937.

Osvald, A., Štefková, J., 2020. The impact of radiant heat on the flexural strength and impact strength in spruce wood bending, in: Makovicka Osvaldova, L., Markert, F., Zelinka, S.L. (Eds.), Wood & Fire Safety, Springer International Publishing, Cham. pp. 72–79.

Pagni, P.J., Joshi, A.A., 1991. Glass breaking in fires. Fire Safety Science 3, 791–802.

Paoletti, I., Nastri, M., 2023. Executive Design of the Façade Systems: Typologies and Technologies of the Advanced Building Envelopes. Springer Nature.

Pasternak, H., Ciupack, Y., 2014. Development of eurocode-based design rules for adhesive bonded joints. International Journal of Adhesion and Adhesives 53, 97–106. Joint Design.

Peng, L., Ni, Z., Huang, X., 2013. Review on the fire safety of exterior wall claddings in high-rise buildings in china. Procedia Engineering 62, 663–670.

Peng, L., Zhaopeng, n., 2016. Experimental study of window-ejected flame and plume on glass curtain walls. MATEC Web of Conferences 46, 05009.

Pereira, D., Gago, A., Proença, J., Morgado, T., 2016. Fire performance of sandwich wall assemblies. Composites Part B: Engineering 93, 123–131.

Pires, V., Rosa, L., Dionísio, A., 2014. Implications of exposure to high temperatures for stone cladding requirements of three portuguese granites regarding the use of dowel–hole anchoring systems. Construction and Building Materials 64, 440–450.

Pyl, L., Schueremans, L., Dierckx, W., Georgieva, I., 2012. Fire safety analysis of a 3d frame structure based on a full-scale fire test. Thin-Walled Structures 61, 204–212. Recent research advances on thin-walled structures.

Quadri, S., 2022. Aldgate fire: Residents raised safety concerns before whitechapel high street blaze. https://www.standard.co.uk/news/london/whitechapel-fire-residents-safety-concerns-east-london-b986722.html. [Online, Accessed: 2023-12-12].

Rackauskaite, E., Flint, G., Maani, A., Temple, A., Kotsovinos, P., 2019. Use of ls-dyna for structural fire engineering, in: 12th European LS-DYNA Conference.

Repubblica Italiana, 2022. Regole tecniche verticali, capitolo v.14 chiusure d'ambito degli edifici civili. https://www.ediltecnico.it/wp-content/uploads/2022/06/RTV_edifici_civile_abitazione_all1_dm_19_5_2022.pdf. [Online, Accessed: 2023-12-12].

Roenner, N., Yuan, H., Krämer, R.H., Rein, G., 2019. Computational study of how inert additives affect the flammability of a polymer. Fire Safety Journal 106, 189–196.

Sabsabi, A., Youssef, M., El-Fitiany, S., Vedrtnam, A., 2021. Simplified structural analysis of framed ordinary non-tempered glass panels during fire exposure. Fire Safety Journal 122, 103357.

Schartel, B., Humphrey, J.K., Gibson, A.G., Hörold, A., Trappe, V., Gettwert, V., 2019. Assessing the structural integrity of carbon-fibre sandwich panels in fire: Bench-scale approach. Composites Part B: Engineering 164, 82–89.

Sciarretta, F., Eslami, J., Beaucour, A.L., Noumowé, A., 2021. State-of-the-art of construction stones for masonry exposed to high temperatures. Construction and Building Materials 304, 124536.

Shahbazian, A., Wang, Y.C., 2014. A fire resistance design method for thin-walled steel studs in wall panel constructions exposed to parametric fires. Thin-Walled Structures 77, 67–76.

Shapiro, A., 2012. Using ls-dyna for heat transfer and coupled thermal-stress problems. Livermore Software Technology Corporation .

Sharma, A., Mishra, K.B., 2021. Experimental investigations on the influence of 'chimney-effect' on fire response of rainscreen façades in high-rise buildings. Journal of Building Engineering 44, 103257.

Siegesmund, S., Ruedrich, J., Koch, A., 2008. Marble bowing: comparative studies of three different public building facades. Environmental Geology 56, 473–494.

Sippel, J., Siegesmund, S., Weiss, T., Nitsch, K.H., Korzen, M., 2007. Decay of natural stones caused by fire damage. Geological Society, London, Special Publications 271, 139–151.

Soja, E., Wade, C., Frank, K., 2022. 4 - flammability tests for building facades, in: Apte, V. (Ed.), Flammability Testing of Materials Used in Construction, Transport and Mining. second ed.. Woodhead Publishing Series in Civil and Structural Engineering, pp. 89–126.

Sorensen, T., Tawadrous, R., Maguire, M., 2022. Thermally efficient corbel connections for insulated sandwich wall panels. Journal of Building Engineering 45, 103424.

Srivastava, G., Nakrani, D., Ghoroi, C., 2020. Performance of combustible facade systems with glass, acp and firestops in full-scale, real fire experiments. Fire Technology 56.

Sulik, P., Kinowski, J., Sędłak, B., 2016. Fire resistance of aluminium glazed curtain walls, test results comparison depending on the side of fire exposure. Applications of Structural Fire Engineering .

Sędłak, B., Kinowski, J., Borowy, A., 2013. Fire resistance tests of large glazed aluminium curtain wall test specimens – results comparison. MATEC Web of Conferences 9, 02009.

Sędłak, B., Kinowski, J., Sulik, P., Kimbar, G., 2018. The risks associated with falling parts of glazed facades in case of fire. Open Engineering 8, 147–155.

Sędłak, B., Roszkowski, P., Sulik, P., 2017. Fire insulation of aluminum glazed partitions depending on the infill solution of framework profiles. Civil And Environmental Engineering Reports 26, 091–107.

Sędłak, B., Sulik, P., Garbacz, A., 2021. Fire resistance of aluminium-glazed partitions depending on their height. Fire and Materials 45, 966–981.

Usmani, A., Rotter, J., Lamont, S., Sanad, A., Gillie, M., 2001. Fundamental principles of structural behaviour under thermal effects. Fire Safety Journal 36, 721–744. Response of Composite Steel Framed Structures to Fire.

Wang, Q., Chen, H., Wang, Y., Sun, J., 2013. Thermal shock effect on the glass thermal stress response and crack propagation. Procedia Engineering 62, 717–724. 9th Asia-Oceania Symposium on Fire Science and Technology.

Wang, Y., Foster, A., 2017. Experimental and numerical study of temperature developments in pir core sandwich panels with joint. Fire Safety Journal 90, 1–14.

Wang, Y., Hu, J., 2019. Performance of laminated glazing under fire conditions. Composite Structures 223, 110903.

White, N., Delichatsios, M., 2015. Fire hazards of exterior wall assemblies containing combustible components .

Yuan, H., Restuccia, F., Richter, F., Rein, G., 2019. A computational model to simulate self-heating ignition across scales, configurations, and coal origins. Fuel 236, 1100–1109.

Yuen, A.C.Y., Chen, T.B.Y., Li, A., De Cachinho Cordeiro, I.M., Liu, L., Liu, H., Lo, A.L.P., Chan, Q.N., Yeoh, G.H., 2021. Evaluating the fire risk associated with cladding panels: An overview of fire incidents, policies, and future perspective in fire standards. Fire and Materials 45, 663–689.

Zeisig, A., Siegesmund, S., Weiss, T., 2002. Thermal expansion and its control on the durability of marbles. Geological Society, London, Special Publications 205, 65–80.